

DURABILITY OF PERFORATED GFRP UNDER VARIOUS
ENVIRONMENTAL CONDITIONS WITH EMPHASIS ON ITS APPLICATION
AS A LINER FOR DIRECTIONAL OIL WELLS

by

Shiva Eslami

Submitted in partial fulfilment of the requirements
for the degree of Doctor of Philosophy

at

Dalhousie University

Halifax, Nova Scotia

May 2013

DALHOUSIE UNIVERSITY
DEPARTMENT OF CIVIL AND RESOURCE ENGINEERING

The undersigned hereby certify that they have read and recommend to the Faculty of Graduate Studies for acceptance a thesis entitled “DURABILITY OF PERFORATED GFRP UNDER VARIOUS ENVIRONMENTAL CONDITIONS, WITH EMPHASIS ON ITS APPLICATION AS A LINER FOR DIRECTIONAL OIL WELLS” by Shiva Eslami in partial fulfilment of the requirements for the degree of Doctor of Philosophy

Dated: May 29, 2013

External Examiner: _____

Research Supervisor: _____

Examining Committee: _____

Departmental Representative: _____

DALHOUSIE UNIVERSITY

DATE: May 29, 2013

AUTHOR: Shiva Eslami

TITLE: DURABILITY OF PERFORATED GFRP UNDER VARIOUS ENVIRONMENTAL CONDITIONS, WITH EMPHASIS ON ITS APPLICATION AS A LINER FOR DIRECTIONAL OIL WELLS

DEPARTMENT OR SCHOOL: Department of Civil and Resource Engineering

DEGREE: PhD CONVOCATION: October YEAR: 2013

Permission is herewith granted to Dalhousie University to circulate and to have copied for non-commercial purposes, at its discretion, the above title upon the request of individuals or institutions. I understand that my thesis will be electronically available to the public.

The author reserves other publication rights, and neither the thesis nor extensive extracts from it may be printed or otherwise reproduced without the author's written permission.

The author attests that permission has been obtained for the use of any copyrighted material appearing in the thesis (other than the brief excerpts requiring only proper acknowledgement in scholarly writing), and that all such use is clearly acknowledged.

Signature of Author

DEDICATION

This thesis is dedicated to my parents and all my family members who have supported me all the way since the beginning of my studies.

TABLE OF CONTENTS

LIST OF TABLES.....	ix
LIST OF FIGURES.....	x
ABSTRACT.....	xiv
ACKNOWLEDGEMENTS.....	xv
CHAPTER 1 INTRODUCTION	1
1.1 FRP (FIBER REINFORCED POLYMER) COMPOSITES IN OIL INDUSTRY	1
1.2 MOTIVATIONS AND OBJECTIVES	1
1.3 EXPERIMENTAL STRATEGY.....	2
1.4 THESIS LAYOUT	4
1.5 REFERENCES	7
CHAPTER 2 LITERATURE REVIEW.....	8
2.1 HORIZONTAL DRILLING	8
2.1.1 APPLICATIONS	9
2.1.2 THE COMPLETION OF HORIZONTAL WELLS FOR PRODUCTION	10
2.2 APPLICATION OF FRP LINERS IN HORIZONTAL WELLS.....	11
2.3 FRP DURABILITY	12
2.3.1 ALKALINITY	12
2.3.2 TEMPERATURE	14
2.3.4 MOISTURE	14
2.3.4.1 MOISTURE ABSORPTION SOLUTIONS	19
2.3.5 INFLUENCE OF ACID	22
2.4 REFERENCES	28
CHAPTER 3 EFFECTS OF AGING TEMPERATURE ON MOISTURE ABSORPTION OF PERFORATED GFRP.....	35
3.1 ABSTRACT	35
3.2 INTRODUCTION	36
3.3 THEORETICAL BACKGROUND.....	38
3.4 SPECIMEN PREPARATION	39
3.5 TESTING PROCEDURE	41

3.6	EXPERIMENTAL RESULTS AND DISCUSSION	42
3.6.1	MOISTURE ABSORPTION BEHAVIOR	42
3.6.2	MECHANICAL CHARACTERIZATION	44
3.6.3	SEM ANALYSIS.....	47
3.7	CONCLUSIONS.....	50
3.8	ACKNOWLEDGEMENTS	51
3.9	REFERENCES	51
CHAPTER 4 LONG TERM HYGROTHERMAL RESPONSE OF PERFORATED GFRP PLATES, WITH/WITHOUT APPLICATION OF CONSTANT EXTERNAL LOADING		54
4.1	ABSTRACT	54
4.2	INTRODUCTION	55
4.3	THEORETICAL BACKGROUND ON MOISTURE ABSORPTION	58
4.4	EXPERIMENTAL INVESTIGATION.....	61
4.4.1	SPECIMEN PREPARATION	61
4.4.2	EXPERIMENTAL PROCEDURE.....	62
4.5	EXPERIMENTAL RESULTS AND DISCUSSION	64
4.5.1	MOISTURE ABSORPTION BEHAVIOR	64
4.5.2	DEGRADATION IN THE MECHANICAL PROPERTIES	68
4.5.3	SEM ANALYSIS.....	75
4.6	CONCLUSIONS	77
4.7	ACKNOWLEDGEMENT.....	77
4.8	REFERENCES	78
CHAPTER 5 EFFECTS OF PERFORATION SIZE ON PERFORATED GFRP COMPOSITES' RESPONSE TO ACIDIC MEDIA.....		81
5.1	ABSTRACT	81
5.2	INTRODUCTION	81
5.3	THEORETICAL BACKGROUND.....	84
5.4	EXPERIMENTAL INVESTIGATION.....	87
5.4.1	SPECIMEN PREPARATION	87
5.4.2	EXPERIMENTAL METHODS	88
5.5	EXPERIMENTAL RESULTS AND DISCUSSION	90

5.5.1	ABSORPTION BEHAVIOR.....	90
5.5.2	MECHANICAL CHARACTERIZATION.....	95
5.5.3	MICROSCOPIC OBSERVATION.....	100
5.6	SUMMARY AND CONCLUSIONS	103
5.7	ACKNOWLEDGEMENTS	103
5.8	REFERENCES	104
CHAPTER 6 EXPERIMENTAL INVESTIGATION OF THE EFFECT OF AGING ON PERFORATED COMPOSITE TUBES UNDER AXIAL COMPRESSIVE LOADING.....		107
6.1	ABSTRACT	107
6.2	A BRIEF REVIEW OF THE RELEVANT RESEARCH.....	108
6.3	EXPERIMENTAL INVESTIGATION.....	109
6.3.1	FABRICATION AND CONDITIONING OF GFRP CYLINDRICAL SPECIMENS	109
6.3.2	TEST EQUIPMENT AND PROCEDURE	111
6.4	RESULTS AND DISCUSSION	113
6.4.1	INFLUENCE OF ACIDIC AND ELEVATED ENVIRONMENT ON THE MATERIAL	114
6.5.2	INFLUENCE OF ACIDIC AND ELEVATED TEMPERATURE ON THE LOAD BEARING CAPACITY OF THE PIPES	117
6.5.3	INFLUENCE OF ACIDIC AND ELEVATED ENVIRONMENT ON THE MICROSTRUCTURE OF THE PIPES	123
6.6	CONCLUSION	126
6.7	ACKNOWLEDGEMENT.....	127
6.8	REFERENCES	127
CHAPTER 7 PERFORATED GFRP PIPES' RESPONSE TO HOSTILE MEDIA		129
7.1	ABSTRACT	129
7.2	INTRODUCTION	129
7.3	LITERATURE REVIEW	131
7.4	EXPERIMENTAL INVESTIGATION.....	133
7.4.1	SPECIMEN PREPARATION	133
7.4.2	EXPERIMENTAL METHODS	135

7.5	EXPERIMENTAL RESULTS AND DISCUSSION	137
7.5.1	ABSORPTION BEHAVIOR.....	137
7.5.2	MECHANICAL CHARACTERIZATION	139
7.5.3	MICROSCOPIC OBSERVATIONS	144
7.6	SUMMARY AND CONCLUSION	146
7.7	REFERENCES	147
6.7	ACKNOWLEDGEMENT.....	148
CHAPTER 8	SUMMARY AND CONCLUSIONS	149
8.1	SUMMARY.....	149
8.2	CONCLUSIONS	150
8.3	RECOMMENDATIONS FOR FUTURE WORKS.....	151
References	153
APPENDIX A	Copyright Permission Letter.....	163

LIST OF TABLES

Table 3.1	The aging scenarios.....	41
Table 3.2	Bending test results for specimens aged at various temperatures (humidity 60%)	45
Table 4.1	Details of the specimens and conditioning scenarios.....	63
Table 4.2	Three-point bending test results (Environment temperature = 60 °C and 100% humidity)	69
Table 5.1	Details of the specimens and test condition	89
Table 6.1	Test specimens' specification	111
Table 6.2	Experimental results of buckling tests	118
Table 7.1	Details of the specimens and test condition	136

LIST OF FIGURES

Figure 1.1	Experimental strategy	5
Figure 2.1	Horizontal drilling phases [6]	9
Figure 2.2	Various operations involved in completion of horizontal wells [10]	14
Figure 2.3	SEM image (3K×) of different fibers in NaOH solution [20]	13
Figure 2.4	Stress Orientation at angle θ with respect to the longitudinal direction of fiber [44]	16
Figure 2.5	Material transportation from a high concentration part to a low concentration part (also referred to as diffusion) [51]	17
Figure 2.6	A thick spherical molecule of matrix with its outer surface under pressure [46]	18
Figure 2.7	A typical curve for the Fickian diffusion [52]	20
Figure 2.8	Typical diffusing molecules in Langmuir model [58]	21
Figure 2.9	X-ray dispersive microanalysis of calcium in E-glass fiber after exposure to 5N H ₂ SO ₄ [60]	24
Figure 2.10	Helical cracks in E-glass fibers exposed to H ₂ SO ₄ [19]	25
Figure 2.11	SEM of E-glass fibers after exposure to 5N H ₂ SO ₄ , showing helical cracking and the skin/core structure [60].	26
Figure 2.12	SEM of E-glass fibers, having been exposed to 5N H ₂ SO ₄ , showing longitudinal cracking [60]	27
Figure 2.13	X-ray dispersive microanalysis for silicon in E-glass fiber after exposure to 5 N H ₂ SO ₄ [60]	27
Figure 2.14	Tensile loading frames used for acid corrosion resistant experiments [63]	28
Figure 3.1	Representative volume used to fabricate the specimens	40
Figure 3.2	Three-point bending test setup	42
Figure 3.3	Moisture absorption of the specimens aged at 40°C, 60°C and 80°C temperature (humidity = 60%)	43
Figure 3.4	Average moisture absorption in different aging condition (humidity = 60%)	44
Figure 3.5	Failure mode observed as a result of the bending tests	45
Figure 3.6	Plot of the average load versus displacement (each curve is the average of 3 specimens) for the specimens conditioned at different temperatures at 60% humidity	46
Figure 3.7	Variation of the flexural stiffness as a function of diffusion coefficient and aging temperatures for specimens aged at various temperatures in 60% humidity	46
Figure 3.8	Comparison of the failure Surfaces of un-aged (virgin) perforated GFRP specimens and aged specimens at various temperatures (at 60% humidity)	49
Figure 3.9	SEM image showing typical (a) voids and (b) cracks in the matrix of the perforated GFRP specimen aged in humidity at 80°C	50
Figure 4.1	Typical perforated specimens (a) prior to, and (b) after mechanical test	58
Figure 4.2	Specimen geometry	61
Figure 4.3	Three-point bending frame setup for SCC testing	63
Figure 4.4	Moisture absorption of the specimens aged in water at 60°C	65

Figure 4.5	Moisture absorption of the specimens subjected to stress corrosion in 60°C water	65
Figure 4.6	Comparison of the moisture absorption predictions of the Langmuir and Fickian models for the specimens aged in water at 60°C temperature	67
Figure 4.7	Comparison of the moisture absorption prediction capability of the Langmuir and Fickian models for the undergone stress-corrosion in water at 60°C temperature	67
Figure 4.8	Comparison of the diffusions coefficients predicted by Shen and Springer equation and proposed model.	68
Figure 4.9	Load versus displacement curves for specimens aged or exposed to SCC with different perforation diameters (each curve represents average response of three specimens)	70
Figure 4.10	Degradation in the flexural strength of the perforated specimens as a function of time and perforation diameter (aged in water specimens and those subject to SCC)	72
Figure 4.11	Degradation in the flexural modulus of elasticity of the perforated specimens as a function of time and perforation diameter (aged in water specimens and those subject to SCC)	72
Figure 4.12	Increase in the ultimate flexural strain of perforated specimens as a function of conditioning time and perforation diameter	73
Figure 4.13	Comparisons of the predicted normalized strength (by Eq. (16)) versus that experimentally obtained: (a) aged in water (b) SCC in water	74
Figure 4.14	Comparison of the typical failure surfaces of the perforated GFRP specimens at before and after conditioning	76
Figure 5.1	Typical specimens geometry	88
Figure 5.2	The frame used to apply external load to the GFRP specimens (in SCC test)	89
Figure 5.3	Specimens under external load immersed in acid	90
Figure 5.4	Mass absorption of the specimens aged 15% sulfuric acid solution at 60 °C	92
Figure 5.5	Mass absorption of the specimens aged 15% sulfuric acid solution at 60 °C, subject to external load (SCC)	92
Figure 5.6	Mass absorption predictions by the Longmuir and Fickian models for the specimens aged in 15% sulfuric acid solution at 60°C; (a) specimens with perforation size: 0 and 5 mm, (b) perforation size: 8 and 11 mm	93
Figure 5.7	Mass absorption predictions by the Longmuir and Fickian models for the specimens aged in 15% sulfuric acid solution at 60°C, subject to external load (SCC); (a) specimens with perforation size: 0 and 5 mm, (b) perforation size: 8 and 11 mm	94
Figure 5.8	White precipitation as a result of chemical reactions between the fibers and sulphuric acid	95
Figure 5.9	Typical GFRP specimens appearance (drastic color change) after being immersed in 15% sulfuric acid solution	97
Figure 5.10	Degradation in the flexural strength of the perforated specimens as a function of time and perforation diameter (aged in sulphuric acid)	97

Figure 5.11	Degradation in the flexural strength of the perforated specimens as a function of time and perforation diameter (aged in sulphuric acid, subject to external load)	98
Figure 5.12	Variation in the ultimate flexural strain of perforated specimens aged in acidic solution as a function of conditioning time and perforation diameter	98
Figure 5.13	Degradation in the flexural modulus of elasticity of the perforated specimens as a function of time and perforation diameter (aged in water & acid)	99
Figure 5.14	The accuracy of the proposed model for estimating the saturation time of the perforated specimens as a function of perforation diameter (aged in 15% sulphuric acid subject to external load)	99
Figure 5.15	Typical delamination seen in the specimens due to the chemical degradation of the resin and fibers	100
Figure 5.16	Typical failure surfaces of the GFRP specimens before and after immersion in acid	101
Figure 5.17	Effect of the acid on fibers surface	102
Figure 6.1	Perforated tube: (a) tube geometry, (b) cross sections showing perforation arrangements	111
Figure 6.2	Buckling test facility	112
Figure 6.3	Typical failure patterns a) un-aged specimen b) aged specimen	114
Figure 6.4	Variation of mass absorption as a function of time for pipe with $d/h=27.5$ aged in 15% sulfuric acid at $60\text{ }^{\circ}\text{C}$	116
Figure 6.5	Variation of mass absorption as a function of time for pipe with $d/h=48.8$ aged in 15% sulphuric acid at $60\text{ }^{\circ}\text{C}$	116
Figure 6.6	Variation of mass absorption as a function of time for pipe with $d/h=71.5$ aged in 15% sulphuric acid at $60\text{ }^{\circ}\text{C}$	117
Figure 6.7	Experimental load versus end-shortening curves (AI and AP, $D/t=48.8$)	118
Figure 6.8	Hoop and axial strains for non-perforated and perforated pipes (AI and AP, $d/h=48.8$)	120
Figure 6.9	Experimental load versus end-shortening curves (BI and BP, $d/h=71.5$)	120
Figure 6.10	Hoop and axial strains for non-perforated pipes in both healthy and aged states (BI, $d/h=71.5$)	121
Figure 6.11	Experimental load versus end-shortening curves (CI and CP, $d/h=27.5$)	122
Figure 6.12	Hoop and axial strains for non-perforated pipes in both healthy and aged states (CI, $d/h=27.5$)	122
Figure 6.13	Comparison of the typical failure surfaces of the virgin and aged specimens	124
Figure 6.14	SEM images (through-the- thickness) of the smallest D/t saturated pipe	125
Figure 6.15	Transverse crack pattern through fibers	125
Figure 7.1	Typical perforated and non-perforated pipe specimens	134
Figure 7.2	Typical perforation arrangement in specimens: (a) tube geometry and longitudinal arrangement of the perforations, (b) cross sections showing the circumferential arrangement of the perforations	135
Figure 7.3	Variation of liquid absorption as a function of time for perforated pipes aged in water and 15% sulfuric acid at $60\text{ }^{\circ}\text{C}$; perforation size: 0, 5, 8 and 11 mm; testing condition: Aging	138

Figure 7.4	Variation of liquid absorption as a function of time for perforated pipes submerged in water and 15% sulfuric acid at 60 °C and subjected to external load (SCC); perforation size: 0, 5, 8 and 11 mm; testing condition: SCC	138
Figure 7.5	Degradation in the flexural modulus of elasticity of the perforated specimens as a function of perforation diameter and environmental conditions	140
Figure 7.6	Degradation in the flexural strength of the perforated specimens as a function of perforation diameter and environmental conditions	140
Figure 7.7	Variation in the ultimate flexural strain of perforated specimens as a function of perforation diameter and test conditions	141
Figure 7.8	Comparison of the postulated model for service life and the regression line from experimental results for GFRP perforated specimens as a function of perforation diameter	143
Figure 7.9	Typical fiber/resin interface of specimens subjected to various conditions	145
Figure 7.10	Helical cracks on the surface of a fiber (in specimens subjected to acidic environment) as a result of a combined state of radial and tangential stresses	146

ABSTRACT

Directional oil wells provide larger pay-zone (extraction zone) than the conventional vertical wells; they are therefore considered to be more economical means for oil extraction. Customarily, perforated steel pipes, called “liners”, are used to stabilize the wells. However, these liners are sensitive to environmental effects (i.e., combined high temperature and aqueous or acidic media), and are susceptible to stress corrosion. Perforated glass fiber reinforced polymer (GFRP) liners have been suggested as an alternative to the perforated steel liners to increase the service life of these liners, thereby offering overall economic benefits. In general, however, the mechanical properties of composites are weakened when exposed to such environmental parameters for a long period of time; therefore, the durability of GFRP liners is of concern. In addition, application of externally applied loads could also change the free volume fraction of the GFRP’s matrix; hence, negatively affect its absorption process and diffusion coefficient.

The main purpose of this thesis is therefore to investigate the effect of perforation size on the mechanical response of GFRP tubes/liners subject to hostile environments, as well as developing an effective model for predicting the post-exposure mechanical properties and residual life of the GFRP. For that, the long-term performance of four groups of perforated GFRP plates and tubes (with 5, 8 and 11 mm dia. perforations) were experimentally investigated. The first group of specimens was aged in water, while the second group was subjected to externally applied load while being aged in water. The third and fourth groups underwent a similar regime, but aging was done in 15% sulfuric acid solution instead of water. All experiments were conducted at 60 °C. The flexural properties of the specimens were evaluated by three-point bending tests during and upon completion of the saturation process. The observed saturation behaviors were then compared to that predicted using the Fickian and non-Fickian solutions. Furthermore, scanning electron microscopy was used to observe the microstructural changes.

Finally, models were developed to predict GFRP’s mechanical properties degradation, as well as its life cycle.

ACKNOWLEDGEMENTS

My deepest gratitude goes to my supervisor, Prof. Farid Taheri, for all his guidance and supports in so many ways, financially, academically and emotionally, throughout my PhD study. His patience and commitment to see the successful completion of this thesis is greatly appreciated. It has been a most rewarding learning experience to work in his research group and his wide knowledge has been of great value for me.

My gratitude also goes to my supervisory committee Dr. Tamunoiyala Koko and Dr. Kevin Plucknett and my external examiner, Dr. Pierre Mertiny for their time for this project and for their study and comments on my thesis.

I would like to express my gratitude to Dr. Fathollah Taheri-Behrooz for his comprehensive support and guidance in my research and also to Dr. Ramadan Esmael for his kind help in this project.

My love goes to my mother for always encouraging me to live my dreams and follow my heart; to my father for his permanent support and love in ups and downs; to my brother, Shahram, for all his support, understanding and encouragement and to my grandparents for their unreserved love.

I am thankful to my aunts, Mahnaz and Mitra for their permanent care, positive thoughts and energy, even when we are thousands of miles away from each other and to Shahram Etefagh for his support with an open heart all along my way coming to Canada.

My appreciation goes to Brian Kennedy and Blair Nickerson, our department's technicians, for all their supports with respect to the experimental side of my project.

My sincere thanks go to my current and previous officemates and colleagues including Mbaraka Mohamed, Morteza Mehrzadi, Babak ahmadi Moghadam, Mohammad Azadeh, Babak Soltannia, Mohammad Yahyaei, Davood Rezaei, Ramin Hosseinzadeh, Kaveh Arjomandi, Nikzad Nourpanah and Shahin Shadlou for their support, friendship and understanding.

I also extend my thanks to Azrah Kaniz, Muhammad Khan, Shaghayegh Vafayei, Ali vahdat, Zahra Pahlevani, Saham Ghazavi, Malihe Rostami, Ali Roshanfekar, Maryam

Nourbakhsh, Michelle Estekanchi and Ehsan Maghsoudlu for their honest and sincere friendship which was a gift for me when I was away from my family .

Also, my sincere gratitude goes to all my non-Iranian and Iranian friends in Halifax, we made great memories together and I will definitely miss you.

Finally, I sincerely appreciate the financial support I received from the National Sciences and Engineering Research Council of Canada (NSERC) which made it possible for me to continue my studies.

CHAPTER 1 INTRODUCTION

1.1 FRP (FIBER REINFORCED POLYMER) COMPOSITES IN OIL INDUSTRY

FRP (Fiber Reinforced Polymer) composite applications have become more established in a variety of structures and components. One of the unique features of FRPs is the use of various material compositions to meet the required strength and stiffness. The effective and efficient design of FRPs requires a wide range of knowledge in understanding their capabilities and limitations. Lack of in-depth understanding of FRP behavior can undoubtedly inhibit the effective exploitation of FRPs for structural applications. The effective and interesting aspects of their mechanical properties have been widely studied, while the influence of the environmental conditions (temperature, humidity, etc.) on the structural performance requires more attention.

Nowadays, FRP applications in the oil and gas industry are gaining attention, so that the life-cycle cost of structures could be reduced. However, in consideration of a possible alternative to current metallic liners, one must explore their response and performance in hostile environmental conditions (e.g., elevated temperature and acidic media), in order to assess the feasibility of the idea.

1.2 MOTIVATIONS AND OBJECTIVES

At present, perforated steel tubes, referred to as “liners”, are installed in oil wells in order to more effectively access the oil reservoir’s strata. Most of the conventional oil collection liners are not favored for installation in directional wellbores. This is due to the fact that significant effort has to be expended for their perforation, transportation and installation. Moreover, corrosion of such liners, which leads to the requirement for their replacement, consumes large expenses.

Therefore, the use of FRPs in producing liners can potentially generate great savings for oil companies, in the long term. Before such considerations, however, the effect of the service environment on the durability of FRP composite materials must be investigated. The temperature of wells that are drilled to low depth oil reservoirs of (up to 2000 m), would be low as 30-50 °C; however, in very deep wells (i.e., more than 5000 m), the well

temperature could reach as high as 160 °C [1, 2]. It should also be noted that in those depths, virtually all wells are surrounded by moisture or moisture vapors and combination of elements of sulfur. When this element is exposed to oxygen and water molecules in such wells, it would lead into formation of sulfuric acid. This service environment will therefore present a degrading effect on all structural components in that environment, including liners. Unfortunately, the current available database regarding the response of GFRP (in terms of physical and mechanical properties) within such real service environment is relatively scarce.

The main objectives of this study are therefore to investigate the influence of various environmental related parameters on cured perforated Glass Fiber Reinforced Polymer (GFRP) liners (tubes), and to develop a model for predicting their durability within directional oil well environment. Therefore, the specific focus will be on investigating the influence of environmental effects (i.e., humidity, temperature, and acidic media) on perforated GFRP pipes. Our literature search revealed that there has been no investigation into the effect of perforations on GFRP pipe's response and durability. Moreover, it appears that there is no model exists by which one could predict the life cycle of perforated GFRP pipes within the said environment.

1.3 EXPERIMENTAL STRATEGY

In order to realize the abovementioned objectives, an experimental strategy was proposed (see Figure 1.1). In this strategy, non-perforated and perforated GFRP plates and pipes hosting three different size perforations (i.e., 5, 8, 11 mm) are immersed in two types of media (i.e., aqueous and 15% sulfuric acid solution), at 60 °C. Then, their flexural response and degradation as a result of the saturation process are investigated. Some specimens are also subjected to an external load while aging. This condition would create the stress corrosion cracking phenomenon (and of course, when immersion is done under no external loading condition, then the pure aging condition would prevail). The results obtained from the outlined experimental program would provide adequate information by which one can develop a practical model for predicting the diffusion rate and life-cycle of the composite under the mentioned conditions.

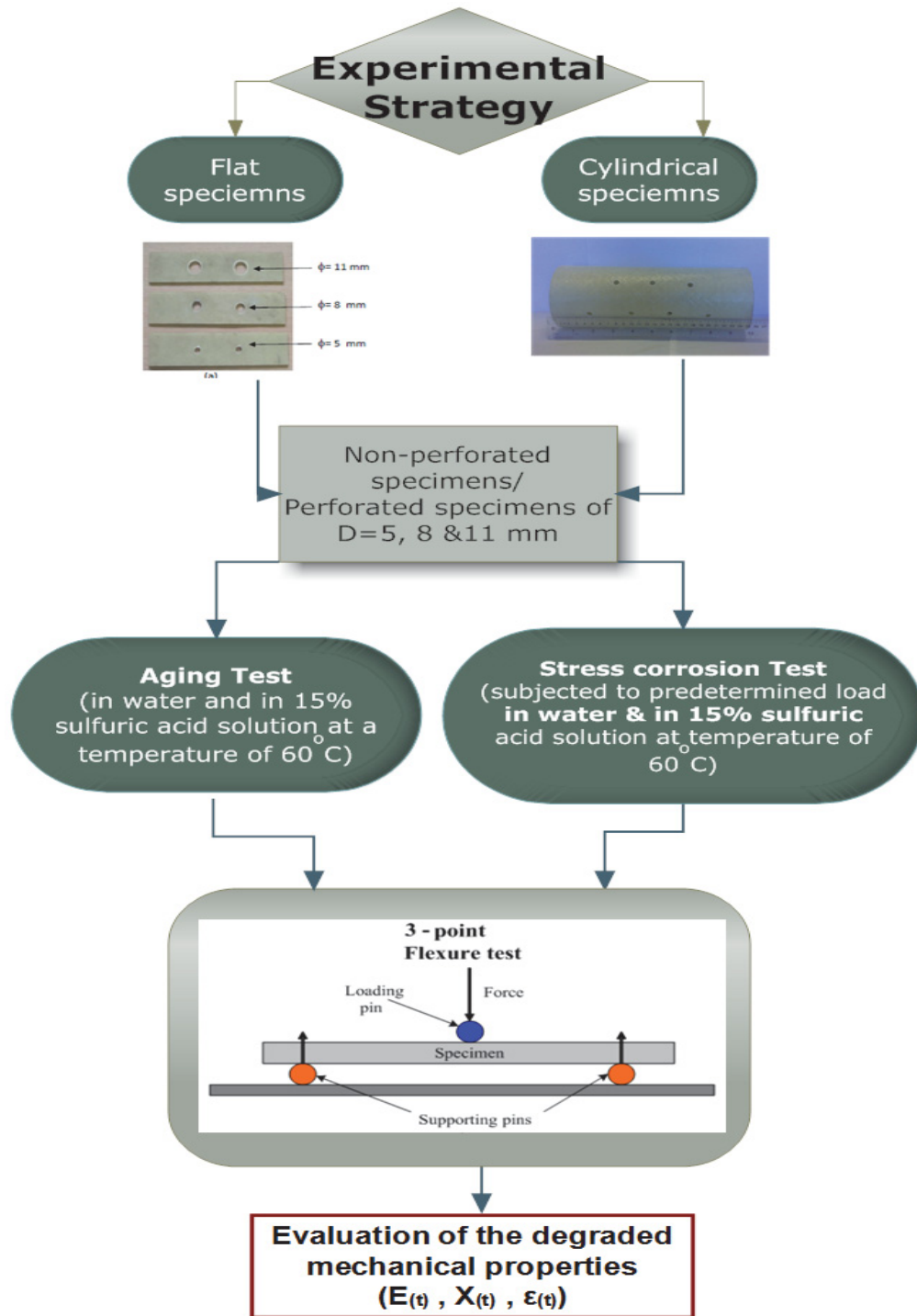


Figure 1.1 Experimental strategy

1.4 THESIS LAYOUT

This thesis consists of eight chapters. These chapter include five peer-reviewed journal manuscripts, either published or under review. The present chapter gives an overview of the overall project, and introduces the main topics included in the subsequent chapters. Chapter Two is the literature review, and covers an introduction to directional drilling, application of FRP liners in horizontal oil wells, and FRP durability response in alkaline, acidic and aqueous media, as well as, being subjected to elevated temperature. Chapters Three to Seven, each presents a journal paper, and each consists of introduction, literature review, main body, summary and conclusions. The main body of each paper explains the experimental investigations, and the results obtained from the conducted tests and microstructural observations. As well, the semi-empirical models developed to predict the specimen's behavior under various environmental situations are also noted. Chapter Eight includes the overall summary of this research, the conclusions and recommendations for future work.

Directional wells will be briefly introduced in chapter two; their importance and applications will be discussed and the currently practiced completion methods for horizontal wells will be introduced. Perforated steel liners are commonly installed in the oil wells in order to facilitate better access to various layers of oil reservoirs. These liners corrode as a result of their specific surrounding environments, thus must be replaced from time to time. The replacement is associated with very high cost, and that is why the use of perforated glass fiber reinforced plastic (GFRP) liners can be viewed as a potential cost-effective alternative to the traditional steel liners. One of the apprehensions for the use of such liners has been the issue of their durability, and the prediction of their life cycle. Consequently, in order to assess the feasibility of the concept, one ought to establish a rational procedure for assessing the long-term durability of perforated GFRP under various environmental conditions (i.e., moisture, elevated temperature and acidic media). Therefore, the environmental effects on the mechanical properties and performances of FRP materials will be reviewed.

Chapter Three will discuss the influence of aging on the flexural stiffness and bending capacity of a perforated glass fiber-reinforced epoxy composite subjected to combined

moisture and elevated temperature. Specimens, in the configuration of one quarter of a perforated GFRP tube were aged at 60% humidity and temperatures of 40, 60 and 80°C, respectively. Moisture absorptions diagrams, bending tests results and the scanning electron microscope (SEM) images were used to evaluate the effects of moisture absorption on the aged specimens. Moreover, a semi-empirical equation were developed to predict the change in the stiffness of the perforated aged GFRP structures.

In Chapter Four, the response of perforated GFRP plates subjected to a hot and humid environment is studied. The applicability and accuracy of Fick's model for establishing the magnitude of moisture absorption by such composites is assessed. Also, the influence of constant external loading on such perforated GFRP, while exposed to a harsh hot and humid environment, is investigated. Moreover, since the strength and stiffness of composites can be significantly affected by environmental parameters, the degradation in the strength and stiffness of the perforated GFRP as a function of time in such environment will be established by introducing a new model. The developed model can also account for the influence of the applied external loading. Chapter Five presents the result of the study onto the response of non-perforated and perforated GFRP plates, in a combined acidic and hot environment. The applicability of Fickian and Langmuir type models for predicting the mass absorption response of the composite, the degradation in the flexural properties of the composite bearing different perforation sizes, the physical effect of the acidic media on the GFRP material are also investigated and analyzed. Moreover, a semi-empirical model is developed, which is capable of predicting the saturation time of the composite. The model is also capable of accounting for the stress induced corrosion. The proposed model can estimate the time period needed for the degradation of the mechanical properties of GFRP composites aged in harsh environments (e.g., acidic and hot environments).

In Chapter Six, the results from the compressive axial loading tests, conducted on non-perforated and perforated GFRP pipes, which were exposed to acidic or aqueous media, with/without the application of external loading, are studied. The degradation of the flexural properties of such components, with different perforation sizes, is investigated. The applicability of the Fickian model for assessing the diffusion in the components is

also discussed. Moreover, scanning electron microscopy was performed to further study the environmental effects on the composite specimens.

In Chapter Seven, a life assessment model is developed for characterizing the response of perforated GFRP pipes, aged in both hot sulfuric acid and aqueous media, subjected to no external, as well as externally applied load. Tests were conducted to investigate the degradation in the flexural properties of the composites hosting different perforation sizes, subjected to various environmental conditions. In these experiments, aging and stress corrosion tests were conducted on perforated GFRP pipes and the influence of perforation diameter on the absorption response and the mechanical degradation of the material are examined. The tests are divided into two main categories; tests in water and tests in sulfuric acid. In each category, the specimens were immersed and kept in the hostile medium until they were saturated under two different testing conditions: (1) aging and (2) stress corrosion, and they were subsequently tested in three-point bending configuration.

The tubular GFRP specimens used in these investigations were fabricated by applying epoxy to a stitched E-glass fabric having a layup sequence of $[45^\circ/-45^\circ/90^\circ]$ (the angles are with respect to the longitudinal axis of the pipes).

A model is also developed by integrating the diffusion coefficient equations, both for non-stressed and stressed (SCC) specimens. This model can be used to predict the degradation in the material's strength as a function of time. In other words, the service life of the structure in sulfuric and aqueous medium and relatively high temperature (a similar environment in open-hole oil wells) can be predicted by the proposed model with reasonable accuracy. Moreover, scanning electron microscopy (SEM) were used to investigate the microstructural changes in the GFRP and the hydrolysis and corrosion caused by the exposed media.

Chapter Eight presents a brief summary of this study, as well as the conclusions and recommendations for future work.

1.5 REFERENCES

[1] The calculation of oil temperature in a well, SPE 17125, Society of Petroleum engineers, 1987

[2] High pressure and temperature wells, Retrieved on 4/6/2012, from:

<https://www.rwe.com/web/cms/en/1475772/rwe-dea/know-how/drilling/high-pressure-and-temperature-wells/>

CHAPTER 2 LITERATURE REVIEW

2.1 HORIZONTAL DRILLING

Due to increasing depletion of hydrocarbon products in the world, there is an increased need for development of more efficient extraction methods for exploitation of oil and gas reservoirs worldwide. Horizontal wells have emerged as a reliable method, with hundreds of them having been installed in every conceivable geologic formation [1]. Horizontal drilling is the process of drilling and completing a production well that begins as a vertical or inclined linear bore and continues at a near-horizontal attitude until the desired location is reached [2]. Various parameters impact the design of the directionality of horizontal oil and gas wells, including characterization of the reservoir rock, temperature, and pressure of the reservoir and reservoir fluids [3, 4].

The conventional vertical wells are typically drilled into a reservoir to produce hydrocarbons from just a few meters of contacted pay zone, located at the bottom of the hole. In the case of a horizontal well, the reservoir contact area is substantially increased by drilling through a radius at the bottom section of the well and then drilled horizontally along the thin pay-zone (see Figure 2.1). The radius of the well's curvature can be ultra-short (less than 1 m), short (6-12 m), medium (100-260 m) or long (greater than 260 m). The gain in the increased contact zone leads to an increase in reservoir productivity and higher ultimate recovery compared to vertical wells. In Canada, many horizontal wells, drilled in the provinces of Alberta, Saskatchewan and Manitoba have targeted thin sandstone reservoirs. In several cases, aquifers underlie these reservoirs, thus creating water coning problems, if vertical wells are to be drilled [5].

Horizontal drilling has many benefits as an effective access technology, with the two most significant advantages being [1]:

- An increase in the linear footage of well screen in contact with the pay zone, compared to a vertical well screen; and
- The ability to drill beneath surface obstructions or ongoing site operations without disturbance, in contrast to either vertical drilling or trenching operations.

However, the oil industry aims to ensure that not only should a horizontal well be the appropriate choice from the perspective of production volume, but it also should be an economical one [3]. There are currently some challenges in regards to the economics of horizontal drilling. Specifically, the achievement of the desired technical objectives comes at a price; a horizontal well can be anywhere from 25 percent to 30 percent more costly to drill and complete for production than a vertical well directed to the same target zone. Even when the drilling technique has been optimized for a target, the expected financial benefits of horizontal drilling must at least offset the increased well costs before such a project could be deemed feasible [2].

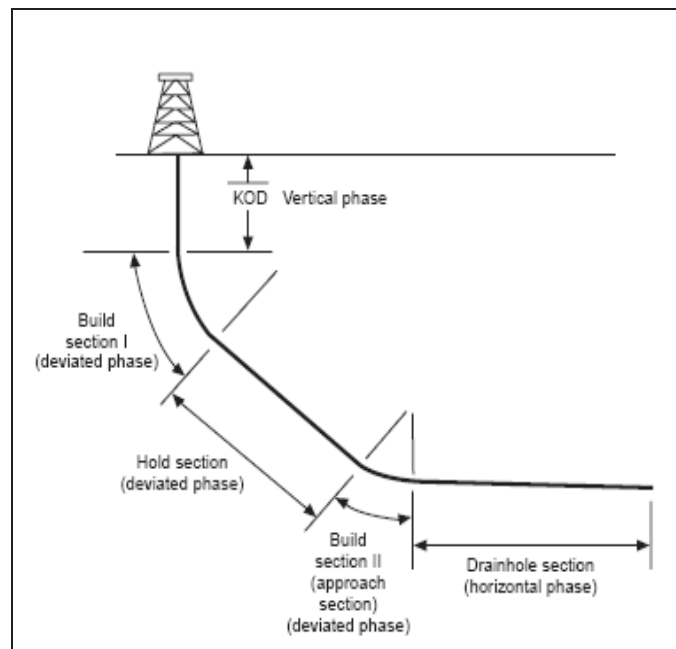


Figure 2.2 Horizontal drilling phases [6]

2.1.1 APPLICATIONS

The reservoir rocks that are potential candidates for horizontal and multilateral drilling applications include the following [6-9]:

- * Naturally fractured reservoirs
- * Low permeability reservoir

- * Channel sand and reef reservoirs
- * Coal bed methane reservoirs
- * Reservoirs with potential water and/or gas coning problems
- * Thin reservoirs
- * Economically inaccessible reservoirs.
- * Water-flood/enhanced oil recovery: compared to conventional vertical injection-vertical production well configurations, a horizontal production well significantly increases the ultimate oil recovery in water-flooding when used after the oil production stops.

2.1.1.2 THE COMPLETION OF HORIZONTAL WELLS FOR PRODUCTION

Drilling and completion methods, including drilling underbalanced, have been developed or customized for horizontal applications to minimize formation damage. These methods can be categorized into the areas of well logging and formation testing, well cleanup and well stimulation, open-hole completion, and cased completion [6].

The following options are usually considered for lateral completions of horizontal wells (Figure 2.2) [10]:

- Barefoot/open hole- used for stable consolidated formations that will not collapse when the well is put into production.
- Pre-drilled or slotted liner- used when there is a doubt about well-bore stability.
- Casing or liner, cemented and perforated- used to minimize the coning problems.
- Open hole with the stand alone screen or gravel pack- used when there are sand control problems.

In many instances, cased completions will be used. The installation (i.e., setting) of a relatively thin-walled casing in the well-bore allows most possible production problems to be avoided. The casing process consists of hanging the casing in the hole, cementing it in place, isolating the producing horizon with some combination of cement plugs and tools called packers, perforating the casing and any cement that exists opposite of the desired producing areas and, perhaps, installing a production liner.

In a fully-cased well, there are two ways to access target producing intervals. The first is to perforate the casing and the cement that may exist opposite to the selected producing horizons, using a perforating gun that contains various shaped explosive charges. The second is to set an un-cemented well liner at the selected horizon in lieu of the casing; then liners are pre-perforated.

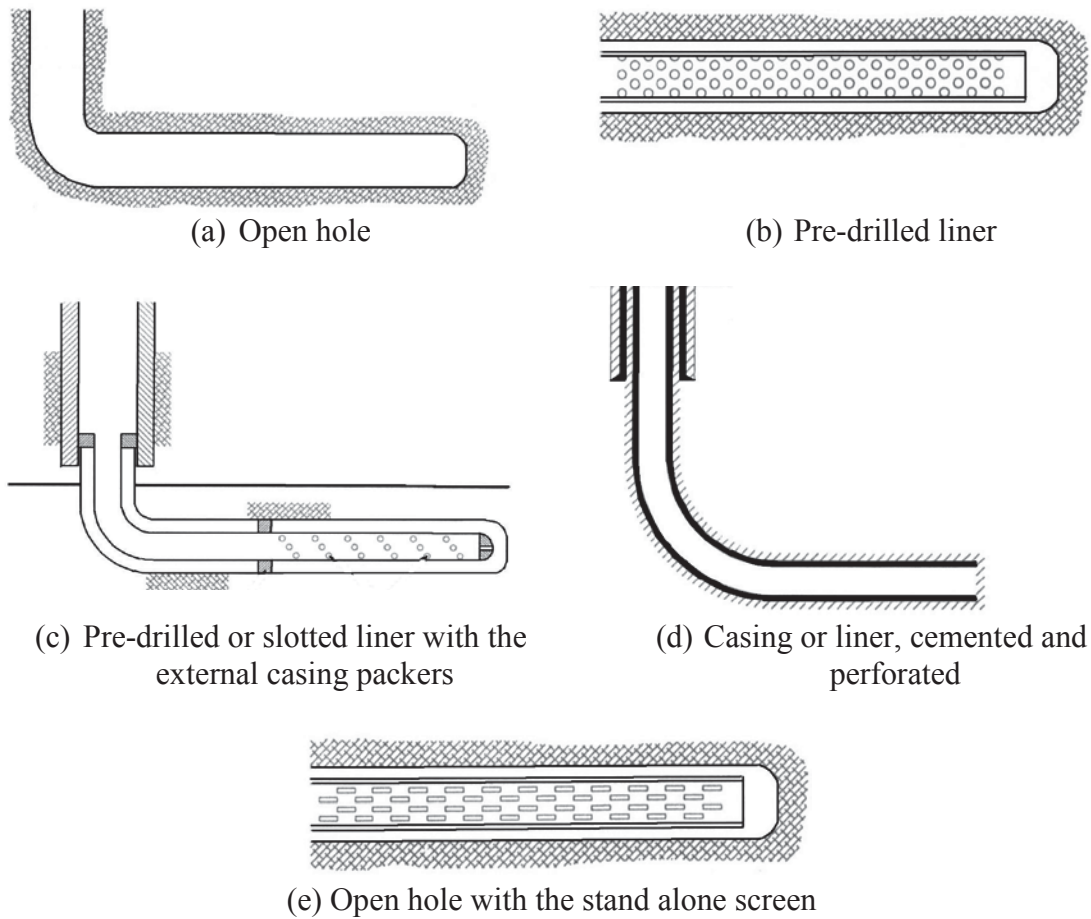


Figure 3.2 Various operations involved in completion of horizontal wells [10]

2.2 APPLICATION OF FRP LINERS IN HORIZONTAL WELLS

At present, there are perforated steel tubes, called liners, which could be installed in the oil wells in order to have better access to various layers of oil reservoirs. Such structures must periodically be replaced due to the corrosion that occurs in harsh environmental conditions. However, as the frequent need for liner replacement incurs high costs on production companies, the use of perforated glass fiber reinforced plastic (GFRP) liners

has been proposed by our research group as a novel idea and an effective alternative for replacing the damaged steel ones, specifically those used in open-hole horizontal wells. However, one of the concerns with the proposition would be the issue of durability and life cycle prediction of the composite used in forming such liners. Therefore, in order to verify the viability of the proposed concept, investigations should be conducted to evaluate the long-term durability of perforated GFRP under various environmental conditions (i.e., moisture, elevated temperature and acidic media).

Although GFRPs have been widely used in various structural applications due to their resistance to corrosion and their high specific strength and elastic modulus [11-18], in order to establish their suitability for the stated application, other aspects of their mechanical properties must be explored [15]. Specifically, their long term performance under various environmental conditions, as mentioned earlier, should be systematically explored.

Existing studies [11-12, 18] have evidenced that thermo-physical, mechanical and chemical properties of FRPs degrade due to moisture diffusing into their polymeric resin. Moreover, when GFRP structures are surrounded by a material with high alkalinity (e.g. concrete), the alkali-resistance of the fibers would be of a major concern. As well, elevated and subfreezing temperatures and freeze-thaw cycles can induce adverse thermal effects on FRPs. For instance, even the combination of a relatively moderately elevated temperature and humidity can lead to excessive creep. Moreover, exposure to ultraviolet light can also cause degradation of FRPs.

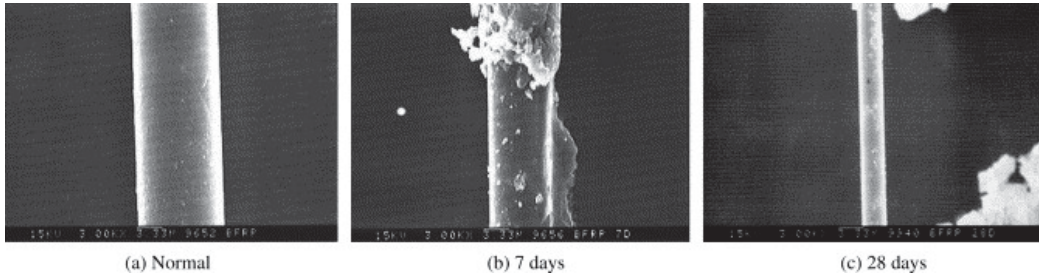
2.3 FRP DURABILITY

The purpose of this section is to outline different aspects of environmental effects on the mechanical properties and performances of FRP materials.

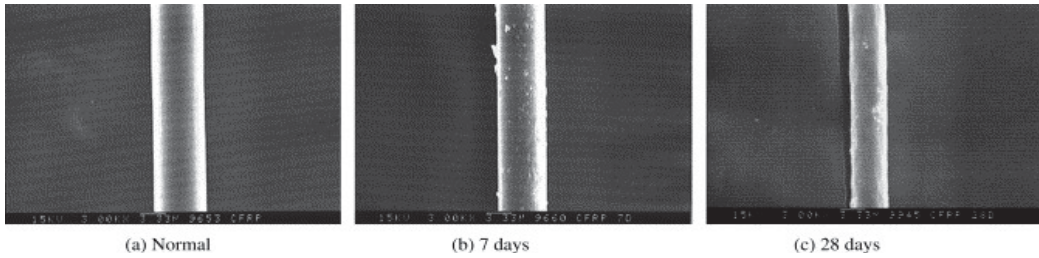
2.3.1 ALKALINITY

Alkalinity impacts mainly GFRP composites by breaking down the silica network of their fiber by attacking hydroxide (OH⁻) ions, and causing eventual dissolution of all the elements of the glass fiber. The glass fibers gradually lose weight, and consequently strength, when in contact with a strong alkaline environment. When a GFRP is kept in a

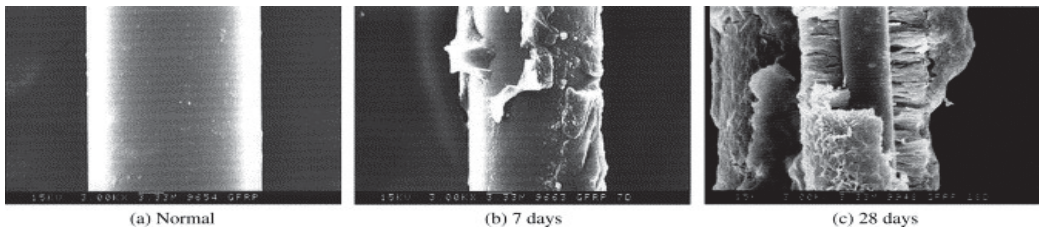
weak corrosive solution for two weeks at room temperature, its strength can be degraded by as much as 30% [19]. Sim et al. [20] investigated the alkali resistance of three types of fibers (basalt, carbon and glass fibers), and found that basalt and glass fiber volumes decreased when subjected to an alkali medium (Figure 2.3). Reactions between the fibers' surface and the alkali medium deteriorate the fibers significantly and thus decrease their volume.



(a) Basalt fibers in NaOH solution



(b) Carbon fibers in NaOH solution



(c) Glass fibers in NaOH solution

Figure 2.4 SEM image (3K \times) of different fibers in NaOH solution [20]

The reaction products were believed to have been created due to the interaction between SiO₂ in the fibers and alkali solution. No such reaction product was observed in their specimens made of carbon fibers.

2.3.2 TEMPERATURE

Adverse effects on composites can be caused by fire, freeze-thaw cycles, elevated and subfreezing temperatures and thermal cycles. Temperatures higher than the in-service temperature can cause intense deterioration of the bulk resin and the fiber-matrix interface. Moreover, with an increase in visco-elastic response, a consequent reduction in mechanical performance could develop when resins are subjected to an elevated temperature range [21-29].

In general, subzero temperatures would harden the matrix, thereby causing micro-cracks and bond degradation [30]. Moreover, combination of freeze-thaw cycles and the presence of salt can cause formation of salt deposits, which, if accompanied by swelling (caused by moisture infusion) and drying, may lead to significant degradation [11]. Further, it has been found that not only the performance of FRP composites affected by temperature, but it also is time dependent [31]. Moreover, when subjected to large loads, failure mechanisms become highly affected by temperature, as even modest degradation due to temperatures could lead to failure. However, when loads are more modest, the time dependency of the degradation has to be considered when characterizing FRP [31-33].

2.3.4 MOISTURE

Moisture absorption changes the thermo-physical and mechanical properties of FRP [37, 38]. Moisture can initiate plasticization and hydrolysis of a polymeric matrix, leading to degradation, which could become more severe at elevated temperatures [39-42]. Moreover, uneven swelling of the matrix as a result of moisture absorption can create unwanted stress concentration regions. Gautier et al. [43] aged two types of glass-fiber reinforced polyester composites in water at different temperatures (30, 50, 70 and 100 °C). Cracking in the matrix and interfacial de-bonding were observed, and a decrease in inter-laminar shear strength was reported, which was caused by interfacial de-bonding resulting from differential swelling.

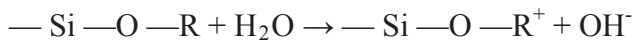
For glass fibers, moisture could cause degradation at the fiber level [19]. The fiber cross sectional shape also has effects on the moisture diffusion rate [14]; fibers with a regular

cross-section (like glass fibers) possess higher diffusivity in comparison to fibers with irregular cross-section (such as most carbon fibers).

Degradation of E-glass fibers in water can mainly be related to leaching of alkali oxides (sodium and potassium oxide) from the fiber surface, resulting in the formation of surface micro-cracks, which act as stress concentrators. The loss of strength can be expected to be permanent at all conditioning temperatures and exposure times [40]. The presence of Na^+ ions in solution slows down the exchange of alkali ions, such as Na^+OH^- , which restricts entry of Cl^- ions into the silic acid network [14]. Chloride ions slow the degradation process, although only slightly. Under the influence of humidity or water the fiber forms a water skin in which the alkali ions (e.g. NaOH^-) are leached from the fiber surface and replaced by protons (H^+). The thickness of the silic acid structure increases with exposure time and is dependent on the temperature and humidity of the surrounding environment. The water surrounding the glass fibers evolves into an aggressive alkali solution as the alkali ions dissolve out of the glass, slowly decomposing the glass fibers. Increased alkali content of the glass tends to reduce environmental attack from water and alkali solutions [18].

In brief, moisture effects on E-glass fibers include [14, 41, and 43]:

- Leaching of alkali oxides (sodium and potassium oxide) from the fiber surface



where R is Na, K, Ca, Mg, Al...

- Formation of surface micro-cracks and stress concentration
- Slow decomposition of glass fibers
- Permanent loss of strength

Several studies have investigated the response of composites to a hygrothermal environment, under loading [44-50]. It has been shown that the free volume fraction change could cause the moisture absorption of composites under externally applied stress. Neumann and Marom [44] showed experimentally that the maximum absorbed moisture would be enhanced with increasing magnitude of the applied tensile stress when the angle between fibers and loading direction (θ) (Figure 2.4) was greater than zero; however,

their experimental results showed the reverse at very small θ angles (close to zero). This could be due to the relatively large stresses induced by the residual swelling in the composite when the fiber angle becomes near zero.

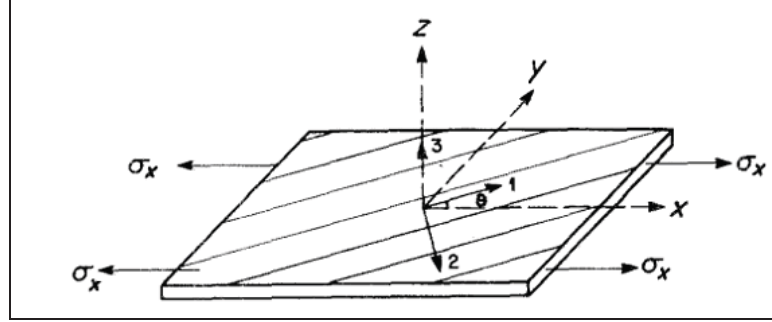


Figure 2.5 Stress Orientation at angle θ with respect to the longitudinal direction of fiber [44]

An equation has been developed for estimating the stiffness loss due to stress-corrosion-cracking (SCC) in glass/epoxy composites by combining the Weibull statistical distribution of the fibers strength with a classical power law type expression defining the sub-critical crack growth rate [45]; the equation is represented as:

$$\frac{S}{S_0}(t) \approx \exp[-K^* t^{nm/n-2} \sigma_{max}^{nm/n-2} \lambda^{nm/n-2}] \quad (1)$$

where S is the stiffness at time t , S_0 is the initial stiffness, K^* is a constant value, m is the Weibull modulus, which characterizes the statistical distribution of the surface defects, n is a power law exponent that characterizes the sub-critical crack growth rates of these defects within a given physico-chemical environment, σ_{max} is the applied stress and λ is a numerical value that can be considered as unity when there is no deviation in the applied strain.

Also, a few investigations have been conducted to assess the effect of stress on the diffusion of water into epoxy using the concept of free volume in polymers.

Diffusion (Figure 2.5) is the process of material transportation from one part of a system to another as a result of accidental molecular movements [52]. The diffusion coefficient represents the rate of diffusion of a matter as a function of absolute temperature, viscosity and size.

The diffusion coefficient can be calculated by an Arrhenius-type equation [53]:

$$D' = D_i \exp\left(\frac{-E_a}{RT}\right)$$

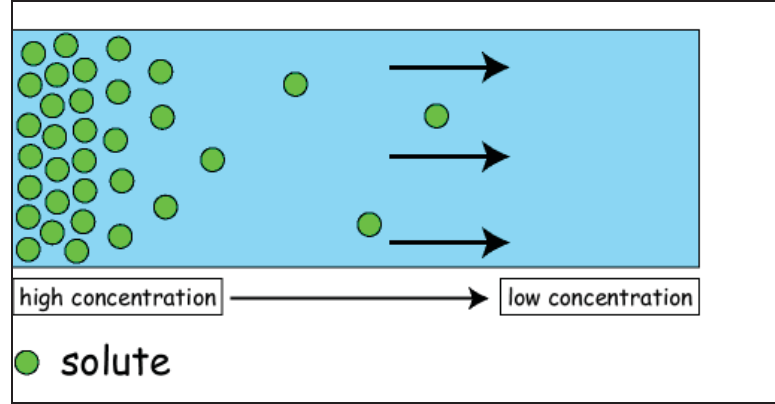


Figure 2.6 Material transportation from a high concentration part to a low concentration part (also referred to as diffusion) [51]

where D_i is a constant, E_a is the activation energy of the diffusion process, T is the absolute temperature in Kelvin and R is the universal gas constant.

Fahmy and Hurt [46] explained how the diffusion coefficient in an stressed polymer, D_σ , could be calculated by using the following equation:

$$\ln\left(\frac{D_\sigma}{D_0}\right) = b \left[\frac{1}{v_{f0}} - \frac{1}{v_{f\sigma}} \right] \quad (2)$$

where D_0 is the diffusion coefficient in the unstressed state, v_{f0} and $v_{f\sigma}$ are the free volume fraction in the unstressed and stressed states, respectively, and b is the outer radius of spherical molecules of the matrix as shown in Figure 2.6.

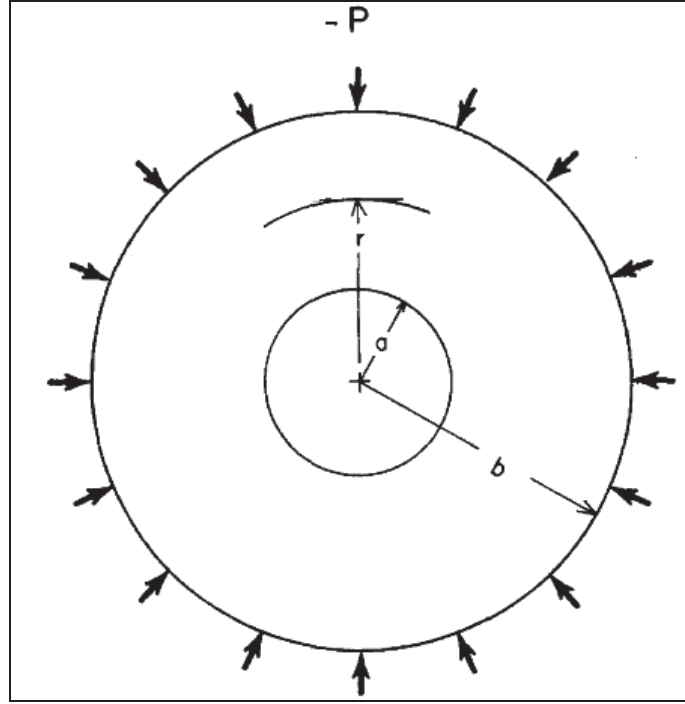


Figure 2.7 A thick spherical molecule of matrix with its outer surface under pressure [46]

The finalized relation between the diffusion coefficient and stress has been expressed in the following form [46]:

$$D_{\sigma} = D_0 \left(1 + A \frac{\sigma}{G} \right) \quad (3)$$

where σ , G and A are the applied stress, shear modulus and a material constant, respectively. For a polymeric composite, the Eq. 2 can be modified as [49]:

$$\ln \left(\frac{D_{\sigma}}{D_0} \right) = \frac{b}{\Phi_m} \left[\frac{1}{v_{f0}} - \frac{1}{v_{f\sigma}} \right] \quad (4)$$

where Φ_m is the volume fraction of matrix.

It should be noted that the presence of a tensile stress would enhance the diffusion coefficient and moisture absorption, while compressive stress would decrease it (though to a lesser extent); however, it has been shown that under bending conditions, D would increase because the increase in the moisture absorption process due to the tensile stress

would be much higher than the resistance to moisture absorption resulting from the compressive stress [46-48].

2.3.4.1 MOISTURE ABSORPTION SOLUTIONS

It is possible to obtain the moisture concentration distribution in an infinitely large polymer composite plate using Fick's equation [54]:

$$\frac{\partial c}{\partial t} = \frac{\partial}{\partial x} D \frac{\partial c}{\partial x} \quad (5)$$

where c is the moisture concentration and D is the mass diffusivity along the laminate thickness direction. Since the temperature and the diffusivity are considered to be constant within the material, the phenomenon can be represented by the following differential equation:

$$\frac{\partial c}{\partial t} = D \frac{\partial^2 c}{\partial x^2}$$

The solution for the moisture absorption, derived by Shen and Springer [54], is as follows:

$$\frac{M_{\%}}{M_{\infty}} = 1 - \frac{8}{\pi^2} \sum_{n=0}^{\infty} \frac{1}{(2n+1)^2} \exp \left[-D(2n+1)^2 \frac{\pi^2 t}{h^2} \right] \quad (6-a)$$

where $M_{\%}$ and M_{∞} are the amount of moisture absorbed at time t and the equilibrium moisture content, respectively; D is the diffusion coefficient and h is the specimen thickness.

The above can be represented in an approximate form as:

$$\frac{M_{\%}}{M_{\infty}} \approx 1 - \exp \left[-7.3 \left(\frac{Dt}{h^2} \right)^{0.75} \right] \quad (6-b)$$

The diffusion coefficient D can be obtained from the following equation [54-56]:

$$D = \pi \left(\frac{h}{4M_{\infty}} \right)^2 \left(\frac{M_2 - M_1}{\sqrt{t_2} - \sqrt{t_1}} \right)^2 \quad (7)$$

where $\left(\frac{M_2 - M_1}{\sqrt{t_2} - \sqrt{t_1}} \right)$ is the slope of the initial linear part of the absorbed moisture-time curve. Figure 2.7 shows a typical curve for Fickian diffusion [52].

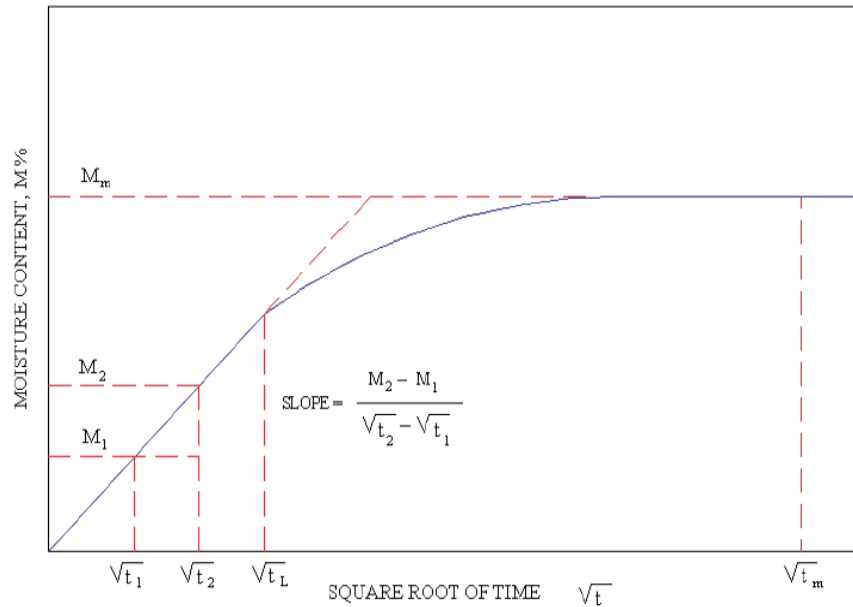


Figure 2.8 A typical curve for the Fickian diffusion [52]

It is worth mentioning that some researchers have claimed that Fick's model cannot adequately predict the moisture absorption in composites. For instance, Carter and Kibler [57] stated that the time required for interactions between moisture and matrix to occur in composites would be longer in comparison to the time required for the migration of water within the matrix; as a result, they proposed a Langmuir-type model. In their model, it is assumed that there would be two types of absorbed water molecules: (i) mobile molecules and (ii) bound molecules, and that the level of final absorbed moisture will depend on the previous saturation level history (see Figure 2.8).

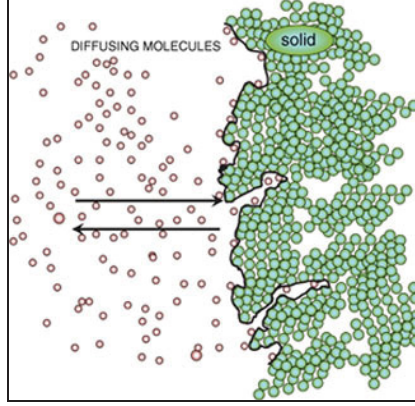


Figure 2.9 Typical diffusing molecules in Langmuir model [58]

They also suggested the following equation for prediction of the level of moisture absorption at time t in specimens that have very low initial moisture content and are subjected to a relatively short exposure time [57]:

$$M_t = \frac{4}{\pi^{3/2}} \left[\frac{\beta}{\beta + \gamma} M_\infty \right] \sqrt{kt} \quad (8)$$

In the above equation, β and γ are the probabilities of molecule bonding and molecule mobility, per unit time, respectively, and k is calculated by the following equation:

$$k = \frac{\pi^2 D}{h^2} \quad (9)$$

where h and D are as described earlier.

Carter and Kibler suggested that the use of the following equation for predicting the level of moisture absorption occurring within a long exposure time [57]:

$$M_t = M_\infty \left[1 - \frac{\gamma}{\beta + \gamma} \exp(-\beta t) \right] \quad (10-a)$$

where β can be determined by taking the derivatives of the above equation [57]:

$$-\left[\frac{dM_t}{dt} \right]^{-1} \left[\frac{d^2 M_t}{dt^2} \right] \approx \text{constant} = \beta \quad (10-b)$$

By substituting the calculated β in the following equation, one can find γ [57]:

$$\exp(-\beta t) \left[\beta \left\langle \frac{dM_t}{dt} \right\rangle^{-1} M_t + I \right] \approx \text{constant} = I + \frac{\beta}{\gamma} \quad (11)$$

Some researchers have demonstrated the agreement of the results of this model to experimental results [52, 59].

The above equations have been proposed for infinite plates, in which the diffusion is assumed to occur mainly through the surfaces; but in finite size plates, diffusion through the edges would have a considerable effect on the maximum value of moisture absorption, thus, such deviations should be considered.

Shen and Springer [54] developed an equation by which the diffusion coefficient was modified for finite size specimens, according to the following equation:

$$D_{F.S} = D \left(1 + \frac{h}{l} + \frac{h}{w} \right)^{-2} \quad (12)$$

In the above equation, $D_{F.S}$ is the modified diffusion coefficient for finite size specimens, l , w and h are the length, width and thickness of the specimen.

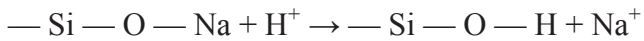
2.3.5 INFLUENCE OF ACID

The chemical corrosion of E-glass fibers, especially in acidic solutions, is well-known to related industries. Despite the knowledge-base, several chemical corrosion induced failure cases have been reported for the GFRP composites. The accepted mechanism of the corrosion process is ion replacements in which metal ions such as Ca^{2+} and Al^{3+} in the glass fiber are exchanged for H^+ in the acid [60]:

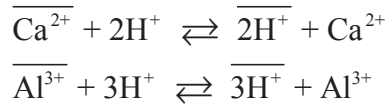


where the bar denotes association of the elements with the glass phase. The smaller size of H^+ compared to metal ions may produce tensile stresses in the surface of the glass, which could lead to cracking.

Among all glass fiber types, E-glass fibers are more susceptible to deterioration by mineral acids (e.g., H₂SO₄ and HCl). Those acids can be present in all chemical factories, industrial locations and even industrial sewages. The ionic exchange of sodium, potassium, calcium, magnesium, boron and aluminum of the fiber will happen in acidic media, when the metallic cations at the glass surface are replaced by the hydrogen ions in the acid solution. Ionic exchange between Na⁺ ions at the fiber surface and the H⁺ ions in the acid solution is as follows [19]:



Given that calcium and aluminum oxides form approximately 35% by weight of the glass, the leaching of these two metallic ions is considerable also [61]:



where the ions denoted by the bar are in the glass phase and the other ions exist in acid solutions.

When a glass structure is exposed to an acidic media, calcium ions can diffuse easily through the silica network of glass and exchange with hydrogen ions [60] (see Figure 2.9); but the aluminum ion is more difficult to move, due to its higher valence and smaller volume relative to the calcium ion [19]. These processes are accelerated at elevated temperatures [61].

Not only the hydrogen ion but also the associated anions in the medium can also be involved in the leaching mechanism. If the reactions between anions in the medium and cations in the glass fiber make complex ions or insoluble deposits; then the cations will be removed from the glass surface and the above reaction will be driven to the right side [19, 60].

Therefore, leaching in acids can generally be characterized either by acid-strength-controlled leaching or by anion-controlled leaching.

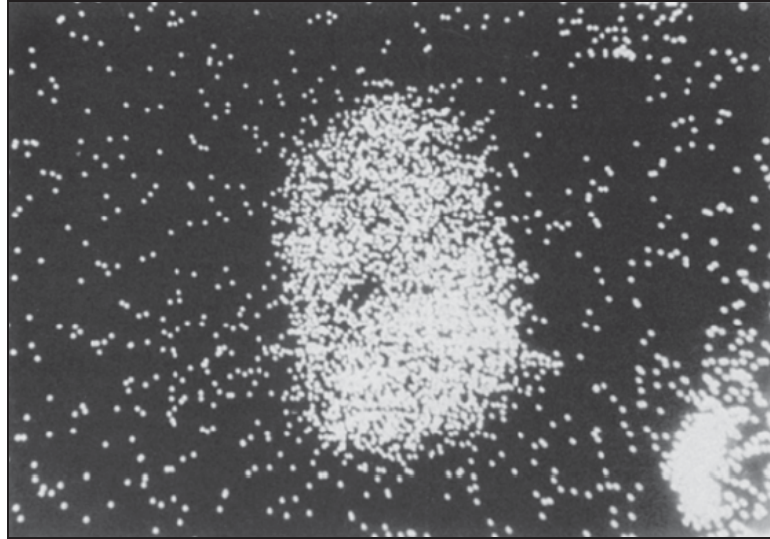
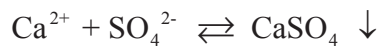


Figure 2.10 X-ray dispersive microanalysis of calcium in E-glass fiber after exposure to 5N H₂SO₄ [60]

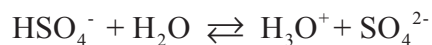
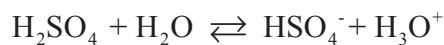
In hydrochloric and nitric acids, leaching is controlled by acid concentration; because the anions in these solutions (Cl⁻ and NO₃⁻) do not make deposits of main metallic cations in the glass [60].

Conversely, sulfuric acid makes an anion-controlled leaching environment for the calcium ion because the product of reaction between the sulfate anion, SO₄²⁻, and the calcium ion in the glass would be a deposit, governed by the following relationship [61]:



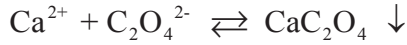
However, as for the aluminum ion, the leaching behavior in sulfuric acid is acid-controlled as the sulfate anion cannot form deposits/complex ions with aluminum ions.

The dissolution of sulfuric acid obeys the following chemical processes [61]:

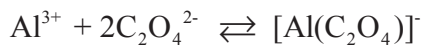
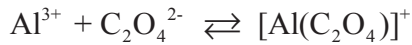


The more the existence of HSO₄⁻, the higher the fiber corrosion will be.

On the other hand, the anion in oxalic acid, $C_2O_4^{2-}$, can form both an insoluble salt with the calcium ion and stable complex ions with the aluminum ion [61]. The formation of the insoluble calcium salt can be expressed by:



The oxalate anion can also form several complex ions with the aluminum ion, such as [61]:



As the outer layer of fibers diminishes, stresses caused by the core of the fiber increase, leading to a decrease in the load capacity of the fiber and initiating cracks. The combination of tangential and radial stresses makes cracks be helical (Figure 2.10).

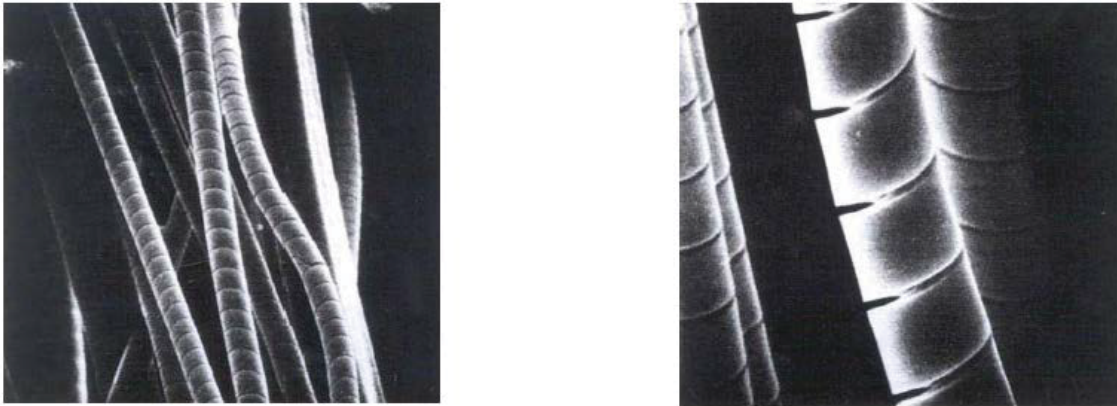


Figure 2.11 Helical cracks in E-glass fibers exposed to H_2SO_4 [19]

The surface crack morphology is dependent onto two different types of stresses [61]: (1) the residual stresses resulting from fiber fabrication, and (2) the shrinkage stresses induced by the volume mismatch between the fiber surface and core, developed out of the fiber corrosion.

It is worthwhile to mention that the depth of ion removal and shrinkage stress can affect the crack shapes [61]. When the depth is relatively small, the overall surface stress is controlled by the axial residual stress and the fracture will be axially dominated. When the crack starts, it grows around the fibers to relax the internal axial stress, with the spiral

crack morphology (see Figure 2.11). However, when the depth of ion removal is large, the fracture in the hoop direction would be eminent. When the hoop stress reaches to a critical limit, axial surface cracks will be formed on the fiber surface (see Figure 2.12). At a specific depth, the fracture causing stresses in the axial and hoop directions cause the mixed morphology of spiral and axial cracks.

There are important findings made by Bledzki et al [62] confirming that the surface crack could not form in the wet acid leaching process, until the water molecules absorbed in the corroded fiber are completely evaporated. Reduction in the shrinkage stress in the wet environment is the main reason for this phenomenon. Water molecules fill the micro-pores in the fiber surface made by the ion exchange process, so that the volumetric stresses would become so small that they would not be able to initiate surface cracks. However, when the fiber surface is dried, the micro-pores will be filled by air and the shrinkage stresses will gradually increase, leading to fiber surface cracking.

In the end, the loss of the silica network on the fiber surface would lead to diminished structural strength and stiffness (see Figure 2.13) [60].

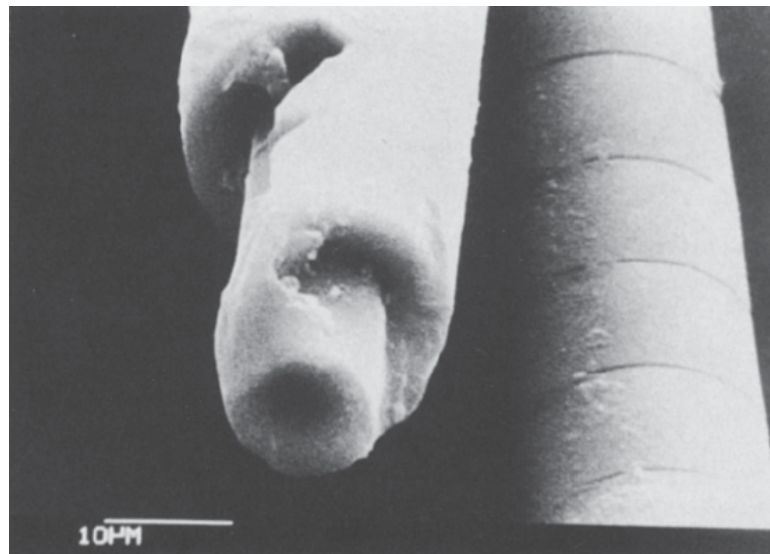


Figure 2.12 SEM of E-glass fibers after exposure to 5N H_2SO_4 , showing helical cracking and the skin/core structure [60].

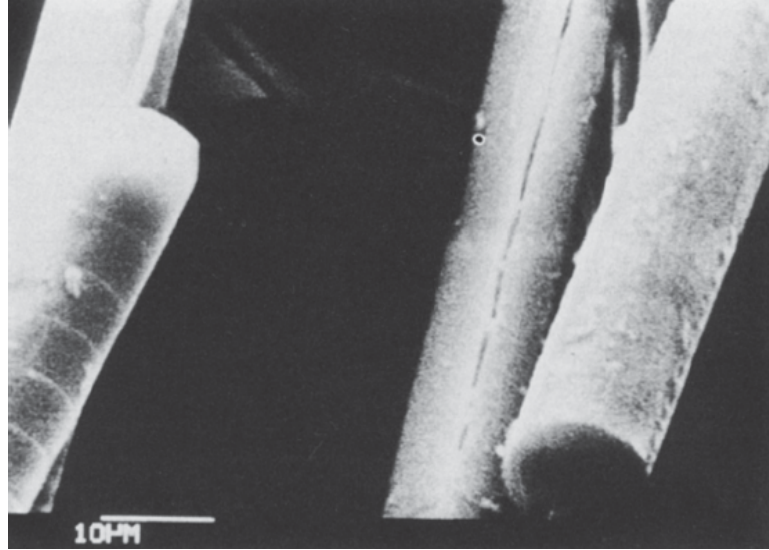


Figure 2.13 SEM of E-glass fibers, having been exposed to 5N H₂SO₄, showing longitudinal cracking [60]

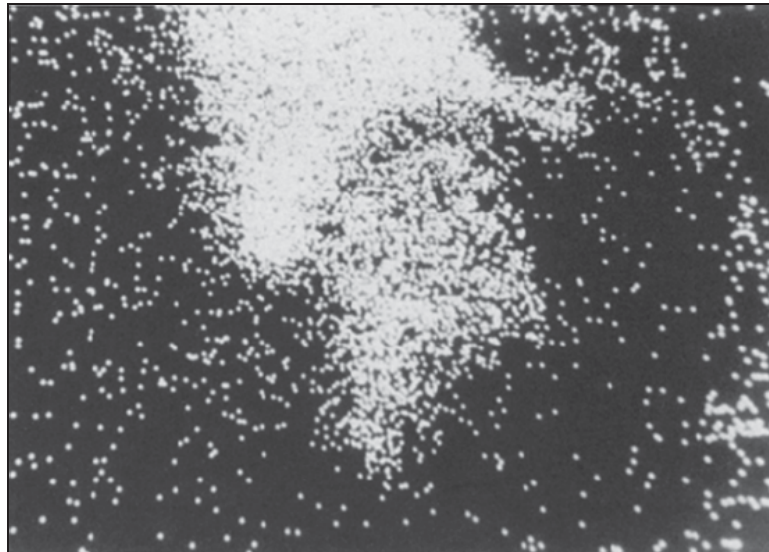


Figure 2.14 X-ray dispersive microanalysis for silicon in E-glass fiber after exposure to 5 N H₂SO₄ [60]

Acids can also penetrate through the matrix to reach to the fibers; therefore, crack initiation is also controlled by the surface conditions. The resistance of glass fibers can be enhanced by changing the chemical composition or chemical sizing (having couplants) the fiber during fabrication to have a barrier coating. Moreover, a protective resin-rich

layer (often referred to as “gel-coat”) approximately 2.54–6.35 mm, is often used on the surfaces of GFRP structures that would be in contact with acid [60].

The resistance to acid corrosion of glass fibers may be assessed by either measuring the time-to-failure of composites under sustained static loading in the acid environment (Figure 2.14), or by allowing stressed or unstressed fibers to remain in an acid environment for a set time, followed by the application of a constant-rate-of strain tensile test to take them to failure [63, 64]. In the latter method, the ratio of failure stress before and after acid immersion may be used as a relative measure of resistance to acid corrosion. The former method of measuring time-to-failure is more time-consuming and gives a characteristic scatter in failure times (i.e., high standard deviations), but may more closely represent in-service behavior [61].



Figure 2.15 Tensile loading frames used for acid corrosion resistant experiments [63]

2.4 REFERENCES

[1] Horizontal Environmental Well Handbook. Prepared by: Directed Technologies Drilling, Inc. 2004.

[2] Strong M, Bozzini Ch, Hood D, Lowder B. Air and Ozone Sparging of TCE Using a Directionally Drilled Horizontal Well. Retrieved on 20/8/2009, from:

<http://www.horizontaldrill.com/resources/articles.htm>

- [3] Drilling Sideways -- A Review of Horizontal Well Technology and Its Domestic Application. A report from: Office of Oil and Gas, U.S. Department of Energy. DOE/EIA-TR-0565. 1993
- [4] Azar J J. "Oil and Natural Gas Drilling" in Encyclopedia of Energy. 2004; 4: 521-34
- [5] Catania P, Wilson M. Horizontal drilling assessment in Western Canada. Appl. Energ. 1999; 64: 331-43
- [6] Catania P. Predicted and actual productions of horizontal wells in heavy-oil fields. Appl. Energ. 2000; 65: 29-43
- [7] Gentzis, Th. Stability analysis of a horizontal coalbed methane well in the Rocky Mountain Front Ranges of southeast British Columbia, Canada. Int. J. Coal Geol. 2009; 77: 328-37
- [8] Hadia N, Chaudhari L, Mitra S K, Vinjamur M, Singh R. Experimental investigation of use of horizontal wells in waterflooding. J Petrol Sci Eng. 2007; 56: 303-10
- [9] Majdi A, Mostafa-zadeh M, Sajjadian V A. Direction and prediction of well priority drilling for horizontal oil and gas wells (A case study). J Petrol Sci Eng. 2005; 49: 63-78
- [10] Bellarby J. 'Chapter 1:Introduction' in Well Completion Design. Developments in Petroleum Science. 2009; 56: 1-14
- [11] Karbhari V M (ed). Durability of composites for civil structural applications. woodhead publishings, Cambridge, UK. 2007
- [12] Lin MW, Berman J B, Khoshbakht M, Feickert C A, Abatan A O. Modeling of moisture migration in an FRP reinforced masonry structure. Build. Environ. 2006; 41: 646-56
- [13] Verghese K N E, Hayes M D, Garcia K, Carrier C, Wood J, Riffle J R, Lesko J J. Influence of matrix chemistry on the short term hydrothermal aging of vinyl ester matrix and composites under both isothermal and thermal spiking conditions. J of Compos. Mater. 1999; 33: 1918-38
- [14] Aditya P K, Sinha P K. Moisture diffusion in variously shaped fibre reinforced composites. Comput. Struct. 1996; 59: 157-66

- [15] Nakai A, Ikegaki S, Hamada H, Takeda N. Degradation of Braided composites in hot water. *Compos. Sci. and Technol.* 2000; 60: 325-31
- [16] Schambron Th, Lowe A, McGregor H V. Effects of environmental ageing on the static and cyclic bending properties of braided carbon fiber/PEEK bone plates. *Compos. Part B: Eng.* 2008; 39: 1216-20
- [17] Scida D, Abourab Z, Benzeggagh M L. The effect of ageing on the damage events in woven-fibre composite materials under different loading conditions. *Compos. Sci. and Technol.* 2002; 62: 551-7
- [18] Hulatt J, Hollaway L, Thorne A. Preliminary investigations on the environmental effects on new heavyweight fabrics for use in civil engineering. *Compos. Part B: Eng.* 2002; 33: 407-14
- [19] Maxwell AS, Broughton WR, Dean G, Sims GD. Review of accelerated aging methods and lifetime prediction techniques for polymeric materials. NLP Report: DEPC MPR 016. 2005
- [20] Sim J, Park Ch, Young Moon D. Characteristics of basalt fiber as a strengthening material for concrete structures. *Compos. Part B: Eng.* 2006; 36: 504-12
- [21] Leone M, Matthys S, Aiello M A. Effect of elevated service temperature on bond between FRP EBR systems and concrete. *Compos. Part B: Eng.* 2009; 40: 85-93
- [22] Tadeu A J B, Branco F J F G. Shear tests of steel plates epoxy-bonded to Concrete under temperature. *J. Mater. Civ. Eng.* 2000; 12: 74-80
- [23] Bai Y, Post N L, Lesko J J, Keller T. Experimental investigations on temperature-dependent thermo-physical and mechanical properties of pultruded GFRP composites. *Thermochimica Acta.* 2008; 469: 28-35
- [24] High-performance concrete: A State-of-the-Art Report, Retrieved on 1/8/2009 from: <<http://www.fhwa.dot.gov/publications/research/infrastructure/structures/hpc/97030/chap5.cfm>>

- [25] Ribeiro M C S, Novoa P R, Ferreira A J M, Marquez A T. Flexural performance of polyester and epoxy polymer mortars under severe thermal conditions. *Cement Concrete Comp.* 2004; 26: 803-9
- [26] Karbhari V M, Zhao L. Use of composites for 21st century civil infrastructure. *Comput. Method. Appl. Mech . Eng.* 2000; 185: 433-54
- [27] Bai Y, Keller T, Vallée T. Modeling of stiffness of FRP composites under elevated and high temperatures. *Compos. Part B: Eng.* 2008; 68: 3099-106
- [28] Elbadry M, Elzaroug O. Control of cracking due to temperature in structural concrete reinforced with CFRP bars. *Compos. Struct.* 2004; 64:37-45
- [29] Mikhail A E, El Damatty A A. Non-linear analysis of FRP chimneys under thermal and wind loads. *Thin-Wall. Struct.* 1999; 35: 289-309
- [30] Dutta P K, Hu, D. Low-temperature and freeze-thaw durability of thick composites. *Compos. Part B: Eng.* 1996; 27: 371-9
- [31] Asaro R J, Lattimer B, Ramroth W. Structural response of FRP composites during fire. *Compos. Struct.* 2009; 87:382-93
- [32] Gu P, Asaro R J. Designing sandwich polymer matrix composite panels for structural integrity in fire. *Compos. Struct.* 2008; 88:300-9
- [33] Bai Y, Vallée T, Keller T. Modeling of thermal responses for FRP composites under elevated and high temperatures. *Compos. Sci.Technol.* 2008; 68: 47-56
- [34] Pillay S, Vaidya U K, Janowski G M. Effects of moisture and UV exposure on liquid molded carbon fabric reinforced nylon 6 composite laminates. *Compos. Sci.Technol.* 2009; 69: 839-46
- [35] Giori C, Yamauchi T. Effects of ultraviolet and electron radiations on graphite-reinforced polysulfone and epoxy resins. *J. Appl. Polym. Sci.* 1984; 29: 237-49
- [36] Woo R. S C, Zhu H, Leung Ch K Y, Kim J K. Environmental degradation of epoxy-organoclay nanocomposites due to UV exposure: Part II residual mechanical properties. *Compos. Sci. Technol.* 2008; 68: 2149-55

- [37] Schutte C L. Environmental durability of glass-fiber composites. *Mater Sci Eng.* 1994; 13: 265-323
- [38] Alawsi G, Aldajah S, Rahmaan S A. Impact of humidity on the durability of E-glass/polymer composites. *Mater and Design.* 2009; 30: 2506-12
- [39] Ellyin F, Rohrbacher C. Effect of Aqueous Environment and Temperature on Glass-Fibre Epoxy Resin Composites. *J. Reinf. Plast. Compos.* 2000; 19: 1405-27
- [40] Perreux D, Suri C. A study of the coupling between the phenomena of water absorption and damage in glass/epoxy composite pipes. *Compos. Sci. Technol.* 1997; 57:1403-13
- [41] Sala G. Composite degradation due to fluid absorption. *Compos. Part B.* 2000; 31(5): 357-73
- [42] Boukhoulda B F, Adda-Bedia E, Madani K. The effect of fiber orientation angle in composite materials on moisture absorption and material degradation after hygrothermal ageing. *Compos. Struct.* 2006; 74:406-18
- [43] Gautier L, Mortaigne B, Bellenger V. Interface Damage Study of Hydrothermally Aged Glass-Fiber Reinforced Polyester Composites. *Compos. Sci. Technol.* 1999; 59: 2329-37
- [44] Neumann S.H, Marom G. Free-volume dependent moisture diffusion under stress in composite materials. *J. Mater. Sci.* 1986; 21: 26-30
- [45] Pauchard V, Grosjean F, Campion-Boulharts H, Chateauminois A. Application of a stress-corrosion-cracking model to an analysis of the durability of glass/epoxy composites in wet environments. *Compos. Sci. Technol.* 2002; 62: 493-98
- [46] Fahmy A A, Hurt J C. Stress dependence of water diffusion in epoxy resin. *Polym. Compos.*, 1980; 1: 77-80
- [47] Whitaker G, Darby M I, Wostenholm G H, Yates B, Collins M H, Lyle A R, Brown B. Influence of temperature and hydrostatic pressure on moisture absorption in polymer resins. *J. Mater. Sci.* 1991; 26: 49-55

- [48] Wan Y Z, Wang Y L, Huang Y, He B M, Han K Y. Hygrothermal aging behaviour of VARTMed three-dimensional braided carbon-epoxy composites under external stresses. *Compos. A.* 2005; 36: 1102-09
- [49] Neumann S, Marom G. Prediction of Moisture Diffusion Parameters in Composite Materials Under Stress. *J. Compos. Mater.* 1987; 21: 68-80
- [50] Neumann S, Marom G. Stress dependence of the coefficient of moisture diffusion in composite materials. *Polym. Compos.* 1985; 6: 9-12
- [51] Diffusion and Osmosis, Retrieved on 30/12/2010 from:
<<http://finleysciencep8.blogspot.com/2010/12/december-21-diffusion-and-osmosis.html>>
- [52] Surathi P, Karbhari V M. Hygrothermal Effects on Durability and moisture Kinetics of Fiber-Reinforced Polymer Composites, Technical Report No. SSRP06/15, University of California, Oakland. 2006
- [53] Rao R, Chanda M, Balasubramanian M. Factors Affecting Moisture Absorption in Polymer Composites, Part II: Influence of External Factors. *J. Reinf. Plast. Compos.* 1984; 3: 246-53
- [54] Shen C H, Springer G S. Moisture Absorption and Desorption of Composite Materials. *J. Compos. Mater.* 1976; 10: 2-20
- [55] Adams R D, Singh M M. The dynamic properties of fibre-reinforced polymers exposed to hot, wet conditions. *Compos. Sci. Technol.* 1996; 56: 977-97
- [56] Ellyin F, Maser R. Environmental effects on the mechanical properties of glass-fiber epoxy composite tubular specimens. *Compos. Sci. and Technol.* 2004; 64: 1863-74
- [57] Carter H G, Kibler K. Langmuir-Type Model for Anomalous Moisture Diffusion in Composite Resins. *J. Compos. Mater.* 1978; 12: 118-31
- [58] Bindslev N. Drug-acceptor Interactions, Retrieved on 20/8/2009 from:
<<http://journals.sfu.ca/coactionbks/index.php/Bindslev/article/view/3/16>>
- [59] Suri C, Perreux D. The effects of mechanical damage in a glass fibre epoxy composite on the absorption rate. *Compos. Eng.* 1995; 5: 415-24

- [60] Lewis G, Bedder S W. Stress corrosion of glass fibers in acidic environments. *J. Mater. Sci. Lett.* 1984; 3: 728-32
- [61] Qiu Q, Kumosa M. Corrosion of E-glass fibers in acidic environments. *Compos. Sci. Tech.* 1997; 57: 497-507
- [62] Bledzki A, Spaude R, Ehrenstein G W. Corrosion phenomenon in glass fibers and glass fiber reinforced thermosetting resins. *Compos. Sci. Technol.* 1985; 23: 263-85
- [63] Renaud C M, Greenwood M E. Effect of Glass Fibres and Environments on Long-Term Durability of GFRP Composites. Retrieved on 1/9/2011 from:
http://www.efuc.org/downloads/CLR_MEG_Paper_on_Advantex_E-CR_Glass.pdf
- [64] Eslami S, Taheri F. Effects of perforation size on the response of perforated GFRP composites aged in acidic media. *Corros. Sci.* 2013; 69: 262-269

CHAPTER 3 EFFECTS OF AGING TEMPERATURE ON MOISTURE ABSORPTION OF PERFORATED GFRP*

Shiva Eslami, Fathollah Taheri-Behrooz and Farid Taheri

Department of Civil and Resource Engineering, Dalhousie University

3.1 ABSTRACT

This paper examines the effects of aging on the flexural stiffness and bending loading capacity of a perforation glass fiber-reinforced epoxy composite subjected to combined moisture and elevated temperature. Specimens, in the configuration of one quarter of a perforated GFRP tube, were aged in 60% humidity and temperatures of 40, 60 and 80°C, respectively. Moisture absorptions of the specimens were measured during the aging process, and bending tests were conducted on the specimens after aging. SEM images were also captured to further examine the effects of the moisture absorption on the aged specimens.

The results indicated that the increase in the aging temperature reduced the diffusion coefficient, thus inducing more moisture absorption by the composite, and in turn causing more reduction in the composite's flexural stiffness and bending capacity.

Moreover, the application of Fick's equation for predicting the moisture absorption rate in such perforated thin-walled composite configuration at various moisture contents and temperatures was also assessed. A semi-empirical equation was developed and proposed by which the reduction of the stiffness in the perforated aged GFRP structures could be predicted.

Keywords: Humidity effect; thermal effect; perforated; moisture absorption; Fickian model; experimental; Diffusion rate.

* Accepted for publication in the Journal of Advances in Materials Science and Engineering Volume 2012, Article ID 303014, 7 pages

3.2 INTRODUCTION

Directional wells are one of the most effective and reliable technologies used nowadays in the oil and gas industry. Hundreds of directional wells have been installed all over the world to increase access to reservoirs, and consequently to increase the productivity and total recovery. From a cost perspective, a horizontal well can be more expensive to drill and complete for production in comparison to a vertical well. Therefore, the oil industry requires assurance that a horizontal well would be the most effective and economical option for a given reservoir. One of the challenges that has often arisen in this field is when one has to replace the so-called “liner” in such wells, usually located often miles under the ground. Liners are conventionally made of perforated steel tubes used to stabilize the directional and vertical wells to access the target producing areas. Annually, hundreds of millions of dollars are spent in replacing the damaged and corroded steel liners in such wells. The concept of replacing steel liners with perforated composite materials such as glass fiber reinforced plastic (GFRP), has been a novel idea that is postulated to be an effective means for replacing aged steel liners.

In general, fiber Reinforced Polymer materials offer better properties in some aspects in comparison to other materials, including superior corrosion resistance, high strength and stiffness to weight ratio, and the ability to be tailored to various configurations. Effective design of components with such materials requires a thorough knowledge of the capabilities and limitations of the constituent materials. Lack of understanding of the behavior of composites under various conditions has indeed impeded wider development of their applications. Despite the fact that various aspects of the mechanical responses of GFRP have been widely studied, , appropriate investigations should be conducted when such materials are to be used in a well environment. An important aspect that would require in-depth evaluation in such circumstances would be the influence of the environmental loading conditions (temperature, humidity, etc) on the structural performance of such composite liners, in order to ensure their long term reliability, since such liners would be in contact with various chemicals during the service life of the oil wells.

It is well known that moisture absorption changes the thermo-physical and mechanical properties of fiber-reinforced plastics (FRP)[1, 2]. Moisture can cause plasticization and hydrolysis of a polymeric matrix, reducing its glass-transition temperature and affecting the fiber–matrix interface bond, leading to loss of mechanical integrity; this degradation would become more adverse at elevated temperatures [3-6].

In FRP, the fiber–matrix interface is the medium for transferring the applied loads from one fiber to another, and hence, it plays an important role in controlling the strength of composites. Previous investigations [7-9] have shown that humidity diffusion through the matrix is accomplished inherently slowly; nonetheless, moisture would diffuse along the fiber/matrix interface more easily and in turn would degrade the interface-bond.

Moreover, the inconsistent swelling of the matrix, as a result of moisture absorption, would create undesirable stress concentration regions. Also, in the case of glass fibers, moisture could also cause degradation at the fiber level. In glass fibers, moisture extracts ions from the fiber, causing changes in its structure, leading to further degradation [10]. In addition, the fiber cross section shape has been found to affect the moisture diffusion rate [11]; for instance, fibers with regular cross-section (like glass fibers) provide more diffusivity in comparison to fibers with arbitrary cross-section (such as most carbon fibers). It has also been commented that glass fibers possess a more permeable nature when subjected to moisture in comparison to carbon fibers [11]. There are also other notable studies investigating the aging effects on woven fiber-reinforced composites [12-14]. For example, Nakai et al [14] studied the degradation of braided glass/epoxy plates in hot water and reported that increasing the exposure time of humidity and temperature would adversely impact the fiber/matrix interface property, first causing degradation at the interface around fiber bundles, but then subsequently, after a long exposure time, the degradation further penetrates inside the fiber bundles.

As stated, several investigations have been conducted examining the effects of moisture and temperature on the mechanical properties of glass/epoxy coupon specimens; however, only a few studies have been documented in consideration of the effects of environmental elements on tubular braided structures. In such cases, although the material may be the same, due to the manufacturing process, the geometry and the

diffusion surface areas would be different [15]. For instance, in comparing the case of a rectangular coupon specimen with a cylindrically shaped specimen, one realizes that moisture diffuses into the specimen through two surfaces and four edges in the rectangular configuration, while in a tube moisture can penetrate through four areas (two surfaces and two edges). Moreover, in general, humidity penetrates quicker into the specimens through the edges, and then moisture will travel along the fibers. It can be therefore appreciated that the diffusion rate would be greater in a rectangular shape specimen in comparison to a tubular configuration. Moreover, when a tube is perforated, then the edge surface areas associated to the perforations would be larger, thus facilitating a higher diffusion rate.

The above observation prompted this study; in order to better understand the diffusion characteristics in perforated configurations, one quarter of a perforated tube will be examined in the present work.

3.3 THEORETICAL BACKGROUND

Although it has been shown that the absorption behavior of some polymeric acid is non-Fickian [16], nonetheless, in general, to estimate the amount of moisture intake in a composite whose matrix is epoxy, one can use Fick's model. Fick's model was originally developed for determining the amount of moisture absorption in materials (for an infinitely large plate of thickness, h), at a given time, t , the solution has been given as [17]:

$$\frac{M_{\%}}{M_m} = 1 - \frac{8}{\pi^2} \sum_{n=0}^{\infty} \frac{1}{(2n+1)^2} \exp \left[-D_c (2n+1)^2 \frac{\pi^2 t}{h^2} \right] \quad (3.1-a)$$

where after some manipulation, the above can be represented in the following form:

$$\frac{M_{\%}}{M_{\infty}} \approx 1 - \exp \left[-7.3 \left(\frac{Dt}{h^2} \right)^{0.75} \right] \quad (3.1-b)$$

where $M_{\%}$ is the percent moisture absorbed at the time t , M_{∞} is the percent moisture absorbed at saturation, h is the specimen thickness and D is the diffusion coefficient of moisture into the specimen.

It should be noted that admissibility of the use of the above equation for estimating moisture absorption in tubular FRP specimens has been examined and confirmed by several researchers [see, e.g., references 15 and 18].

By plotting the graph of moisture content versus time, one can calculate the magnitude of D through the slope of the linear portion of the curve; mathematically, it can be calculated by [15]:

$$D = \pi \left(\frac{h}{4M_\infty} \right)^2 \left(\frac{M_2 - M_1}{\sqrt{t_2} - \sqrt{t_1}} \right)^2 \quad (3.2)$$

where t_2 and t_1 are arbitrary times selected along the linear portion of the curve, and M_1 and M_2 are the corresponding amount of absorbed moistures, respectively.

Moreover, d'Almeida et al. [18] reported that the following equation would better fit the experimental data when fiberglass pipes were tested:

$$\frac{M_{\%}}{M_\infty} = \tanh \left(\frac{4}{h} \sqrt{\frac{Dt}{\pi}} \right) \quad (3.3)$$

It has been shown [18 and 19], that moisture induced degradation of the fiber/matrix interface could significantly reduce the stiffness of the FRP pipes under bending, shear and compression loading conditions, while the tensile strength would not be as significantly affected. This is because debonded fiber/matrix interfaces act mainly as inter-laminar cracks, and therefore, would induce less impact on the strength of the pipes, especially under tensile loading.

In this research, bending tests were conducted on perforated glass/epoxy specimens having a quarter tube configuration and through the experimental data, a model was developed by which the stiffness of the perforated GFRP structures could be predicted.

3.4 SPECIMEN PREPARATION

The material used in this research was 7781 woven E-glass/ NB321 epoxy cross-ply prepreg produced by Newport (Irvin, CA). The tensile modulus and strength of the composite were determined experimentally in-house as $E_{\text{tensile}}=24.75$ GPa, $S_{\text{tensile}}= 370.5$ MPa, respectively. The GFRP composite was selected due to its widespread usage in the

applications where corrosion is of primary concern, as well as its relatively lower cost. Experimental specimens were fabricated in the configuration of one quarter of a perforated tube to study the influence of the hygrothermal effect on the composite, under applied loading.

In order to fabricate the one quarter tube with perforation, prepreg materials were first cut into 30 mm wide tapes (with a 3 mm thickness), and then they were laid on a steel mandrel in $\pm 45^\circ$ orientation, leaving 2 mm space among the tapes to create the perforated region. Figure 3.1 shows the representative volume's schematic, used to form the geometry and the manufactured specimen, respectively. The final geometry was a quarter of a 250 mm long tube with a 150 mm diameter having $2 \times 2 \text{ mm}^2$ perforations.

The layup sequence of all specimens was $[\pm 45^\circ]_4$, and the curing process was carried out according to the vendor's instruction; that is, curing at 135°C for 2 hrs, and subsequently cooled down to the room temperature. The specimens were then trimmed and prepared for the experiment. The specimens' thickness was in the range of 2.7–3.2 mm. The initial weight of each specimen was recorded for the subsequent moisture absorption studies. The fiber content of each specimen was also determined according to ASTM D3171-09 [20]; the average fiber content was at 55% by weight.

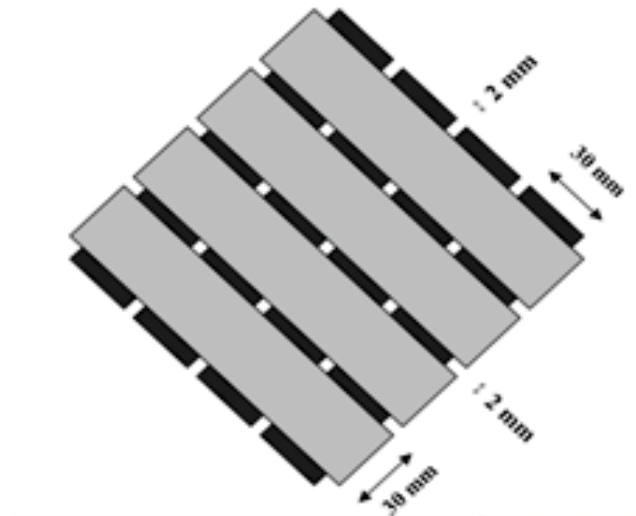


Figure 3.1 Representative volume used to fabricate the specimens

3.5 TESTING PROCEDURE

The aging scenario adopted in this study is summarized in Table 3.1. Specimens were put in a controlled environmental chamber and aged at 60% humidity at temperatures of 40, 60, 80 °C (3 specimens tested at each temperature). The temperatures were chosen such that they were below the glass transition temperature of the resin (which was 150°C). The saturation times for the specimens at various temperatures are also noted in Table 3.1. During the aging process, the moisture absorption percentile and its rate were measured in accordance to ASTM D5229 standard [21]. In our experiment, the saturation point was established as the stage when the change in the measured moisture content of the material at the selected interval was less than 0.01% with respect to the previously recorded moisture content. After reaching to the saturated conditions, the specimens were removed and the bending tests were conducted on the aged specimens and the reference virgin specimens, which were not exposed to temperature and humidity.

Table 3.1 The aging scenarios

Environment	Aging temperature (°C)	Number of specimens	Saturation time (Days)
All specimens at 60% Moisture content	40	3	55
	60	3	38
	80	3	30

The supporting jig (frame) and loading jig, conformed to the exact shape of the specimens, are shown in Figure 3.2. The specimens were supported at their ends, on 9.5 mm diameter bars, and were loaded to failure by a MTS universal testing machine, equipped with an Instron 8500+ electronic controller. The tests were conducted under displacement-controlled condition, with a loading rate of 1.0 mm/min, at room temperature.

Subsequently, the fracture surfaces of the specimens were analyzed with a scanning electron microscope (SEM) to further characterize the influence of the combined moisture/temperature on the materials.

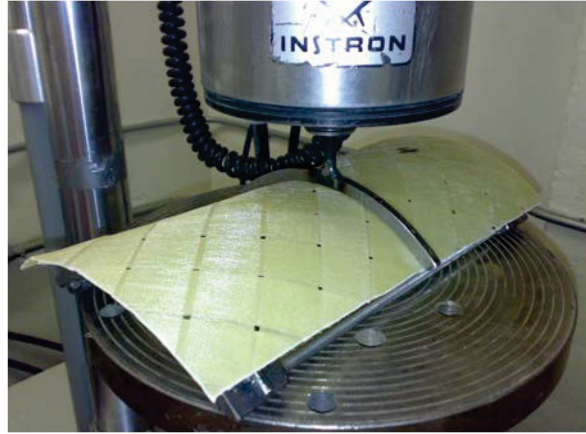


Figure 3.2 Three-point bending test setup

3.6 EXPERIMENTAL RESULTS AND DISCUSSION

3.6.1 MOISTURE ABSORPTION BEHAVIOR

Moisture absorption percentage was calculated using the following equation and is presented as a function of square root of the exposure time:

$$M_t = \frac{m - m_0}{m_0} 100\% \quad (3.4)$$

where M_t is the percent moisture content at time t , m_0 is the weight of the specimen at its dry stage and m is the specimen weight at time t .

Figure 3.3 shows the variation in weight gain (i.e., moisture absorption), as a function of the square root of exposure time for all specimens. In this figure, solid symbols, solid line and dashed line depict the experimental results, the results obtained using the hyperbolic tangent method (i.e., Eq. 3.3) and those obtained by Fick's solution (obtained by Eq. 3.1), respectively. The Fickian model can better describe the moisture absorption response at the lower temperature aging condition, but at the high temperatures, the hyperbolic tangent model (i.e., Eq. 3.3) could provide better prediction. It is postulated that the assumption of equal values for D_x , D_y and D_z used in these models would be a

cause for the observed discrepancy. It is believed that these values would not be equal in the case of a perforated tubular configuration; as a result, their variation as a function of temperature would also be different. Despite this fact, Fick's solution succeeded in predicting the results at the lower temperature, while the hyperbolic tangent model could more accurately predict the absorption behavior at the higher temperatures.

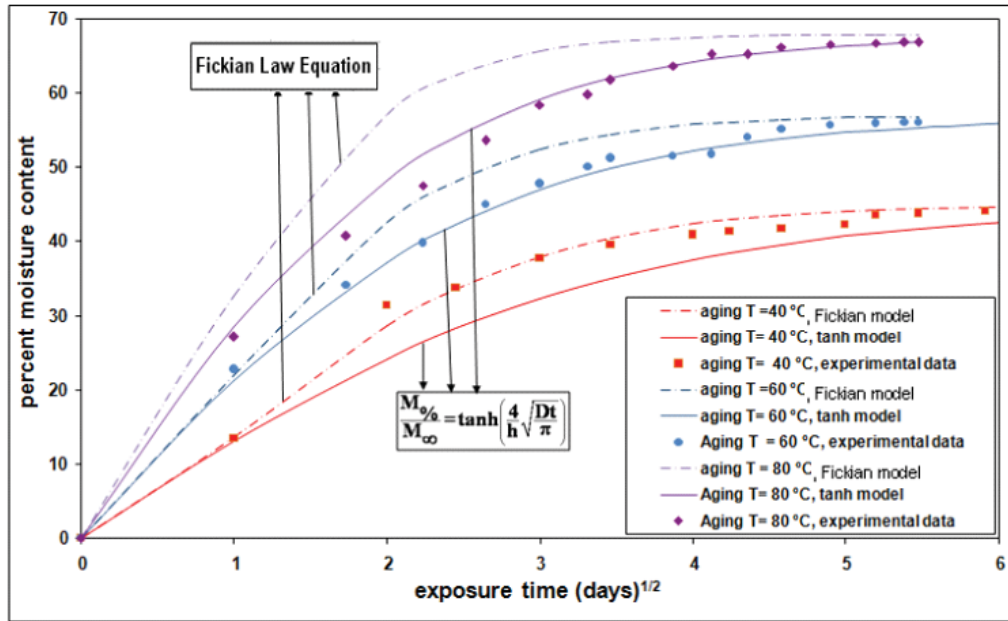


Figure 3.3 Moisture absorption of the specimens aged at 40°C, 60°C and 80°C temperature (humidity = 60%)

Comparison of the variation in the rate of moisture absorption at different aging temperatures (illustrated in Figure 3.4) reveals that when a longitudinal section of a perforated pipe was exposed to humidity, the increase in the exposure temperature from 40°C to 80°C increased the moisture absorption at saturated condition from 45%, to 68%, respectively. Moreover, the diffusion coefficient, D , which represents the slope of the linear portion of the curves of the perforated specimen, increased from 0.16 to 0.35 mm²/day, respectively, when aged at the noted temperatures. d' Almeida et al [18] have reported D as 0.57 mm²/day for their aged pipe specimens and De La Osa et al [22] have reported GFRPs diffusion coefficients for different temperatures: 0.16, 0.47 and 0.97 mm²/day, for temperatures 20, 40 and 60 °C, respectively. Our results can be considered in agreement with the reported experiments.

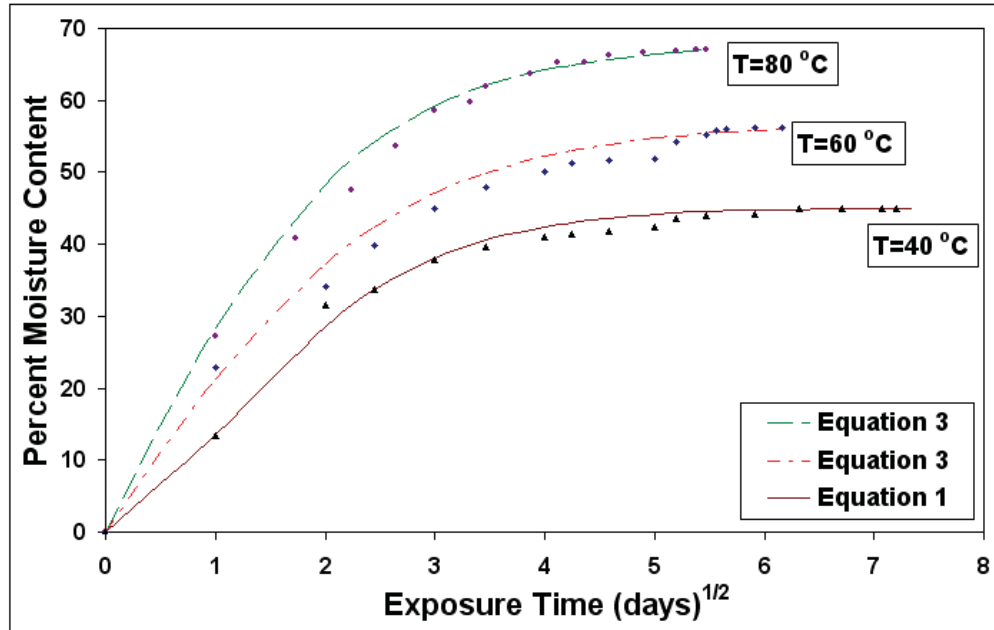


Figure 3.4 Average moisture absorption in different aging condition (humidity = 60%)

(Note: solid lines represent the best fit lines obtained by the noted respective equations)

3.6.2 MECHANICAL CHARACTERIZATION

Three-point bending tests were conducted on the specimens after aging. Figure 3.5 illustrates the typical damage initiation and growth in the specimens, when subjected to the bending test. In all specimens the damage occurred near the load line and the crack propagated along the tape boundary through the perforations.

The bending test results have also been summarized in Table 3.2. It was observed that the increase in the aging temperature decreased the failure load, stiffness and the maximum mid-span displacement of the specimens. As seen in Figure 3.6, the trace of the bending curves for all test specimens was linear up to the fracture point, which reflects the brittle behavior of this composite component. The slope of the load-displacement curves reflects the stiffness of the perforated composite structure under bending. Figure 3.7 shows that with increasing the aging temperature and hence the diffusion rate and the resulting moisture content, the flexural stiffness of this perforated material decreased as much as 8.5%. In the figure, the dot symbols represent the experimental results and the dashed line is the least-square fitted line to the experimental data.

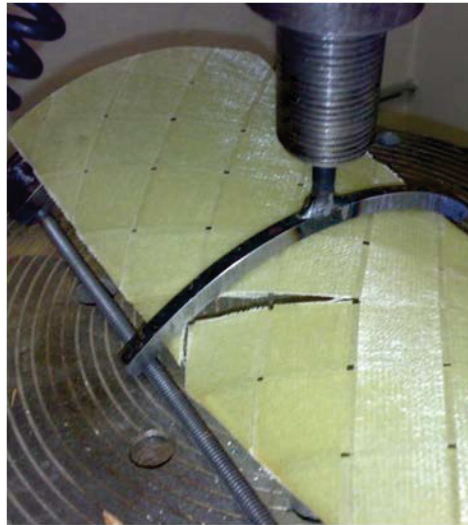


Figure 3.5 Failure mode observed as a result of the bending tests

Table 3. 2 Bending test results for specimens aged at various temperatures (humidity 60%)

Specimen / condition	Failure force (N)*	Max. displacement (mm)	Stiffness, K (N/mm)*	Standard Deviation
R-01 / original	176.05	2.2	82.5	0.104
H 4 / T=40 °C	153.16	1.9	80.3	0.102
H 6 / T=60 °C	139.08	1.8	78.2	0.104
H 8/ T=80 °C	123.24	1.6	76.6	0.106

Note: The reported data are the mean values of 3 results for each category

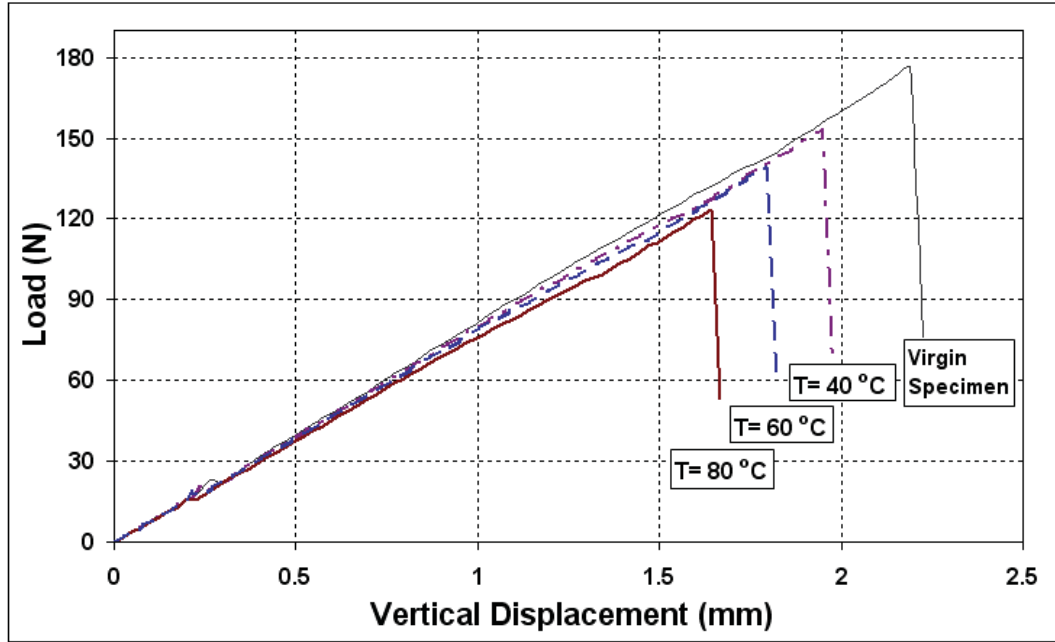


Figure 3.6 Plot of the average load versus displacement (each curve is the average of 3 specimens) for the specimens conditioned at different temperatures at 60% humidity

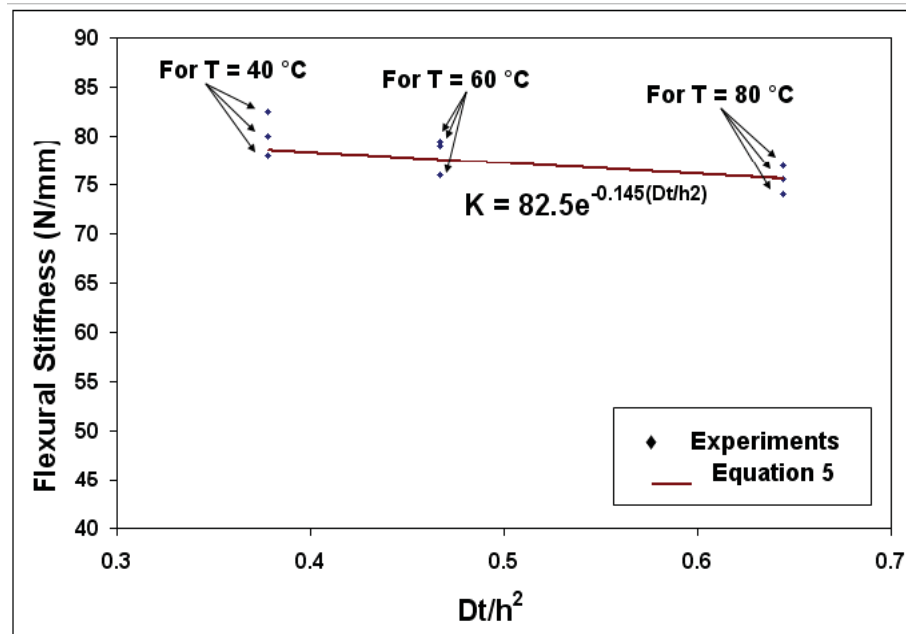


Figure 3.7 Variation of the flexural stiffness as a function of diffusion coefficient and aging temperatures for specimens aged at various temperatures in 60% humidity

Noting the above results, it can be concluded that the flexural stiffness of a perforated pipe could be markedly affected by the diffusion rate and aging temperature. In consideration of the fact that according to Eq. 3.1 the moisture content changes exponentially as a function of the diffusion coefficient, and that the diffusion coefficient changes as a function of the aging temperature (see also Figure 3.4), a simple model is developed and proposed by which the change in the stiffness of a GFRP specimen, aged in humidity at elevated temperature, is related to the influencing variables (that is, the environmental parameters (i.e. the aging temperature and humidity), geometrical factors, and the physical and mechanical properties.) The following represents the semi-empirical exponential function:

$$K_a = K_{ua} \times \exp\left(-0.145 \times \left(\frac{Dt}{h^2}\right)\right) \quad (3.5)$$

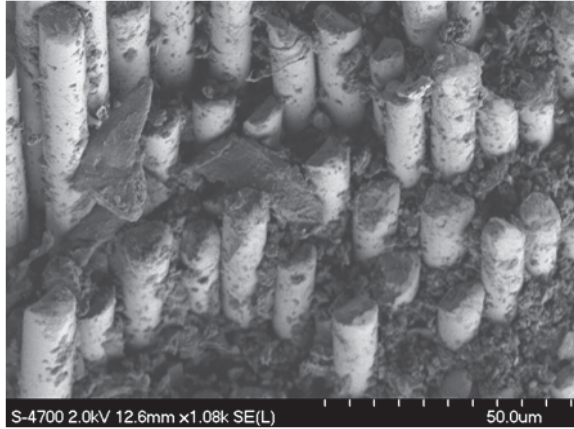
where K_a is the flexural stiffness of the aged structure (in N/mm), K_{ua} is the flexural stiffness of the un-aged material (in N/mm) at time $t = 0$ sec. before the material is exposed to moisture, D is the diffusion coefficient (in mm^2/day) and $\frac{Dt}{h^2}$ is a non dimensional parameter.

3.6.3 SEM ANALYSIS

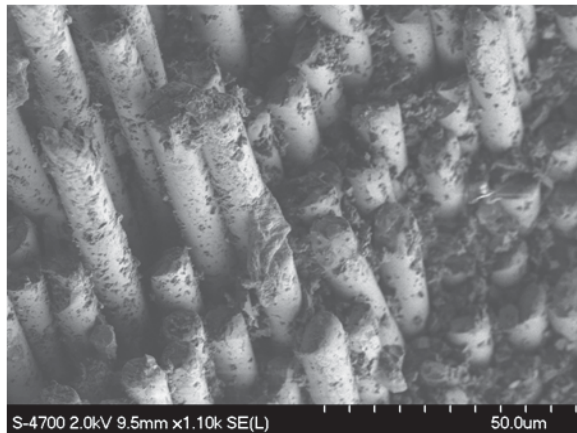
As stated earlier, to gain more insight into the physical effect of the moisture diffusion, scanning electron microscopy (SEM) was conducted on the fracture surfaces. Figure 3.8 shows the fracture surfaces of the glass/epoxy structure before and after the moisture immersion at 40°C and 80°C , at 60% humidity. From the SEM generated images one can observe that in the case of the virgin material (i.e., material that was not exposed to moisture and high temperature), good adhesion of resin to fibers is evident by the presence of large resin clusters; even after the fracture, the least amount of relative debonding is observed between the fibers and matrix (Figure 3.8 (a)). This confirms the existence of a strong bond at the fiber and the matrix interface in the virgin specimens. However, with exposure to humidity and increasing temperature, the interface bond is degraded. This is demonstrated by a decrease in the volume of the resin surrounding the fibers. Comparison of Figures 3.8(a) and 3.8(b), and then Figures 3.8(a) and 3.8(c)

reveals that there is less of a decrease in the resin content in the specimen aged at 40°C, while, the resin degradation is much more pronounced in the specimen aged at 80°C (see Figures. 3.8(b) and 3.8(c)).

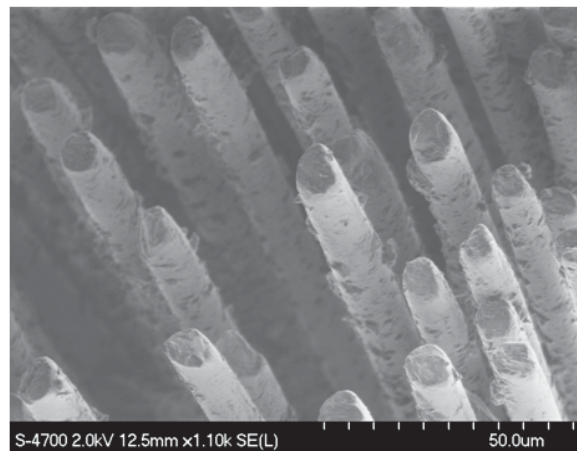
Ingress of moisture into the matrix causes the matrix to swell and the fiber/matrix interface tends to debond. In the presence of elevated temperature, the water molecules ingress into the voids in the matrix, and as the molecule's temperature is increased, their volume increases, thereby creating stress concentration and subsequently cracking the matrix [15]. The microscopic observation of our aged specimens revealed the presence of void content and cracks in the matrix of the specimens subjected to humidity and high temperature (see Figure 3.9).



(a) Virgin



b) at 40°C



(c) at 80°C

Figure 3.8 Comparison of the failure Surfaces of un-aged (virgin) perforated GFRP specimens and aged specimens at various temperatures (at 60% humidity)

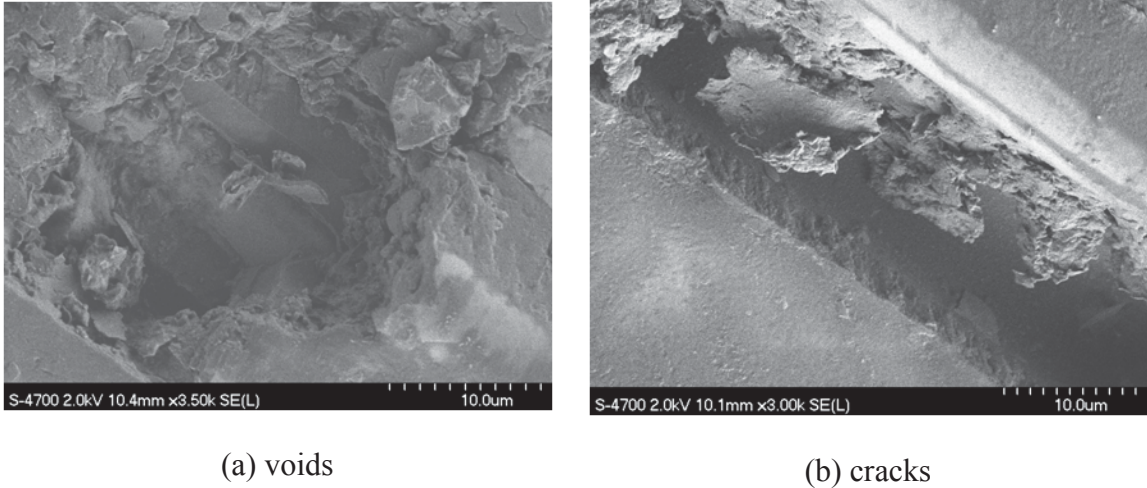


Figure 3.9 SEM image showing typical (a) voids and (b) cracks in the matrix of the perforated GFRP specimen aged in humidity at 80°C

3.7 CONCLUSIONS

A short-term aging experimental investigation was conducted on curved perforated GFRP composite specimens, by which the effect of thermal variation on the moisture absorption kinetics and on the flexural stiffness of the GFRP specimens was investigated. The findings of this study can be summarized as follows:

- Fick's model could describe the moisture absorption rate of the perforated GFRP specimens that were aged at relatively low temperatures, while the hyperbolic tangent model produced better predictions for the specimens conditioned at higher temperatures.
- Moisture causes degradation in the resin matrix and in turn reduces the bending stiffness of the structures made of composite materials. As it is also known that Fick's model assumes that the moisture content varies exponentially as a function of diffusion coefficient, and that the diffusion coefficient also changes as a function of the aging temperature. In concert with Fick's model, a simple semi-empirical model was proposed; by this model one can predict the degradation in GFRP, when exposed to 60% humidity and various elevated temperatures, as a function of diffusion rate of the material and the exposure (conditioning) time.
- Moreover, the increase in the temperature degraded the interface between the fibers and the matrix. The SEM analysis evidenced a dependency of the strength of GFRP to the

reduction in the fiber/resin interfacial strength, through reducing the stress transfer in the GFRP.

An important concluding outcome of the investigation is that when perforated GFRP tubes are used to form liners in horizontal oil well applications, the influence of moisture/temperature must be carefully considered, and the design limits must be adjusted accordingly.

3.8 ACKNOWLEDGEMENTS

The financial support of the Natural Sciences and Engineering Council of Canada (NSERC) in support of this work is gratefully acknowledged. The access to IRM (Institute of Research for Materials) SEM facilities is greatly appreciated.

3.9 REFERENCES

- [1] Schutte C L. Environmental durability of glass-fiber composites. *Mater Sci Eng.* 1994; 13: 265-323
- [2] Alawsi Gh, Aldajah S, Rahmaan S A. Impact of humidity on the durability of E-glass/polymer composites. *Mater and Design.* 2009; 30: 2506-12
- [3] Ellyin F, Rohrbacher C. Effect of Aqueous Environment and Temperature on Glass-Fibre Epoxy Resin Composites. *J. Reinf. Plast. Compos.* 2000; 19: 1405-27
- [4] Perreux D, Suri C. A study of the coupling between the phenomena of water absorption and damage in glass/epoxy composite pipes. *Compos. Sci. Technol.* 1997; 57:1403-13
- [5] Sala G. Composite degradation due to fluid absorption. *Compos. Part B.* 2000; 31(5): 357-73
- [6] Boukhoulida B F, Adda-Bedia E, Madani K. The effect of fiber orientation angle in composite materials on moisture absorption and material degradation after hygrothermal ageing. *Compos. Struct.* 2006; 74:406-18
- [7] Bao L R, Yee L F. Moisture diffusion and hygrothermal aging in bismaleimide matrix carbon fiber composites: part II—woven and hybrid composites. *Compos. Sci. Technol.* 2002; 62: 2111-19

- [8] Assarar M, Scida D, El Mahi A, Poilane C, Ayad R. Influence of water aging on mechanical properties and damage events of two reinforced composite materials: flax fibres and glass fibres. *Mater Design*. 2011; 32: 788-795
- [9] Huang G, Sun H. Effect of water absorption on the mechanical properties of glass/polyester composites. *Mater Design*. 2007; 28 : 1647-50
- [10] Maxwell AS, Broughton WR, Dean G, Sims GD. Review of accelerated aging methods and lifetime prediction techniques for polymeric materials. NLP Report: DEPC MPR 016. 2005
- [11] Aditya P K, Sinha P K. Moisture diffusion in variously shaped fibre reinforced composites. *Comput. Struct*. 1996; 59: 157-66
- [12] Imielinska K, Guillaumat L. The effect of water immersion ageing on low-velocity impact behaviour of woven aramid–glass fibre/epoxy composites. *Compos. Sci. Technol*. 2004; 64: 2271-8
- [13] Scida D, Abourab Z, Benzeggagh M L. The effect of ageing on the damage events in woven-fibre composite materials under different loading conditions. *Compos. Sci. and Technol*. 2002; 62: 551-7
- [14] Nakai A, Ikegaki S, Hamada H, Takeda N. Degradation of Braided composites in hot water. *Compos. Sci. Technol*. 2000; 60: 325-31
- [15] Ellyin F, Maser R. Environmental effects on the mechanical properties of glass-fiber epoxy composite tubular specimens. *Compos. Sci. Technol*. 2004; 64: 1863-74
- [16] Berketis K, Tzetzis D, Hogg PJ. The influence of long term water immersion aging on impact damage behaviour and residual compression strength of glass fibre reinforced polymer (GFRP). *Mater Design*. 2008; 29: 1300-10
- [17] Springer GS. *Environmental Effects on Composite Materials*. vol. 3, Chapter 1 Lancaster, PA: Technomic Pub. Co. 1981
- [18] d’Almeida J R M, de Almeida R C, de Lima W R. Effect of water absorption of the mechanical behavior of fiberglass pipes used for offshore service waters. *Compos. Struct*. 2008; 83: 221-5

- [19] Akay M, Kong A, Mun S, Stanley A. Influence of moisture on the thermal and mechanical properties of autoclaved and oven-cured Kevlar-49/epoxy laminates. *Compos. Sci. Technol.* 1997; 57: 565-71
- [20] ASTM D3171-09. Standard Test Methods for Constituent Content of Composite Materials.
- [21] ASTM D5229. Standard Test Method for Moisture Absorption Properties and Equilibrium Conditioning of Polymer Matrix Composite Materials.
- [22] De La Osa O, Alvarezand V, Va' Zquez A. Effect of Hygrothermal History on Water and Mechanical Properties of Glass/Vinylester Composites. *J. Compos Mater.* 2006; 40(22): 2009-23

CHAPTER 4 LONG TERM HYGROTHERMAL RESPONSE OF PERFORATED GFRP PLATES, WITH/WITHOUT APPLICATION OF CONSTANT EXTERNAL LOADING*

Shiva Eslami, Fathollah Taheri-Behrooz and Farid Taheri

Department of Civil and Resource Engineering, Dalhousie University

4.1 ABSTRACT

The use of glass fiber-reinforced polymer composites (GFRP) is increasingly being considered in various applications where the composite is subjected to harsh hot and humid conditions. Although information on the performance of GFRP under hot and humid conditions is available, the characteristics and the response of perforated GFRP under such conditions have not been fully explored.

In this paper, the response of perforated GFRP plates subjected to hot and humid environment is examined. The applicability and accuracy of Fick's model for establishing the amount of moisture absorption by such composites is examined, and an improved model is proposed. The paper also demonstrates the influence of constant external loading on such perforated GFRP while undergoing conditioning in a hot and humid environment.

Moreover, since the strength and stiffness of composites can be significantly affected by harsh environments, the degradation in the strength and stiffness of the perforated GFRP as a function of time is established. A new model is proposed wherein degradation of the strength of such perforated composites may be established as a function of time and geometric entities. The model can also account for the influence of the applied loading.

Keywords: GFRP, perforated, moisture absorption, stress corrosion, hot and humid condition, Fick's solution, experimental.

* Accepted for publication in the Journal of Polymer Composites
Volume 33, Issue 4, pages 467–475, April 2012

4.2 INTRODUCTION

Perforated steel tubes, also referred to as “liners”, are conventionally installed in the oil directional wells in order to generate larger surface contact area in oil reservoirs, thus increasing output. Having been subjected to harsh environments and corrosion, such structures have to be replaced at certain intervals, thus increasing overall production costs. The use of perforated glass fiber reinforced plastic (GFRP) liners — as a novel idea to replace the damaged steel ones, specifically in open-hole horizontal wells — has been considered by our research group. While the problems of the formation of such a liner and its cost-effective manufacturing have been resolved, its durability has to be effectively established. For that, systematic experimental investigations are under way for evaluating the long term durability of such perforated GFRPs in various environmental conditions (i.e., moisture, high temperature and acidic media). Moreover, even after the long-term response the material to environmental loadings is established, one should also investigate the impact of sustained constant loading in addition to the harsh environmental loadings, known as “stress corrosion.”

In general, mechanical properties of composites are compromised when exposed to various long duration environmental loadings [1-3]. A hygrothermal environments, defined as an environment with combined moisture and temperature, could degrade the polymeric matrix and result in overall softening of the composite [3-7]. This is a consequence mainly of moisture diffusion arising from long-term exposure, accelerated further due to an elevated temperature [8]. Moreover, such combined environmental loadings may exert dimensional changes, subsequently inducing stress concentration in the structure. This usually occurs in a direction that is transverse to the fiber’s orientation, tending to swell the matrix and affects the matrix/fiber interface adversely. In glass fiber polymer composites, moisture may also be active in extracting ions from the fiber and degrade the fiber’s surface [9].

Moreover, several related interesting investigations have also considered the response of composites subject to a constant externally applied load within a hygrothermal environment [10-16]. It has been shown that due to the free volume fraction change, the moisture absorption of composites could be greatly affected and increased when

subjected to externally applied stresses. Neumann and Marom [10] showed experimentally that when the angle between fibers and loading direction (θ) was reasonably large, the maximum absorbed moisture would be enhanced with increasing magnitude of the applied tensile stress; however, at very small θ -angles (close to zero), their experimental results showed the opposite trend. This phenomenon was postulated to be due to the relatively large stresses induced by the residual swelling in the composite in the case of $\theta = 0^\circ$. Pauhard et al. [11] developed an equation for estimating the stiffness loss due to stress-corrosion-cracking (SCC) in GFRP by combining the Weibull statistical distribution of the fiber strengths with a classical “power law“-type expression defining the sub-critical crack growth rate. Accordingly, the relative stiffness loss could be calculated by:

$$\frac{S(t)}{S_0} \approx \exp[-K^* t^{nm/n-2} \sigma_{max}^{nm/n-2} \lambda^{nm/n-2}] \quad (4.1)$$

where S is the stiffness at time t , S_0 is the initial stiffness, K^* is a constant value, m is the Weibull modulus, which characterizes the statistical distribution of the surface defects, n is the power-law exponent, which characterizes the sub-critical crack growth rates of these defects within a given physico-chemical environment, σ_{max} is the applied stress and λ is a numerical value that may be taken as 1 when there is no deviation in the applied strain.

Fahmy and Hurt [12] used the concept of free volume in polymers and explained the effect of stress on the diffusion of water into epoxy. They stated that the diffusion coefficient in the stressed polymer, D_σ , would be a function of free volume fraction according to the following relation [16]:

$$\ln\left(\frac{D_\sigma}{D_0}\right) = b \left[\frac{1}{v_{f0}} - \frac{1}{v_{f\sigma}} \right] \quad (4.2)$$

where D_0 is the diffusion coefficient in the unstressed state, v_{f0} and $v_{f\sigma}$ are the free volume fraction in the unstressed and stressed states, respectively, and b is the outer radius of spherical molecules of the matrix.

After some manipulations, they finalized the relation between the diffusion coefficient and stress in the following form [12]:

$$D_{\sigma} = D_0 \left(1 + A \frac{\sigma}{G} \right) \quad (4.3)$$

where σ , G and A are applied stress, shear modulus and a constant, respectively. In consideration of a polymeric composite, Eq. 4.2 can be written as [15]:

$$\ln \left(\frac{D_{\sigma}}{D_0} \right) = \frac{b}{\Phi_m} \left[\frac{l}{\nu_{f0}} - \frac{l}{\nu_{f\sigma}} \right] \quad (4.4)$$

where Φ_m is the volume fraction of matrix.

It has also been shown [12-14] that the diffusion coefficient and moisture uptake would increase under a tensile stress and decrease under a compressive stress (though to a lesser extent in the latter case). However, under bending, D would increase, thus increasing the gain in moisture. This phenomenon has been attributed to the fact that the increased intensity in the moisture absorption process caused by the tensile stress would be much greater than the resistance to moisture absorption due to the compressive stress.

As stated above, several investigations have been conducted for examining the effects of aqueous environments on the mechanical properties of laboratory scale GFRP specimens; however, no studies have been documented that take the effect of perforation on the resulting infusion in an aqueous environment into consideration. In general, humidity (moisture) penetrates more quickly into the specimens through the edge surfaces, and then traveling along the fibers. Comparing a perforated coupon specimen with a non-perforated coupon specimen, one could appreciate that the diffusion rate would be greater in a perforated specimen due to the larger edge surface areas associated with the perforations.

In an attempt to quantify the influence of perforation on moisture absorption and the resulting impact on the mechanical properties of GFRP composite, 3-point bending tests were conducted on non-perforated and perforated specimens, first in their virgin state (i.e., not exposed to moisture and heat), as well after conditioning the specimens (see Figure 4.1). The study includes an examination of the influence of perforation diameter

and moisture absorption on the flexural stiffness, the strength of such perforated structural component after aging, as well as the influence of stress corrosion conditions at elevated temperatures. Moreover, a semi-empirical model was developed for predicting the strength degradation in perforated GFRP composites as a result of stress corrosion and aging time.

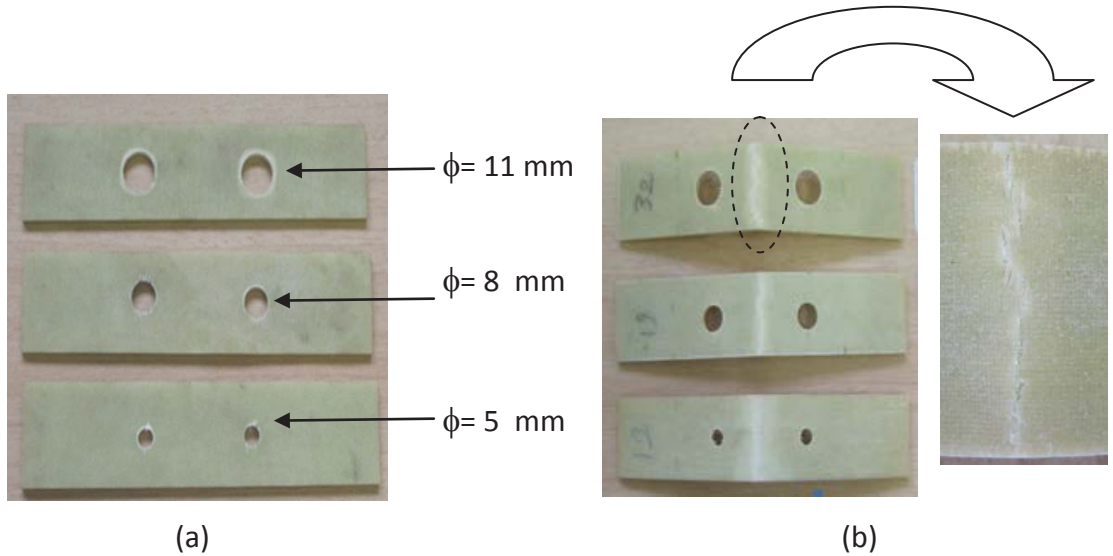


Figure 4.1 Typical perforated specimens (a) prior to, and (b) after mechanical test

The investigation also examined the ability of Fick's model for predicting the level of water absorption into the material as a result of perforation diameter, when the composite was subjected to moisture content at various temperatures.

Scanning electron microscopy was used to examine the matrix/fiber interface degradation caused by moisture absorption in the specimens.

4.3 THEORETICAL BACKGROUND ON MOISTURE ABSORPTION

Moisture absorption by an infinitely large polymer composite plate may be quantified by using Fick's solution, described by the following mathematical equation [17]:

$$\frac{M_{\%}}{M_{\infty}} = 1 - \frac{8}{\pi^2} \sum_{n=0}^{\infty} \frac{1}{(2n+1)^2} \exp\left[-D(2n+1)^2 \pi^2 t / h^2\right] \quad (4.5-a)$$

where $M_{\%}$ and M_{∞} are the amount of moisture absorbed at time t and at the equilibrium state, respectively; D is the diffusion coefficient and h is the

specimen thickness.

The Eq. 4.5-a can be represented in an approximate form as:

$$\frac{M_{\%}}{M_{\infty}} \approx 1 - \exp \left[-7.3 \left(\frac{Dt}{h^2} \right)^{0.75} \right] \quad (4.5-b)$$

The diffusion coefficient D is obtained from the following equation [17-19]:

$$D = \pi \left(\frac{h}{4M_{\infty}} \right)^2 \left(\frac{M_2 - M_1}{\sqrt{t_2} - \sqrt{t_1}} \right)^2 \quad (4.6)$$

where $\left(\frac{M_2 - M_1}{\sqrt{t_2} - \sqrt{t_1}} \right)$ represents the slope of the initial linear part of the absorbed moisture-time curve.

It should be noted that several examples have shown that moisture absorption in composites cannot be accurately predicted using Fick's model, and that the diffusion process in a polymeric matrix composite is totally non-Fickian [5-7]. Carter and Kibler [20] claimed that the time needed for interactions between water and matrix molecules would be longer in comparison to the time required for the migration of water within the matrix; as a result, they proposed a Langmuir-type model. In their model, they assumed that there are two types of absorbed water molecules: (i) mobile molecules and (ii) bound molecules. They further explained that the level of final absorbed moisture would depend on the previous saturation level history. Carter and Kibler [20] suggested the following equation for determining the moisture content after time t in specimens that have very low initial moisture content and that are subject to a relatively short exposure time [20]:

$$M_t = \frac{4}{\pi^{3/2}} \left[\frac{\beta}{\beta + \gamma} M_{\infty} \right] \sqrt{kt} \quad (4.7)$$

In the above equation, β and γ are the probabilities of molecule bonding and molecule mobility per unit time, respectively, and k is calculated from the following equation:

$$k = \frac{\pi^2 D}{h^2} \quad (4.8)$$

When the exposure time is relatively long, the following approximation can be used for determining the moisture content [20]:

$$M_t = M_\infty \left[1 - \frac{\gamma}{\beta + \gamma} \exp(-\beta t) \right] \quad (4.9-a)$$

$$-\left[\frac{dM_t}{dt} \right]^{-1} \left[\frac{d^2 M_t}{dt^2} \right] \approx \text{constant} = \beta \quad (4.9-b)$$

from which the value of β is evaluated, and substituted in the next equation to obtain the value of γ :

$$\exp(-\beta t) \left[\beta \left\langle \frac{dM_t}{dt} \right\rangle^{-1} M_t + 1 \right] \approx \text{constant} = 1 + \frac{\beta}{\gamma} \quad (4.10)$$

Finally, knowing the values of β and γ , one can use equation 4.9-a to evaluate the moisture absorption [20].

The integrity of the above model has been verified against experimental data by a few researchers [21, 22]. Further verification of the model is presented in the current paper.

It has to be mentioned that the above equations have been proposed for infinite plates, in which the diffusion is assumed to occur mainly through the surfaces. However, in finite-sized plates, through-the-edge diffusion would contribute significantly toward the overall absorption. Shen and Springer [17] suggested the following coefficient for modification of the diffusion coefficient.

$$D_{F.S} = D \left(1 + \frac{h}{l} + \frac{h}{w} \right)^{-2} \quad (4.11)$$

where $D_{F.S}$ is the modified diffusion coefficient for finite size specimens, l is the length and w is the specimen's width.

It may be appreciated that such a modification would also be necessary when considering components with perforations. In order to take into account the effect of perforation on moisture absorption of our perforated GFRP specimens, the geometrical coefficient of the

Langmuir model has been modified. The integrity of the modified model is examined by comparing the theoretical results with our experimental results.

4.4 EXPERIMENTAL INVESTIGATION

4.4.1 SPECIMEN PREPARATION

Cross-ply glass-fiber epoxy prepreg, supplied by Newport Adhesives and Composites Inc. (Irvine, CA) was used to form our laminates, with $[0/90]_{7,s}$ layup sequence. The laminates were cured in an oven at the 135 °C for 2 hrs and cooled down to room temperature in the oven, as per the manufacturer's instructions. Following the ASTM D3171-09 [23] procedure, the average fiber content of the laminates was determined to be 55% by weight.

Rectangular specimens were extracted from the plates using a professional water jet system. The specimens were prepared according to the ASTM D790 [24] with standard geometry suitable for a test method used for establishing the flexural properties. The specimens had dimensions of 120 mm (length), 25 mm (width) and 2.8-3.2 mm (thickness) with two circular perforations of various diameters created by a milling machine at a constant centre-to-centre distance of 30mm (see Figure 4.2). The diameters of the perforations were selected as 0 (i.e., no perforation), 5, 8 and 11 mm. The initial weight of each specimen was recorded prior to the subsequent moisture absorption studies.

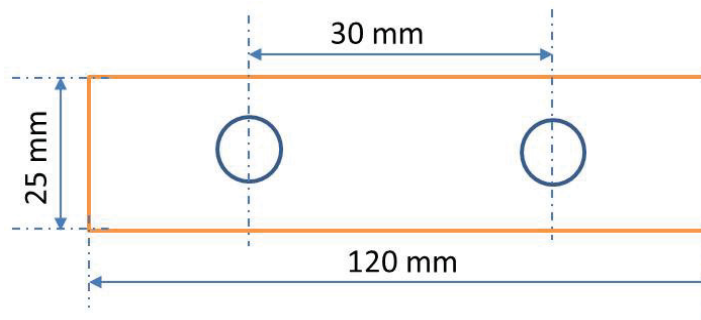


Figure 4.2 Specimen geometry

4.4.2 EXPERIMENTAL PROCEDURE

The specific test parameters are summarized in Table 4.1. The first group of perforated specimens (i.e., three perforation diameters, and three test specimens per perforation size), were put in a controlled environmental chamber and aged in water at 60 °C. The second group of specimens was loaded onto in-house designed/fabricated stress corrosion (SC) loading fixtures (one of the fixtures is shown in Figure 4.3.) The fixture and specimens were also put in water at 60 °C to promote stress corrosion. The test temperature was selected to be as far below the glass transition temperature of this composite material (i.e., 150 °C). It should also be noted that the stress corrosion test specimens were exposed to the environment with various regimes as shown in Table 1.

To establish their moisture absorption characteristics, the specimens were weighed at a specific logical interval during the test, up to the saturation point, as per ASTM D5229 standard [25]. Upon reaching a certain saturation level, some of the specimens were removed and their flexural mechanical properties were evaluated by subjecting the specimens to a three-point bending test. Three time intervals were selected for evaluating the specimen's flexural properties (two during the moisture absorption regime, and one at the fully saturated state). The results were then compared with that of the reference (virgin) specimens (virgin specimens were not subjected to moisture and heat).

The specimens were tested within a MTS universal testing machine, controlled by an Instron digital controller (Model 8510). The load was applied at a rate of 1.0 mm/min, at room temperature.

The specimens were also probed by the aid of a scanning electron microscope (SEM) to study the influence of the moisture absorption and temperature, especially on the matrix/fiber interface.

Table 4.1 Details of the specimens and conditioning scenarios

Environment Condition	Aging temperature (°C)	Perforation size (mm)	Number of specimens	Exposure time (Days)
Aging in water	60	5	3	90
		8	3	90
		11	3	90
Stress corrosion in water	60	5	3	75
		8	3	70
		11	3	70

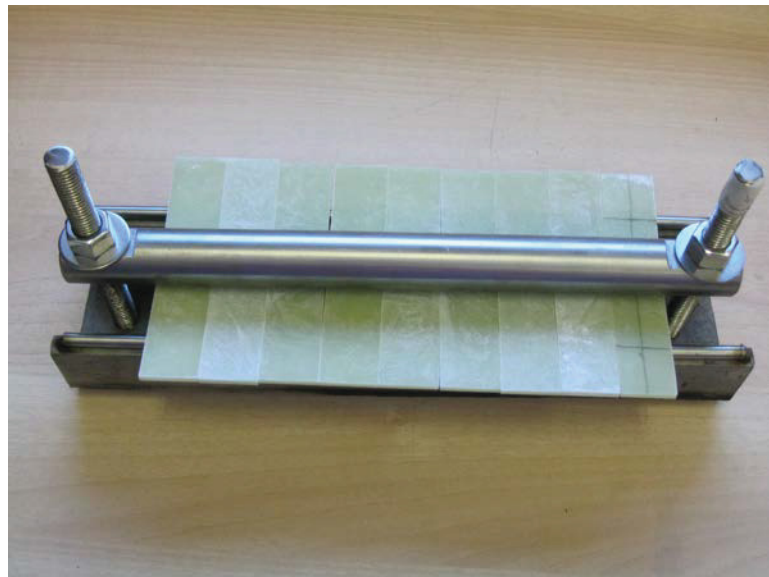


Figure 4.3 Three-point bending frame setup for SCC testing

4.5 EXPERIMENTAL RESULTS AND DISCUSSION

4.5.1 MOISTURE ABSORPTION BEHAVIOR

The weight change rate due to the water absorption in the specimens is determined by the following expression:

$$M_t = \frac{m - m_0}{m_0} 100\% \quad (4.12)$$

where M_t is the weight change at time t , m_0 is the initial specimen mass and m is the mass of the specimen containing water at time t .

The curves of weight-gain versus the square root of exposure time during aging and SCC conditions have been shown in Figures 4.4 and 4.5 for the perforated specimens. In these figures, solid symbols illustrate the experimental results and solid lines represent the predictions based on Fick's equation (i.e., Eq.(4.5)). The curves indicate that the saturation level of the perforated specimens aged in water at elevated temperature increased with increasing perforation diameter. Specifically, the ultimate saturation level for specimens with 5 mm to 11 mm diameter perforations increased from 10%, to 30%, respectively. Moreover, the combined exposure of the perforated specimens to load and humidity (i.e., stress corrosion) under a constant temperature of 60 °C increased the percent gain in moisture from approximately 7% to 30%. Increasing the perforation diameter from 5 to 11 mm, also increased the diffusion coefficient, D , from 2 to 8 %, respectively, in the aged specimens, while the variation was from 3.1 to 6.25 %, respectively, in specimens exposed to the stress corrosion condition (tested at the same temperature and humidity as the aged specimens).

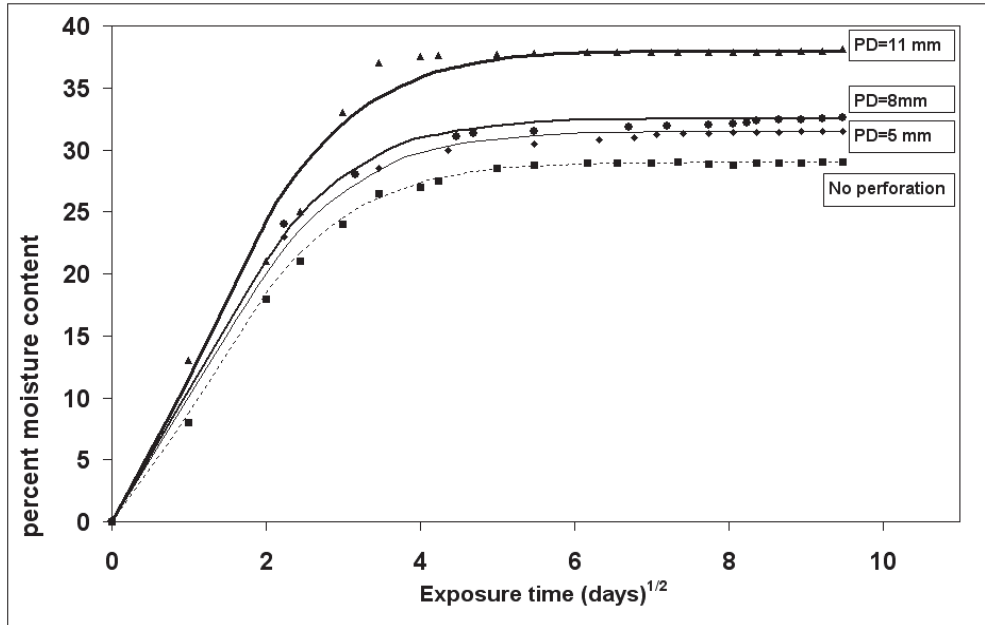


Figure 4.4 Moisture absorption of the specimens aged in water at 60°C

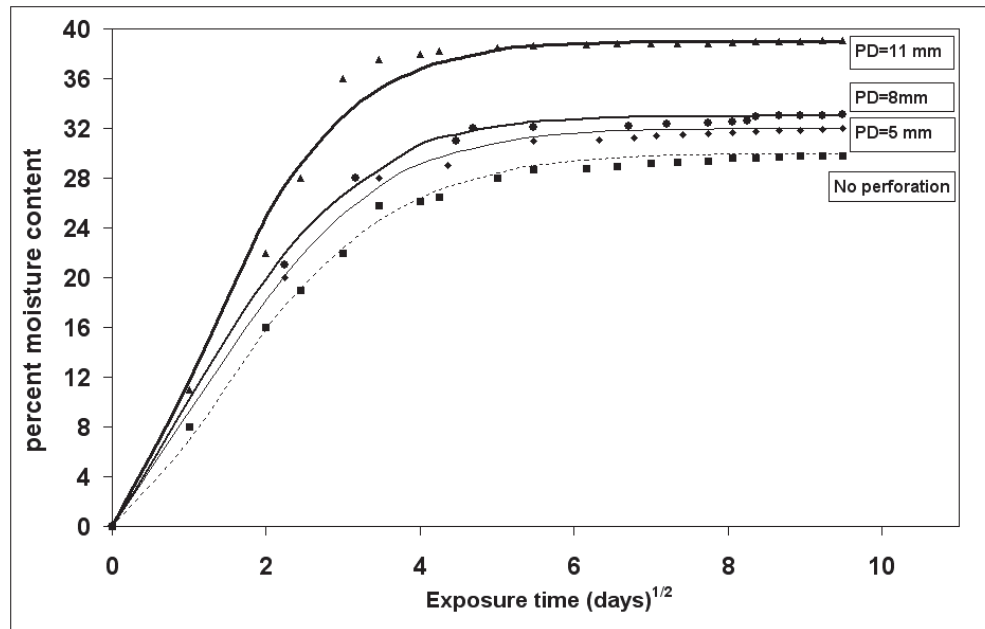


Figure 4.5 Moisture absorption of the specimens subjected to stress corrosion in 60°C water

As stated, to obtain a better prediction of the experimental result, a Langmuir-type model was developed. Figures 4.6 and 4.7 show the comparison of the results obtained based on the application of the Fickian and Langmuir type models with those obtained

experimentally for both groups of aged and SCC perforated specimens. It can be observed that while both models produce good predictions, nonetheless, the moisture uptake of the composite as a function of time could be predicted by the Langmuir-type model more accurately. It should be noted that the curves illustrated in Figure 4.6 and 4.7 were constructed using two equations; Eq. 4.7 was used to plot the initial part (the relatively straight part) of the Langmuir mode curves, while Eq. 4.9-a was used to plot the second part of the curves. As a result, a fictitious peak region can be noted at the intersection point of the two curves.

As mentioned above, Eq. (4.5) was originally developed based on the assumption that moisture absorption takes place only through the top and bottom (finite) surfaces of the material. In other words, the model ignores the through-the-edge diffusion mechanism; hence, the effect of diffusion due to the perforations would be neglected.

With the aim of improving the model, the following modification to the diffusion coefficient is suggested:

$$D_{MFS} = D \left(1 + \frac{h}{l} + \frac{h}{w} + \frac{n\pi dh}{2lw} \right)^{-2} \quad (4.13)$$

where d is perforation's diameter, and n is the number of the circular perforations; the remaining parameters are the same as those in Eq. (4.11). The equation in the parentheses is the summation of all the surface and edge areas divided by areas of the top and bottom surfaces, perpendicular to the thickness.

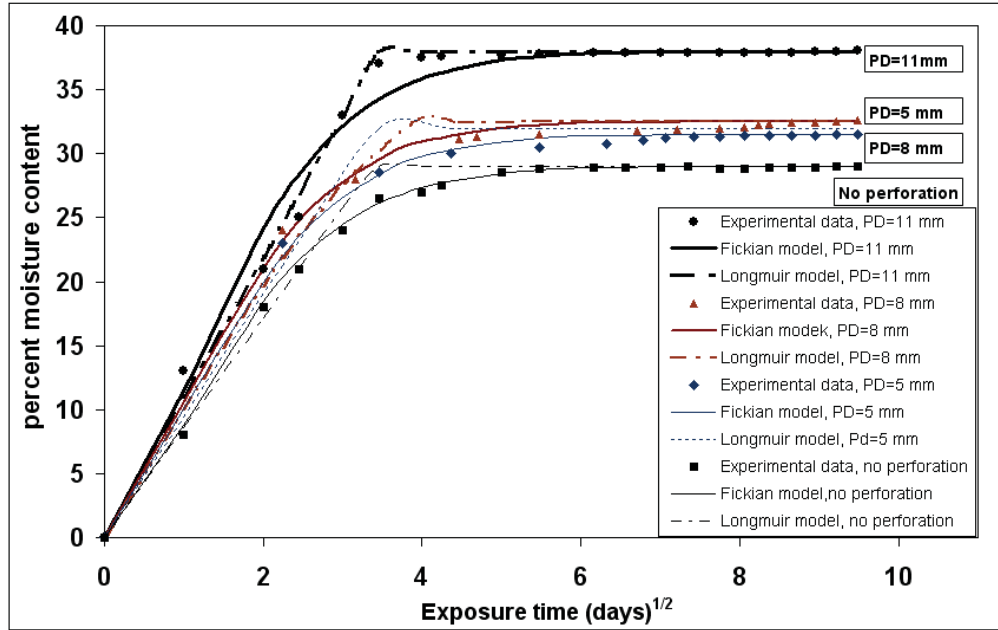


Figure 4.6 Comparison of the moisture absorption predictions of the Langmuir and Fickian models for the specimens aged in water at 60°C temperature

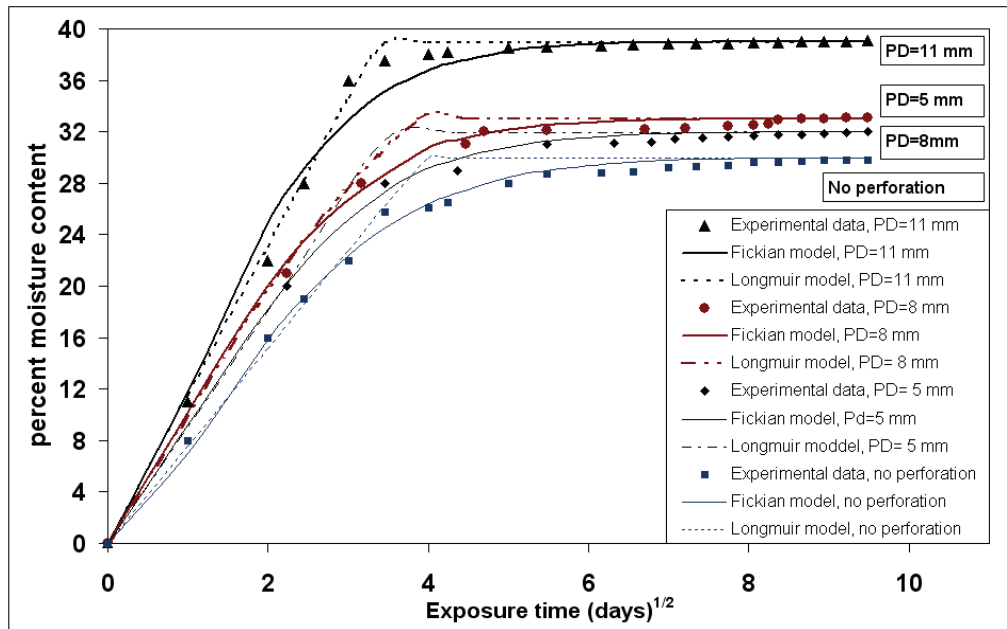


Figure 4.7 Comparison of the moisture absorption prediction capability of the Langmuir and Fickian models for the undergone stress-corrosion in water at 60°C temperature

The integrity of the proposed modified equation in comparison to the one proposed by Shen and Springer [17] (i.e., Eq. (4.11)) is illustrated in Figure 4.8. The suitability and stability of the proposed equation is shown by its stationary nature, while the prediction of the other equation varies as the diameter varies.

By substitution of Eq. (4.13) into Eq. (4.5), we obtain the following equation, which can be used to establish the moisture absorption of perforated GFRP with a better accuracy.***

$$\frac{M_{\%}}{M_{\infty}} \approx 1 - \exp \left[-7.3 \left(\frac{Dt}{h^2} \right)^{0.75} \left(1 + \frac{h}{l} + \frac{h}{w} + \frac{n\pi dh}{2lw} \right)^{-1.5} \right] \quad (4.14)$$

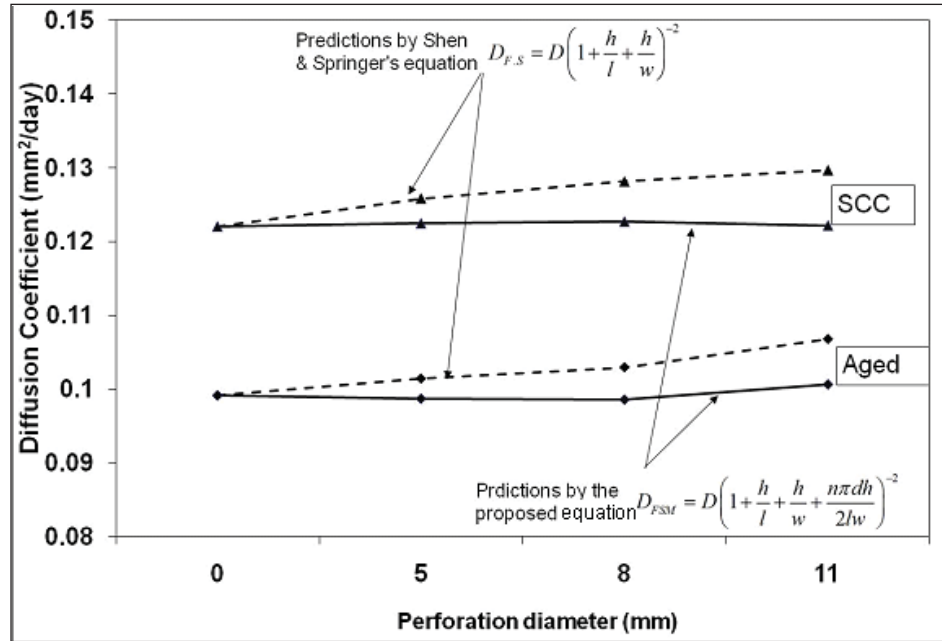


Figure 4.8 Comparison of the diffusions coefficients predicted by Shen and Springer equation and proposed model.

4.5.2 DEGRADATION IN THE MECHANICAL PROPERTIES

As stated, to evaluate the influence of moisture absorption and SCC on the mechanical response of the composite, each specimen was subjected to a three-point bending test at certain interval during the process of moisture absorption, and after becoming fully

saturated. The typical failure mode of the specimens is shown in Figure 4.1(b). All specimens underwent a sudden softening at their mid-span and fractured.

Table 4.2 presents three-point bending test results. As can be seen, the increase in the perforation diameter decreased the flexural strength and stiffness of the specimens; however, the ultimate strain slightly increased, which is believed to be due to the matrix plastization that usually occurs as a result of exposure to an aqueous environment. Figure 4.9 shows the typical load-displacement response of the specimens aged at different environmental conditions, as well as the virgin specimens. As seen, the specimens responded virtually linearly up to the ultimate load, though a slight nonlinearity could be observed in the response of aged and SCC specimens in comparison to the original specimens. Moreover, regardless of the existence of the perforations, the mechanical properties of the aged and SCC specimens were significantly compromised in comparison to the virgin specimens.

Table 4.2 Three-point bending test results (Environment temperature = 60 °C and 100% humidity)

Pre-test Environment Condition of specimens	Specimen ID	Perforations dia. (mm)	Flexural strength (MPa)/ (standard deviation)	Ultimate flexural strain (%)/ (standard deviation)	Flexural modulus of elasticity (GPa)/ (standard deviation)
Aging in water	PA 5	5	280/(0.102)	3.12/(0.103)	15.5/(0.102)
	PA 8	8	190/(0.104)	3.18/(0.102)	13.8/(0.102)
	PA 11	11	150/(0.105)	3.30/(0.107)	12/(0.105)
Stress corrosion in water	PS 5	5	160/(0.107)	3.33/(0.102)	9.5/(0.104)
	PS 8	8	115/(0.11)	3.40/(0.106)	7.7/(0.108)
	PS 11	11	100/(0.103)	3.48/(0.109)	5.9/(0.104)

Note: The reported data are the mean values of 3 results for each category

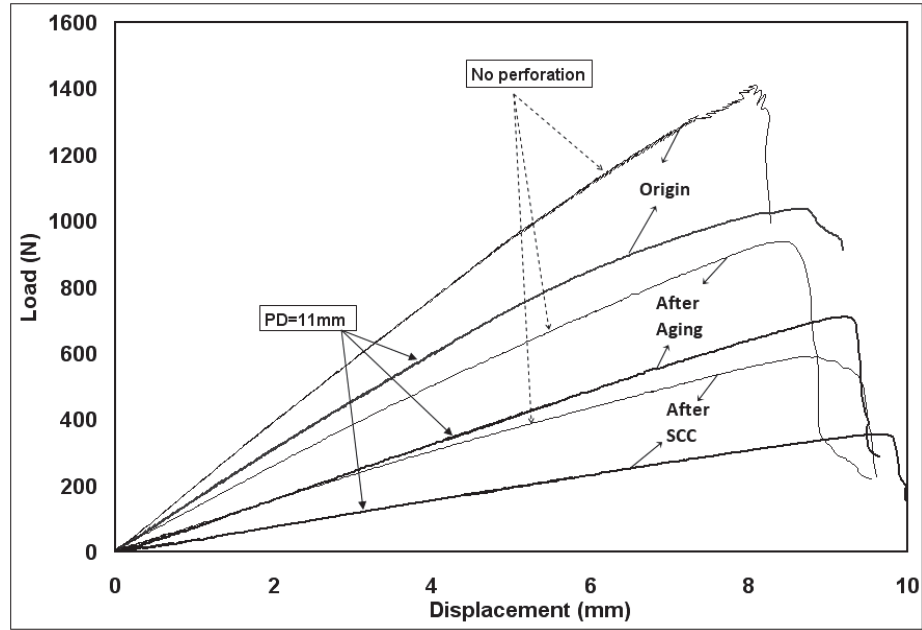


Figure 4.9 Load versus displacement curves for specimens aged or exposed to SCC with different perforation diameters (each curve represents average response of three specimens)

To further examine the influence of aging and SCC on the mechanical response of the composite, the variation in the flexural properties as a function of time and perforation diameter is illustrated in Figures 4.10-4.12. The results reveals that increase in perforation diameter, which also increases the rate of moisture absorption and the final moisture content, significantly influences the residual flexural strength of the composite. The maximum degradation in the strength was observed to be approximately 50-70%, after aging and as high as 70-80% after having been subjected to SCC. Similar compromise was seen in the flexural stiffness of the specimens (as high as 37% for the aged and 68% for SCC specimens, respectively).

By considering the exponential nature of Eq. (4.1) and (4.5), and combining Eq. (4.3), (4.6) and (4.13), an equation is derived by which the degradation in the flexural strength of the GFP as a function of perforation diameter, as well as the exposure time and applied stress, due to stress-corrosion in water can be predicted with good accuracy. The equation has the following form:

$$\frac{\sigma_{residual}}{\sigma_0} = e^{-\left[\frac{D}{\phi^2}\right](A+B\sigma_{app})t} \quad (4.15)$$

In the above equation $\sigma_{residual}$ is the flexural strength of the structure at time t , σ_0 is the flexural strength of the virgin material, D is the diffusion coefficient calculated by equation 4.6, σ_{app} is the applied stress (which would be zero if the material is only subject to the aging processes). A and B are empirical material constants. The constant A (i.e., the “aging constant”) is obtained from a basic aging test results; while factor B , or the “stress coefficient”, signifies the influence of the applied constant stress; its value is obtained from a basic SCC test. Finally, ϕ is a geometric factor, calculated by the following equation:

$$\phi = \left(1 + \frac{h}{l} + \frac{h}{w} + \frac{n\pi dh}{2lw}\right) \quad (4.16)$$

where h , l and w are thickness, length and width of the specimen, respectively, d is the perforation diameter, n is the number of perforations.

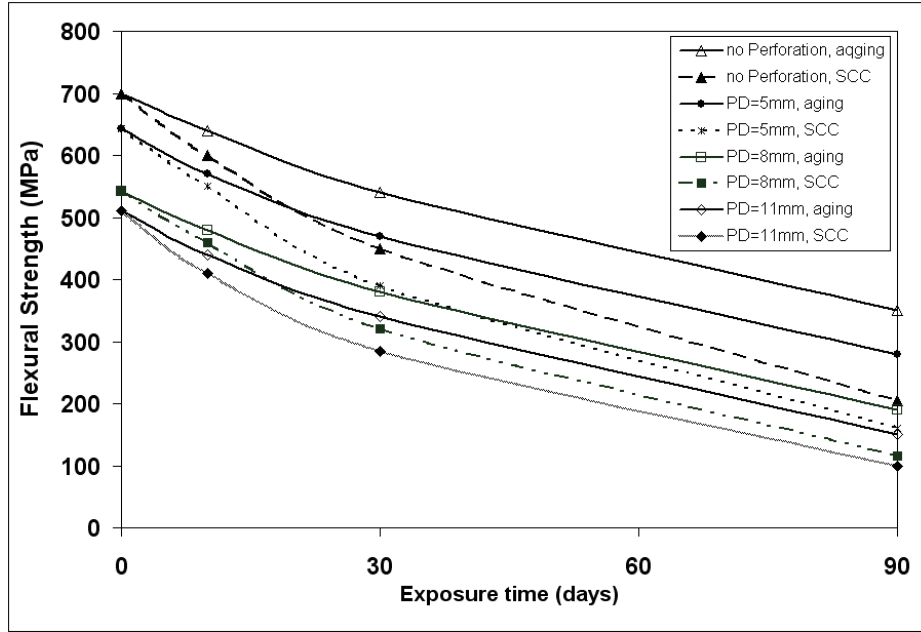


Figure 4.10 Degradation in the flexural strength of the perforated specimens as a function of time and perforation diameter (aged in water specimens and those subject to SCC)

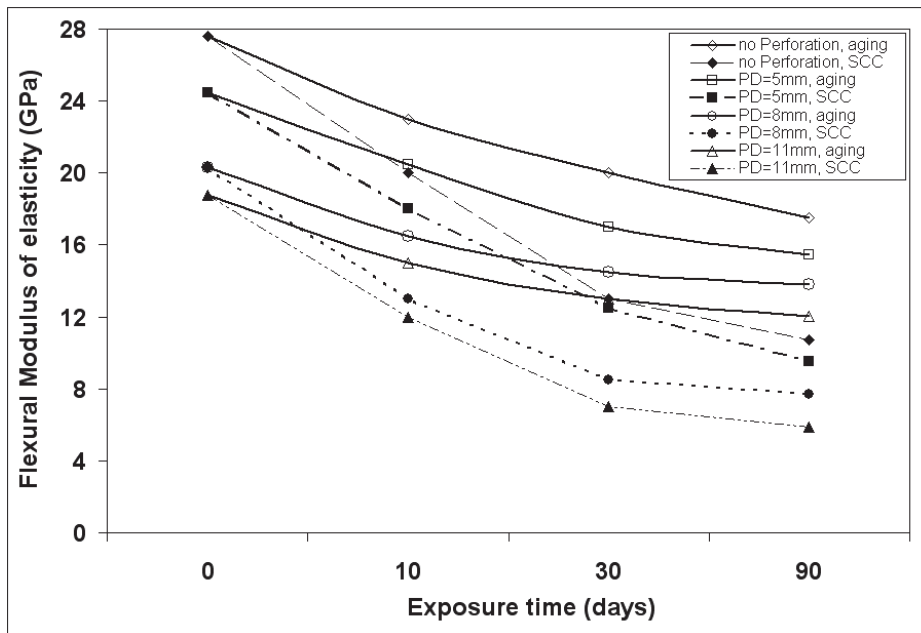


Figure 4.11 Degradation in the flexural modulus of elasticity of the perforated specimens as a function of time and perforation diameter (aged in water specimens and those subject to SCC)

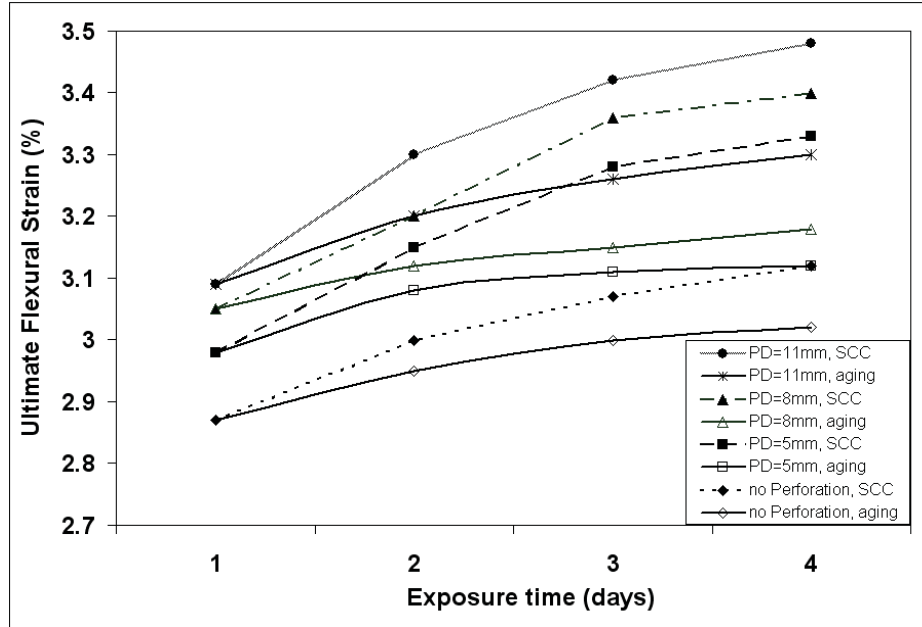
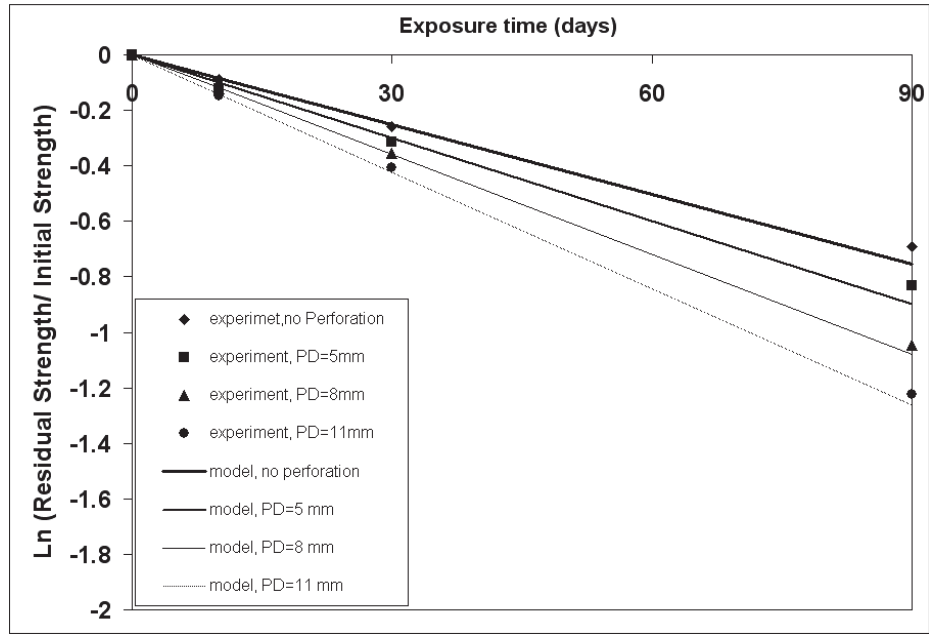


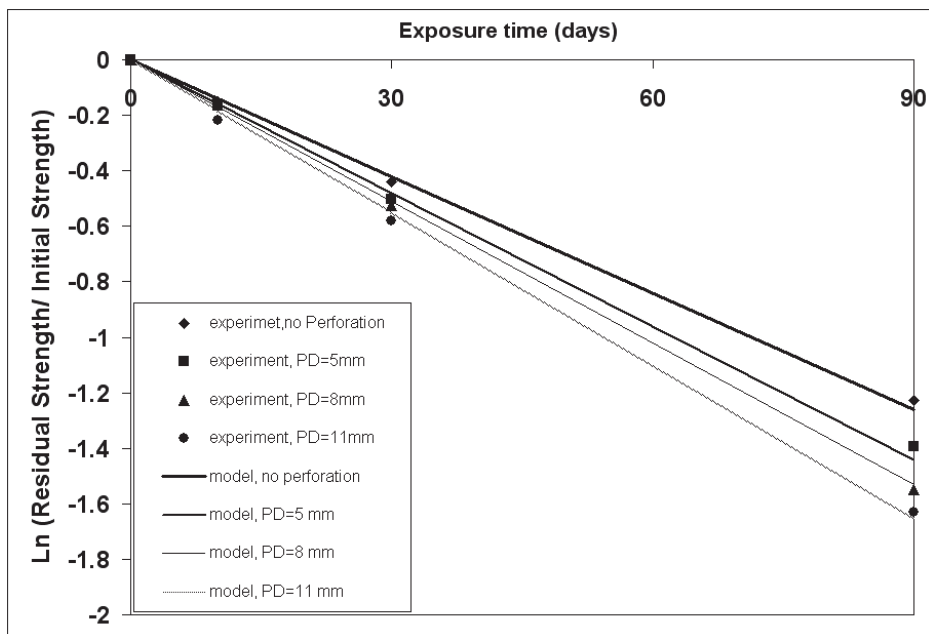
Figure 4.12 Increase in the ultimate flexural strain of perforated specimens as a function of conditioning time and perforation diameter

Figure 4.13 illustrates the comparison between the normalized flexural strengths obtained experimentally (solid points) and those (dashed lines), obtained through the proposed equation, for different perforation diameters, as a result of exposure to the aging and SCC conditions. As it can be seen, the model produces good prediction of the residual strength.

In general, therefore, it can be seen that the diffusion magnitude and perforation diameter (i.e., the cross-sectional surface area of the perforations), could significantly alter the flexural properties of perforated composites.



(a)



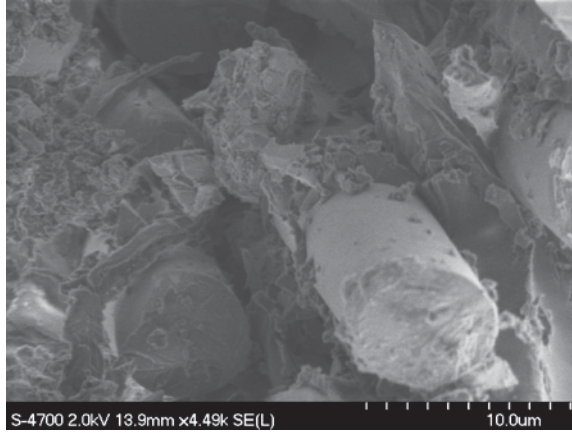
(b)

Figure 4.13 Comparisons of the predicted normalized strength (by Eq. (16)) versus that experimentally obtained: (a) aged in water (b) SCC in water

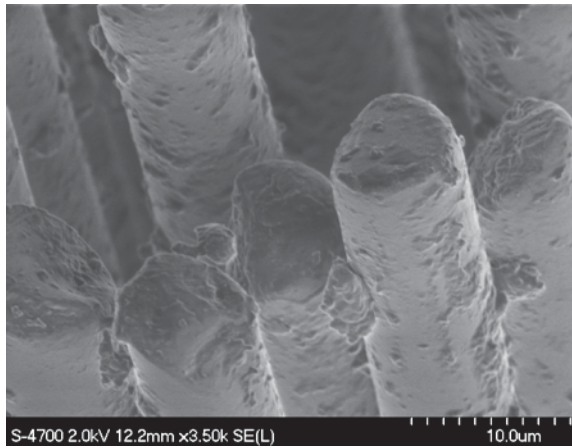
4.5.3 SEM ANALYSIS

Figure 4.14 shows the SEM images of the GFRP specimens, before and after water immersion, for specimens subjected to aging in water and SCC conditions. It can be seen that when a specimen was not exposed to moisture and high temperature (i.e., virgin), there was good adhesion between the fibers and matrix, evident by the large amount of matrix surrounding the fibers. However, after exposing the specimens to humidity and temperature, the bond between fibers and matrix weakened, evident by the large number of scattered clusters of matrix and enlarged voids surrounding the fibers (as shown in Figures 4.14(b) and 4.14(c)).

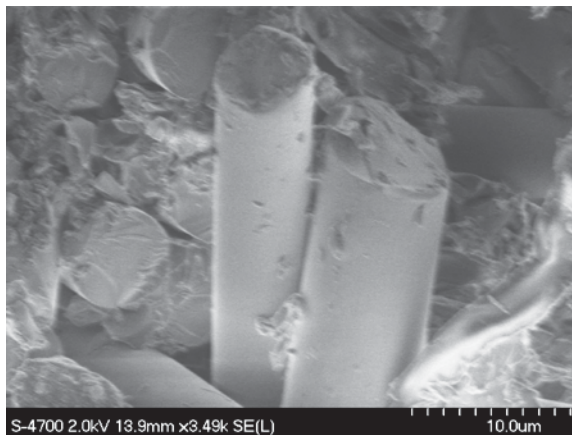
During aging in water, the water molecules penetrate (diffuse) into voids of the polymeric matrix; as temperature increases, the voids grow into larger cavities and cracks. It has been shown that immersion of fiber-reinforced epoxy matrix in water caused swelling of the matrix, thereby causing debonding of the fiber/matrix interface [26]. This is consistent with the observation made in our experiments; that is the observations of more voids and cracks in the matrix of the specimens subjected to humidity and high temperature, as opposed to the un-exposed (virgin) specimens.



(a) Virgin



b) after aging



(c) after SCC

Figure 4.14 Comparison of the typical failure surfaces of the perforated GFRP specimens at before and after conditioning

4.6 CONCLUSIONS

Aging and stress corrosion (SCC) experiments were conducted on perforated GFRP composite specimens. The influence of perforation diameter on the moisture absorption rate and change in the flexural properties of the composite was studied. The applicability of Fick's solution for establishing the level of moisture absorption was examined, and an improved model was developed. The proposed model was demonstrated to be capable of establishing the rate and amount of the moisture absorption of the perforated GFRP specimens that were exposed to aging and stress corrosion experiments at 60 °C temperature with a better accuracy.

The mechanical tests conducted on post-aged and SCC specimens revealed that an increase in the perforation diameter led to an increase in the diffusion surface, hence increasing the moisture absorption. Moisture absorption resulted in matrix degradation, thereby reducing the flexural strength and stiffness of the composite; however, the ultimate flexural strain of the material was increased as a result of matrix plastization. Moreover, in consideration of the exponential nature of the moisture content as a function of the diffusion coefficient, a semi-empirical model was also developed by which the time varying degradation in the strength of the composite aged in an aqueous hot environment and/or subject to SCC could be predicted with good accuracy. From the physical perspective, the SEM investigation of the fiber resin interface of the specimens revealed a distinct degradation in the interface as a result of the high moisture absorption.

In conclusion, while such a composite could be effectively used in applications involving harsh environments (such as that in directional oil wells), nevertheless, special provisions should be made to incorporate the influence of the environment on the structural integrity of the composite, thereby the durability of the structure.

4.7 ACKNOWLEDGEMENT

The financial support of the Natural Sciences and Engineering Council of Canada (NSERC) in support of this work is gratefully acknowledged. The access to IRM (Institute of Research for Materials) SEM facilities is greatly appreciated.

4.8 REFERENCES

- [1] Chou P J C, Ding D. Characterization of Moisture Absorption and Its Influence on Composite Structures. *J. Thermoplast. Compos. Mater.* 2000; 3: 207-25
- [2] Mula S, Bera T, Ray P K, Ray B C. Effect of hydrothermal aging on mechanical behavior of sub-zero weathered GFRP composites. *J. Reinf. Plast. Compos.* 2006; 25: 673-80
- [3] Davies P, Mazeas F, Casari P. Sea Water Aging of Glass Reinforced Composites: Shear Behaviour and Damage Modelling. *J. Compos. Mater.* 2001; 35: 1343-72
- [4] Shirrell C D, Leisler W H, Sandow F A. Moisture-Induced Surface Damage in T300/5208 Graphite/Epoxy Laminates, in *Nondestructive Evaluation and Flaw Criticality for Composite Materials*, ASTM STP 696, R. B. Pipes. ed. American Society for testing and materials, West Conshohocken, USA. 1979:209-23
- [5] Weitsman Y. Moisture in Composites: Sorption and Damage, chap. 9, *Fatigue of Composite Materials*, Elsevier Science Publishers B.V. Amsterdam. 1991: 385-429
- [6] Roy S. Prediction of Anomalous Hygrothermal Effects in Polymer Matrix Composites. *J. Reinf. Plast. Compos.* 1999; 19: 1197-207
- [7] Aditya P K, Sinha P K. Diffusion Coefficients of Polymeric Composites Subjected to Periodic Hygrothermal Exposures. *J. Reinf. Plast. Compos.* 1992; 11: 1035-47
- [8] Sereir Z, Adda-Bedia E A, Tounsi A. Effect of temperature on the hygrothermal behaviour of unidirectional laminates plates with asymmetrical environmental conditions. *Compos. Struct.* 2006; 72: 383-92
- [9] Maxwell A S, Broughton W R, Dean G, Sims G D. Review of accelerated aging methods and lifetime prediction techniques for polymeric materials, NLP report, DEPC MPR 016, National Physical Laboratory, Teddington, UK. 2005.
- [10] Neumann S.H, Marom G. Free-volume dependent moisture diffusion under stress in composite materials. *J. Mater. Sci.* 1986; 21: 26-30

- [11] Pauchard V, Grosjean F, Campion-Boulharts H, Chateauminois A. Application of a stress-corrosion-cracking model to an analysis of the durability of glass/epoxy composites in wet environments. *Compos. Sci. Technol.* 2002; 62: 493-98
- [12] Fahmy A A, Hurt J C. Stress dependence of water diffusion in epoxy resin. *Polym. Compos.*, 1980; 1: 77-80
- [13] Whitaker G, Darby M I, Wostenholm G H, Yates B, Collins M H, Lyle A R, Brown B. Influence of temperature and hydrostatic pressure on moisture absorption in polymer resins. *J. Mater. Sci.* 1991; 26: 49-55
- [14] Wan Y Z, Wang Y L, Huang Y, He B M, Han K Y. Hygrothermal aging behaviour of VARTMed three-dimensional braided carbon-epoxy composites under external stresses. *Compos. A.* 2005; 36: 1102-09
- [15] Neumann S, Marom G. Prediction of Moisture Diffusion Parameters in Composite Materials Under Stress. *J. Compos. Mater.* 1987; 21: 68-80
- [16] Neumann S, Marom G. Stress dependence of the coefficient of moisture diffusion in composite materials. *Polym. Compos.* 1985; 6: 9-12
- [17] Shen C H, Springer G S. Moisture Absorption and Desorption of Composite Materials. *J. Compos. Mater.* 1976; 10: 2-20
- [18] Adams R D, Singh M M. The dynamic properties of fibre-reinforced polymers exposed to hot, wet conditions. *Compos. Sci. Technol.* 1996; 56: 977-97
- [19] Ellyin F, Maser R. Environmental Effects on the Mechanical Properties of Glass-Fiber Epoxy Composite Tubular Specimens. *Compos. Sci. Technol.*, 2004; 64: 1863-74
- [21] Suri C, Perreux D. The effects of mechanical damage in a glass fibre epoxy composite on the absorption rate. *Compos. Eng.* 1995; 5: 415-24
- [22] Surathi P, Karbhari V M. Hygrothermal Effects on Durability and moisture Kinetics of Fiber-Reinforced Polymer Composites, Technical Report No. SSRP06/15, University of California, Oakland. 2006
- [23] ASTM D3171-09. Standard Test Methods for Constituent Content of Composite Materials. West Conshohocken, USA. 2009

[24] ASTM D790-10. Standard test methods for flexural properties of unreinforced and reinforced plastics and electrical insulating materials. West Conshohocken, USA. 2010.

[25] ASTM D5229-04. Standard Test Method for Moisture Absorption Properties and Equilibrium Conditioning of Polymer Matrix Composite Materials. West Conshohocken, USA. 2004.

[26] d'Almeida J R M, de Almeida R C, de Lima W R. Effect of water absorption of the mechanical behavior of fiberglass pipes used for offshore service waters. Compos. Struct. 2008; 83: 221-5

CHAPTER 5 EFFECTS OF PERFORATION SIZE ON PERFORATED GFRP COMPOSITES' RESPONSE TO ACIDIC MEDIA*

Shiva Eslami and Farid Taheri

Department of Civil and Resource Engineering, Dalhousie University

5.1 ABSTRACT

The response of non-perforated and perforated GFRP specimens, aged in a combined acidic and hot environment, under an externally applied load (stress corrosion), and no external load conditions, is investigated. The applicability of Fickian and Langmuir type models for predicting the mass absorption response of the composite is also examined, and the degradation in the flexural properties of the composite bearing different perforation sizes is also established. The results indicate that the perforation size, immersion time, and the presence of external load (during aging) all directly influence the flexural properties of the composite.

Keywords: A. Glass; B. SEM; C. Acid corrosion; C. Stress corrosion

5.2 INTRODUCTION

In the oil extraction industry, “liners” are specific structural components that are utilized to stabilize the directional wells. These wells provide increased surface contact areas in hard-to-reach reservoirs, thus can increase the productivity of the pay zone. The commonly used liners are usually made of perforated steel tubes; these liners are usually subjected to hostile and corrosive environments in oil wells. As a result, they would have to be replaced periodically, thus increasing the overall cost of oil extraction. Recognizing this fact, the concept of using perforated glass fiber reinforced plastic (GFRP) liners, especially in the open hole horizontal wells has been deemed as a logical alternative.

* Accepted for publication to the Journal of Corrosion Science
Volume 69, April 2013, Pages 262–269

However, in order to explore the viability and feasibility of the concept, the durability and life-cycle performance of such liners had to be thoroughly investigated.

Although various researchers have reached the conclusion that acidic media may cause severe degradation in fiber-reinforced plastics (FRP), nevertheless, most of the investigations conducted thus far have considered carbon-epoxy composites, and the database for characterization of the response of GFRP to the aforementioned media, especially at elevated temperature is relatively limited. This is despite the fact that E-glass fibers, owing to their superior strength and abrasion properties (amongst their many other positive attributes), are the most widely used fiber in various industrial applications [1–4].

Nevertheless, the main factor responsible for corrosion degradation of GFRPs could be attributed to the glass fibers rather than the matrix, since most matrices protect fibers from the corrosive environment [5–8]. On the other hand, if the resin/fiber interface is somehow damaged (e.g., due to presence of micro-cracks), while exposed to acidic media, the mechanical properties of the fiber would be degraded significantly. This is mainly due to chemical attack on the fiber surface, as a result of which the fibers would fracture at a stress considerably lower than their ultimate strength [9–11].

From the chemical perspective, the protons (H^+) from the acid could replace the metal ions on the surface of glass fibers. Due to the smaller size of H^+ , a tensile stress would consequently be generated on the surface of fibers, thereby causing cracking of the surface. It can be therefore concluded that H^+ concentration could be a governing factor on the corrosion rate.

Moreover, the anions in the acidic media, jointly with the metals cations, could form an insoluble complex ion accumulating on the fiber, thus accelerating the leaching process of the cations from the fiber surface [12, 13].

Dimensional changes due to swelling, and color changes due to the deformation in the polymer chains of GFRP, have been frequently reported when GFRP specimens were immersed in acidic media [9, 14]. It has been observed that such specimens would show more plasticity under loading, in comparison to the virgin specimens.

As stated above, E-glass fibers are more susceptible to deteriorate by acids (specifically mineral acids such as H_2SO_4). Those acids can be present in all chemical factories, industrial locations, and in oil reservoirs. The metallic cations at the glass surface can be replaced by the hydrogen ions of the acid solution; as a result, elements like sodium, potassium, magnesium, boron and mainly calcium and aluminum ions (due to high weight percentage of their oxides in the glass fiber), can be leached to the acidic solution [9, 12].

In consideration of the kinetics of corrosion of E-glass fibers in sulfuric acid, Jones and Stewart [15] found that increasing the temperature could cause a considerable increase in the corrosion rate, although the concentration of sulfuric acid had no obvious effect on the rate of corrosion; it was shown that the precipitation was the main reason of the removal of calcium from the glass in sulfuric acid and not the replacement of the acid ions.

Based on a survey of the pertinent literature, it could be concluded that although degradation in the mechanical properties of GFRPs has been explored broadly, nevertheless, to the best of our knowledge, the influence of perforation on the resulting diffusion rate of GFRP, especially in their stress corrosion cracking (SCC) process have not been studied.

In general, solutions would penetrate into a GFRP plate faster through the edge surfaces (as opposed to the top and bottom surfaces). The solution would then travel along the length of the fibers. In comparison to a non-perforated GFRP plate, perforated GFRP plate specimens would present a larger edge surface area for solution penetration, thus increasing the rate of the diffusion.

The main aim of this study is to assess the influence of perforations in GFRP plates on acid absorption to an elevated temperature, and the resulting degradation in the flexural properties of the materials. Both perforated and non-perforated specimens were therefore considered and they were aged at elevated temperatures, and they were also subjected to a stress corrosion processes in a sulfuric acid solution.

Moreover, using a scanning electron microscopy, the physical effect of the acidic media on the GFRP material was also investigated and the change in their microstructures was analyzed.

5.3 THEORETICAL BACKGROUND

In general, the mechanical properties of GFRP composites are degraded when such materials are exposed to corrosive environments for long durations [6, 11]. As stated earlier, the process causes the hydrogen ions present in the acidic media to extract ions from the glass fibers and degrade their surface morphology [9]. In fact, all the ions of the fiber's surface structure could be leached into the acidic solution; the more abundant the ions, the greater the leaching [16]. Jones and Betz [16] have shown that there would be an optimum concentration of the acidic by which the maximum corrosion could be caused, and that the corrosion rate of E-glass fibers would significantly increase as the temperature increases. They also suggested the following model for evaluating the loss in strength as a result of exposure to elevated temperatures:

$$\text{Strength retention} = Ae^{-kt} \quad (5.1)$$

where A is the overall strength loss, k is a temperature dependent constant related to the rate of decay of the material, and t is the time of exposure in hours.

The mass absorption process by an infinitely large polymer composite plate immersed in a solution can be modeled by applying the Fickian equation presented, illustrated by [17]:

$$\frac{M_{\%}}{M_{\infty}} = 1 - \frac{8}{\pi^2} \sum_{n=0}^{\infty} \frac{1}{(2n+1)^2} \exp\left[-D(2n+1)^2 \frac{\pi^2 t}{h^2}\right] \quad (5.2-a)$$

which can be approximated as:

$$\frac{M_{\%}}{M_{\infty}} \approx 1 - \exp\left[-7.3\left(\frac{Dt}{h^2}\right)^{0.75}\right] \quad (5.2-b)$$

where $M_{\%}$ is the absorbed mass at time t , M_{∞} is the maximum content and h is the specimen thickness, respectively. In the above equation, D is the diffusion coefficient, which can be calculated for infinite plates using the following relation [17]:

$$D = \pi \left(\frac{h}{4M_{\infty}} \right)^2 \left(\frac{M_2 - M_1}{\sqrt{t_2} - \sqrt{t_1}} \right)^2 \quad (5.3)$$

where $\left(\frac{M_2 - M_1}{\sqrt{t_2} - \sqrt{t_1}} \right)$ is the slope of the initial linear portion of the graph of the absorbed mass versus time.

Moreover, the following coefficient has been suggested for modification of the diffusion coefficient in the case of non-perforated finite size specimens [17]:

$$D_{F.S} = D \left(1 + \frac{h}{l} + \frac{h}{w} \right)^{-2} \quad (5.4-a)$$

where $D_{F.S}$ is the modified diffusion coefficient for finite size specimens, l is the length and w is specimens width.

Considering the presence of perforations, which present added areas for diffusion (i.e., that related to the perforation edge regions, here referred to as A), the modified diffusion coefficient (D_{MFS}) for perforated specimens can be estimated by the following equation [18]:

$$D_{MFS} = D \left(1 + \frac{h}{l} + \frac{h}{w} + \frac{A}{2lw} \right)^{-2} \quad (5.4-b)$$

In the case of a plate hosting equal diameter circular perforations, the equation takes the following form:

$$D_{MFS} = D \left(1 + \frac{h}{l} + \frac{h}{w} + \frac{n\pi dh}{2lw} \right)^{-2} \quad (5.4-c)$$

where d is the perforation diameter, and n is the number of the perforations.

Using eq. 5.4-c, the following equation can be used conducted for predicting the mass absorption of perforated GFRP plates:

$$\frac{M_{\%}}{M_{\infty}} \approx 1 - \exp \left[-7.3 \left(\frac{Dt}{h^2} \right)^{0.75} \left(1 + \frac{h}{l} + \frac{h}{w} + \frac{n\pi dh}{2lw} \right)^{-1.5} \right] \quad (5.5)$$

Moreover, a few some researchers have demonstrated that externally applied load would influence the diffusion in epoxy resins [19]. It has been suggested that diffusion coefficient in a stressed member, D_{σ} , can be evaluated by the following equation [19]:

$$D_{\sigma} = D_0 \left(1 + A \frac{\sigma}{G} \right) \quad (5.6)$$

Where D_0 , σ , G and A are the diffusion coefficient in the unstressed stat, applied stress, shear modulus and a constant (evaluated experimentally), respectively. If the material is subjected to a tensile stress, then the diffusion coefficient would increase; conversely, the application of a comprehensive stress would reduce the diffusion coefficient and hence the mass absorption. However, when the material is subjected to a flexural stress, the relative influence of the tensile stress would be considerably higher than the deceleration in the mass absorption caused by the compressive stress counterpart, therefore, there would be a net increase in the diffusion [19, 20].

However, some investigations have shown that the diffusion process in a FRP composite could be non-Fickian [6], and that instead a Langmuir-type model could estimate the mass absorption in by FRP composites [21]. A representative Langmuir-type model that could be used to estimate the level of absorption of a FRP specimens immersed in a media for a relatively long time period, t , takes the following form:

$$M_t = M_{\infty} \left[1 - \frac{\gamma}{\beta + \gamma} \exp(-\beta t) \right] \quad (5.7)$$

In the above equation, β and γ are the probability of molecule bonding per unit time and probability of molecule mobility per unit time, respectively.

The value of β can be derived using the following equation [21]:

$$-\left[\frac{dM_t}{dt}\right]^{-1}\left[\frac{d^2M_t}{dt^2}\right] = \text{constant} = (\beta) \quad (5.8)$$

and then by substituting β into the following equation, γ could be evaluated [21]:

$$\exp(-\beta t)\left[\beta\left\langle\frac{dM_t}{dt}\right\rangle^{-1}M_t + 1\right] = \text{constant} = 1 + \frac{\beta}{\gamma} \quad (5.9)$$

One of the aims of this study is also to investigate the viability and predictive accuracy of the Langmuir-type and Fickian models for mass absorption response of GFRP composites aged in the acidic media.

5.4 EXPERIMENTAL INVESTIGATION

5.4.1 SPECIMEN PREPARATION

The GFRP specimens used in our investigation were fabricated using 7781 woven E-glass/ NB321 epoxy cross-ply prepreg, supplied by Newport Adhesives and Composites Inc. (Irvine, CA). The layup sequence of the GFRP plates made from the prepreg was $[0/90]_{7,s}$. The plates were vacuumed bagged and cured at 135 °C for 2 hrs, and then cooled down to room temperature in the oven. Next, the plates were trimmed (i.e., 3/4" width strips along plates perimeter were removed), and rectangular specimens were extracted by using a special diamond saw. Perforations of different sizes (5, 8 and 11 mm diameters) were then carefully machined into the specimens (coupons). The coupons were prepared according to ASTM D790 guidelines [22], with final dimensions of 120 mm length, 25mm width and 2.8-3.2 mm thickness. Each perforated coupon had two circular perforations (diameters of 5, 8 and 11 mm) with a centre-to-centre distance of 30mm, as shown in Figure 5.1.

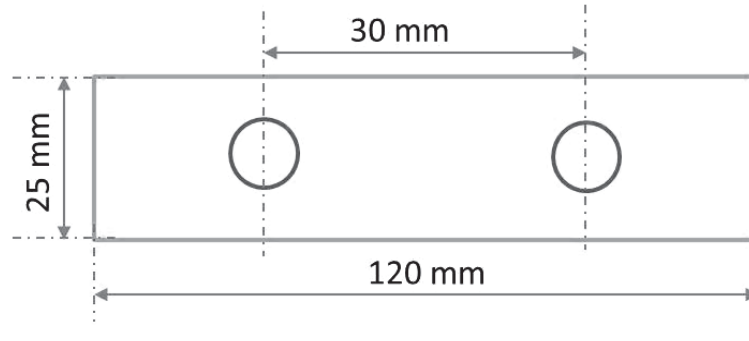


Figure 5.1 Typical specimens geometry

5.4.2 EXPERIMENTAL METHODS

The specimens were immersed and kept in acidic bath until they were fully saturated. After that stage, they were tested in a three-point bending configuration.

The aging conditions of the specimens are summarized in Table 5.1. After recording the initial weight of each specimen, the first group of specimens, referred to AG (acronym for aging group), included three perforation sizes. The specimens in this group were placed in a controlled environmental chamber, aged in a 15% sulfuric acid solution at a temperature of 60 °C. The second group of specimens, referred to SCG (acronym for stress corrosion group), were subjected to a predetermined stress level (25% of the ultimate strength of the specimens) through a frame designed in-house, made of corrosion resistant steel alloy, and submerged in 15% sulfuric acid solution at a temperature of 60 °C (see Figures 5.2 and 5.3). This temperature is well below the glass transition temperature of the resin (i.e., 150 °C). The test was conducted as per ASTM D5229 [23] standard, and the specimens were weighed during the test in a logical sequence until the saturation point.

The specimen's weight gain was determined at three intervals within the test period. Some of the specimens were removed from the chamber and underwent a three-point bending test, using a servo-hydraulic INSTRON testing machine, controlled with 8500⁺ electronics, in order to evaluate their flexural response. The results were then compared with those obtained from virgin specimens (i.e. those not subjected to acid and heat).

Table 5.1 Details of the specimens and test condition

Specimen Type	Environment	Aging temperature (°C)	Test type	Perforation size (mm)	Number of specimens
Plates	15% sulfuric acid solution	60	Aging	0	3
				5	3
				8	3
				11	3
			Stress corrosion	0	3
				5	3
				8	3
				11	3

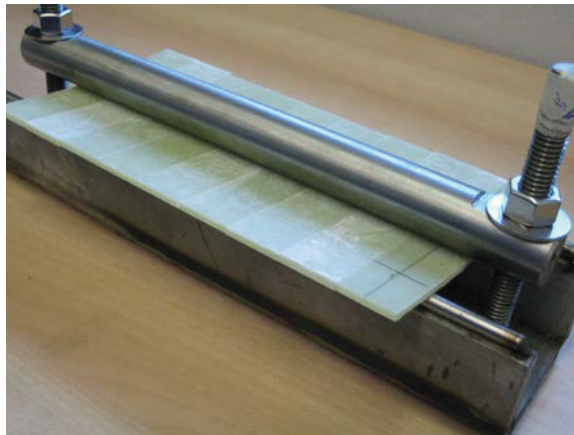


Figure 5.2 The frame used to apply external load to the GFRP specimens (in SCC test)



Figure 5.3 Specimens under external load immersed in acid

5.5 EXPERIMENTAL RESULTS AND DISCUSSION

5.5.1 ABSORPTION BEHAVIOR

The percent of the absorbed solution (mass absorption), M_t , in the specimens was calculated by the following equation:

$$M_t = \frac{m - m_0}{m_0} 100\% \quad (5.10)$$

where m_0 is specimen's mass at the initial stage and m is the mass at time t .

The effect of perforation size on specimen mass absorption has been shown in Figures 5.4 and 5.5; it can be seen that an increase in the perforation size (which in turn increases the edge surface area) lead to an increase in the diffusion surface. Therefore, the specimens with larger perforations became fully saturated at a faster rate. Observation of the absorption trends (for different perforation sizes) indicates that when a perforated coupon was aged in 15% sulfuric acid, at an elevated temperature of 60 °C, an increase in the perforation diameter from 5 mm to 11 mm increased the absorption at the initiation of the saturation roughly from 50% to 100%, respectively. Moreover, comparison of the results for the SCC specimens (those aged in acid at the same temperature while subjected to an applied load) indicates that the specimens having 5 mm dia. perforations experienced mass absorption of approximately 3% compared to 50% gain in mass absorption by for the SCC specimens with 11 mm perforations. As a result the diffusion magnitude also increased for both groups of specimens and perforation sizes.

The rate of mass absorption data versus the square root of exposure time are compared to Fickian and Langmuir-type models in Figures 5.6 and 5.7. The results indicate that the absorption trend of aged and SCC specimens could not be predicted accurately by the Langmuir model. However, the experimental results were in better agreement to the predication of the Fickian model, and the discrepancies were not very significant.

Another important observation was the presence of white sediment accumulated on the chamber walls (see Figure 5.8). The sediment is believed to be calcium sulfate, formed as a result of a chemical reaction between the calcium ions on the fiber's surface and anions in the acid solution.

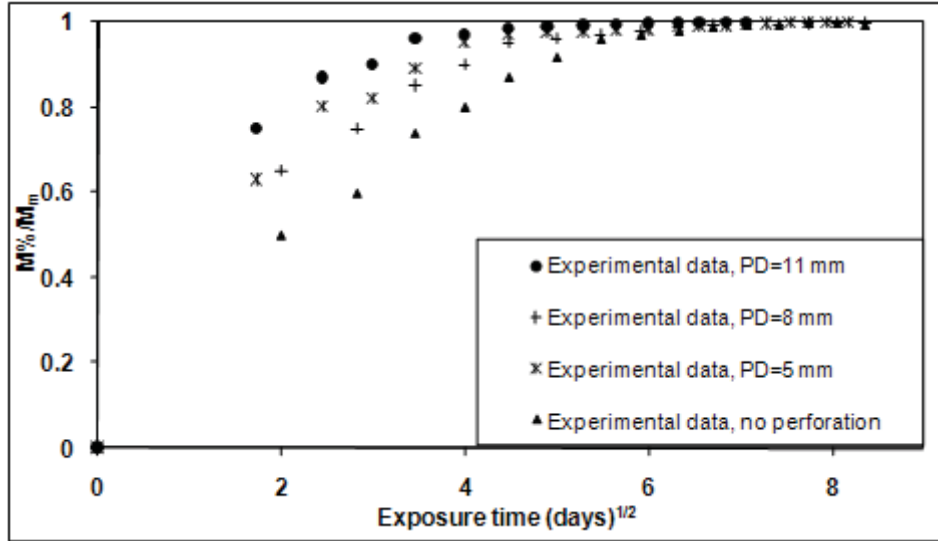


Figure 5.4 Mass absorption of the specimens aged 15% sulfuric acid solution at 60 °C

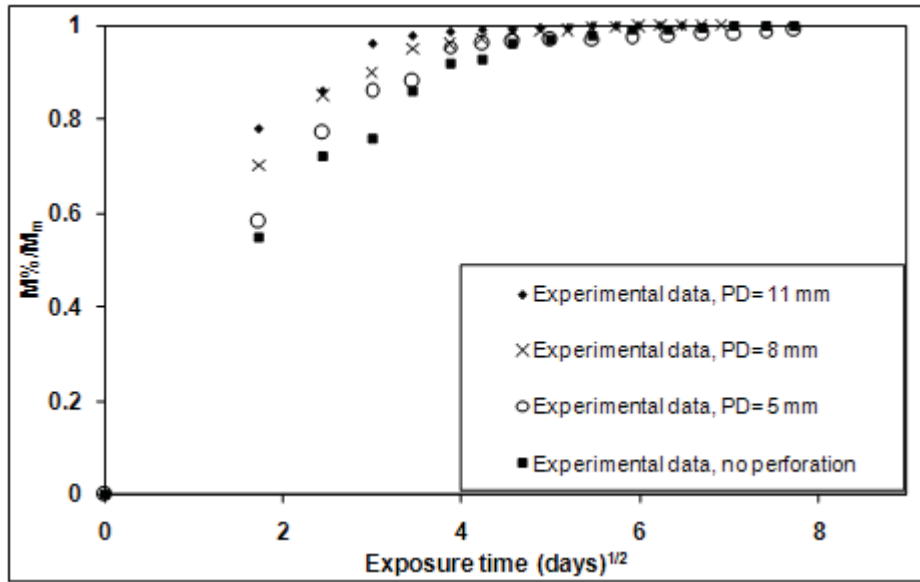
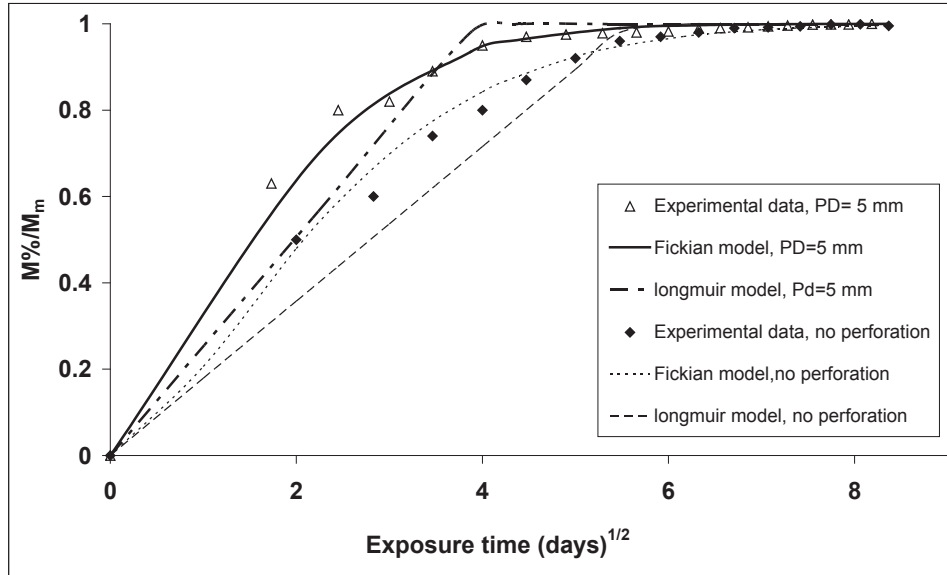
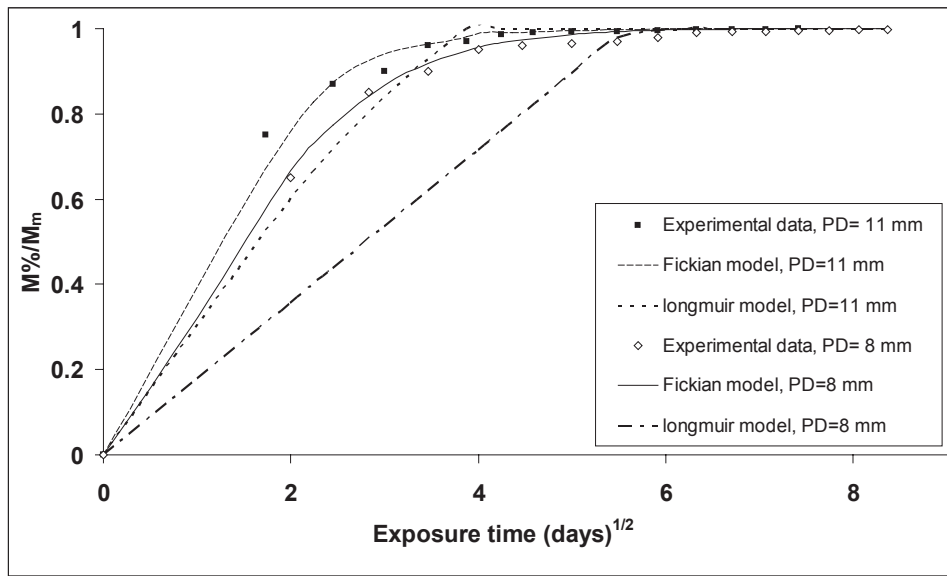


Figure 5.5 Mass absorption of the specimens aged 15% sulfuric acid solution at 60 °C, subject to external load (SCC)

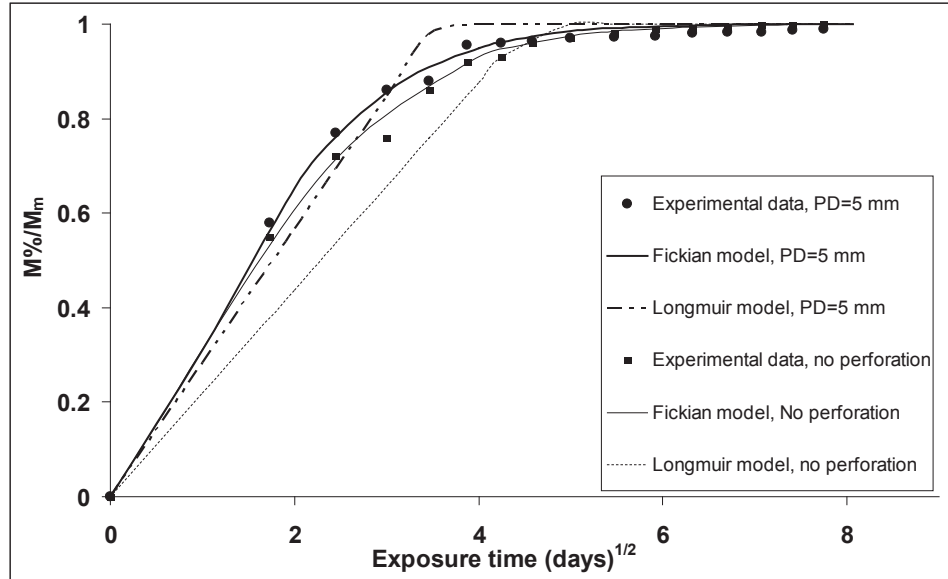


(a)

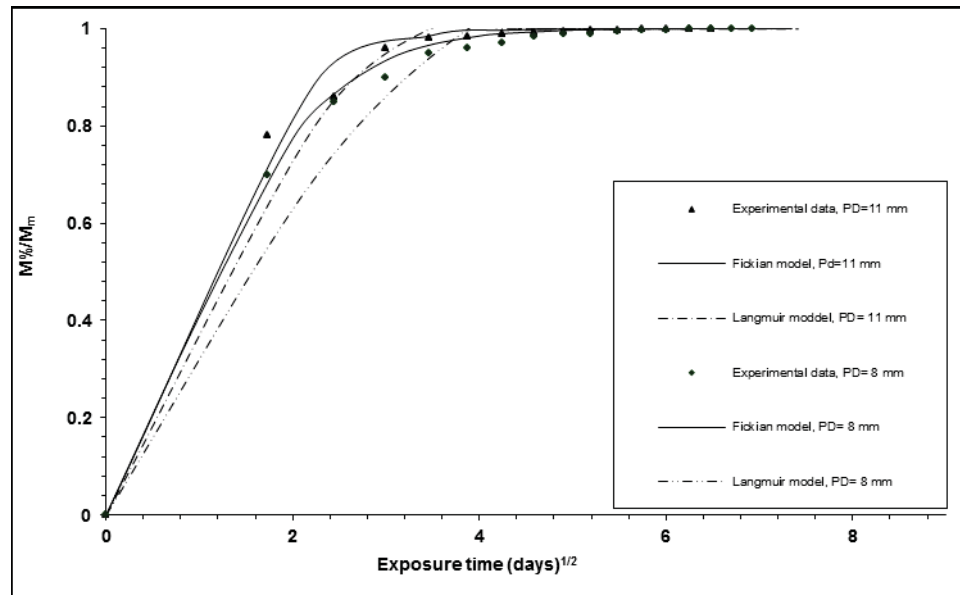


(b)

Figure 5.6 Mass absorption predictions by the Longmuir and Fickian models for the specimens aged in 15% sulfuric acid solution at 60°C; (a) specimens with perforation size: 0 and 5 mm, (b) perforation size: 8 and 11 mm



(a)



(b)

Figure 5.7 Mass absorption predictions by the Longmuir and Fickian models for the specimens aged in 15% sulfuric acid solution at 60°C, subject to external load (SCC); (a) specimens with perforation size: 0 and 5 mm, (b) perforation size: 8 and 11 mm



Figure 5.8 White precipitation as a result of chemical reactions between the fibers and sulphuric acid

5.5.2 MECHANICAL CHARACTERIZATION

As stated, to further investigate the influence of acid absorption and high temperature on the mechanical response of the GFRP, the specimens were subjected to three-point bending tests, during and after the saturation process (the appearance of typical specimens after the saturation process can be seen in Figure 5.9).

To stimulate the behavior of GFRP plates in the given aging conditions, the strength loss curve for each group of specimens was plotted, and is illustrated in Figures 5.10 and 5.11. It can be seen that an increase in the perforation sizes can decrease their resistance to failure and the stress corrosion acidic media can accelerate the strength loss in the specimens more significantly, when compared to aging conditions in the same medium.

The variations of the other flexural properties (i.e., the “Maximum” strain and modulus) have been illustrated in Figure 5.12 and 5.13. As anticipated and clearly evident, increasing the perforation diameter leads to higher diffusion area and hence higher mass absorption, thereby increasing the flexural strain in the aged and SCC conditioned specimens. The resulting response is more plastic in nature, accompanied by a reduction in stiffness (modulus of elasticity) of the perforated coupons by 25% for AG specimens and up to 50% for SCC specimens.

The saturation time, t , can be postulated using the general form of Eq. (5.2) [17]:

$$t = \frac{h^2}{D} \left[\frac{-1}{7.3} \ln \left(1 - \frac{M_{\%}}{M_{\infty}} \right) \right]^{1/0.75} \quad (5.11)$$

By applying Eqs. 5.4-c and 5.6, and considering the influence of the external loading on the diffusion coefficient and perforation sizes, the integration of these equations results in a semi-empirical model that can be used to predict the saturation time for a GFRP composite plate exposed to aging or SCC in acidic solutions:

$$t = \frac{h^2}{D_0 \left(1 + \frac{h}{l} + \frac{h}{w} + \frac{n\pi dh}{2lw} \right)^{-2} (A + B\sigma_{app})} \left[\frac{-1}{7.3} \ln \left(1 - \frac{M_{\%}}{M_{\infty}} \right) \right]^{1/0.75} \quad (5.12)$$

where t is the required time for a specific saturated point, D_0 is the diffusion coefficient in the unstressed status, σ_{app} is the applied stress, which takes a value for SCC specimens, but remains as null for ordinary aged specimens (i.e., not subject to an applied stress); and A and B are empirical constant. The value of A is obtained from the conventional aging test results, while B is obtained from the SCC test results.

Figure 5.14 illustrates the results obtained by the semi-empirical equation (5.12). As can be seen, the normalized predicted results are in reasonably good agreement with the actual test results. Moreover, although the predicted saturation time values are slightly lower for shorter exposure periods, they approach the measured values as the exposure time increases.

From the physical perspective, severe chemical reaction caused visible delamination at the perforation boundaries (see Figure 5.15), which in turn caused swelling of the material.

In summary, it was observed that the increase in perforation diameter, which created larger edge surface areas, ultimately increased the absorption intensity. Greater acid diffusion resulted in increased matrix and fiber corrosion, thereby degrading the flexural properties of the GFRP composite.

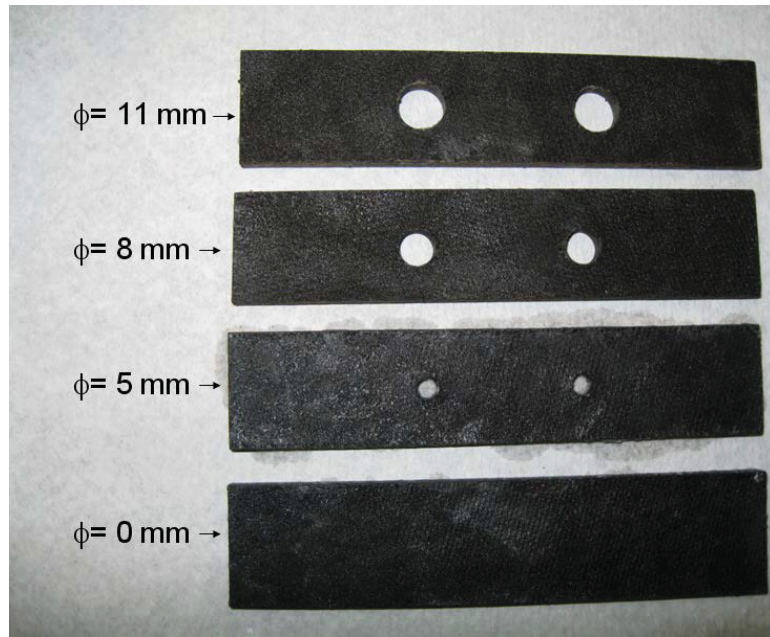


Figure 5.9 Typical GFRP specimens appearance (drastic color change) after being immersed in 15% sulfuric acid solution

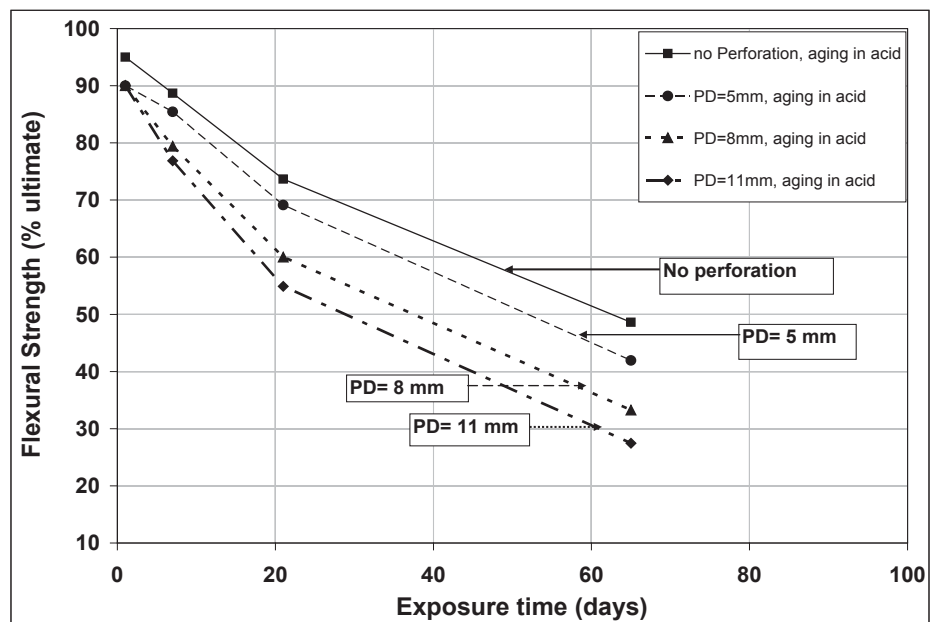


Figure 5.10 Degradation in the flexural strength of the perforated specimens as a function of time and perforation diameter (aged in sulphuric acid)

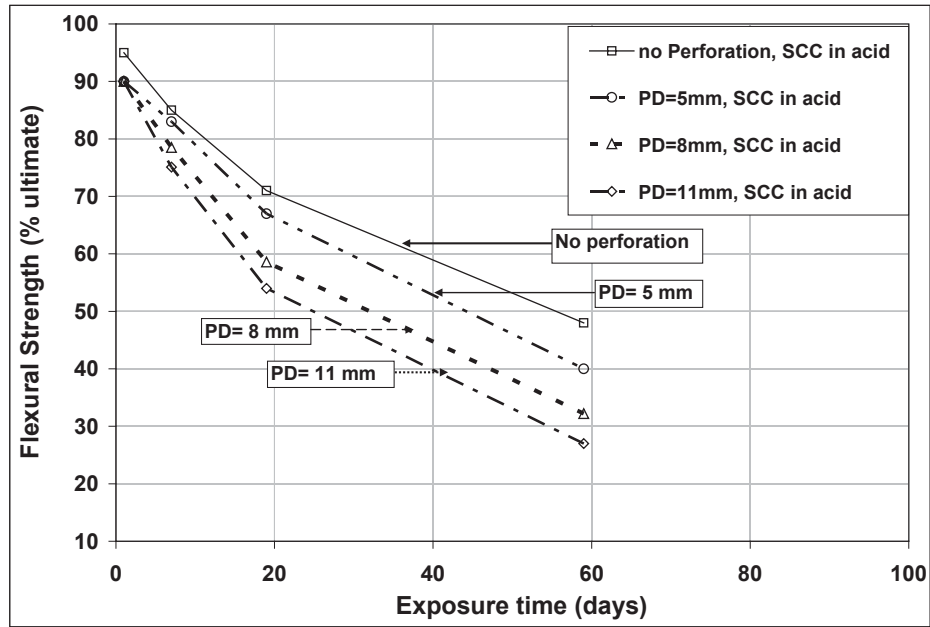


Figure 5.11 Degradation in the flexural strength of the perforated specimens as a function of time and perforation diameter (aged in sulphuric acid, subject to external load)

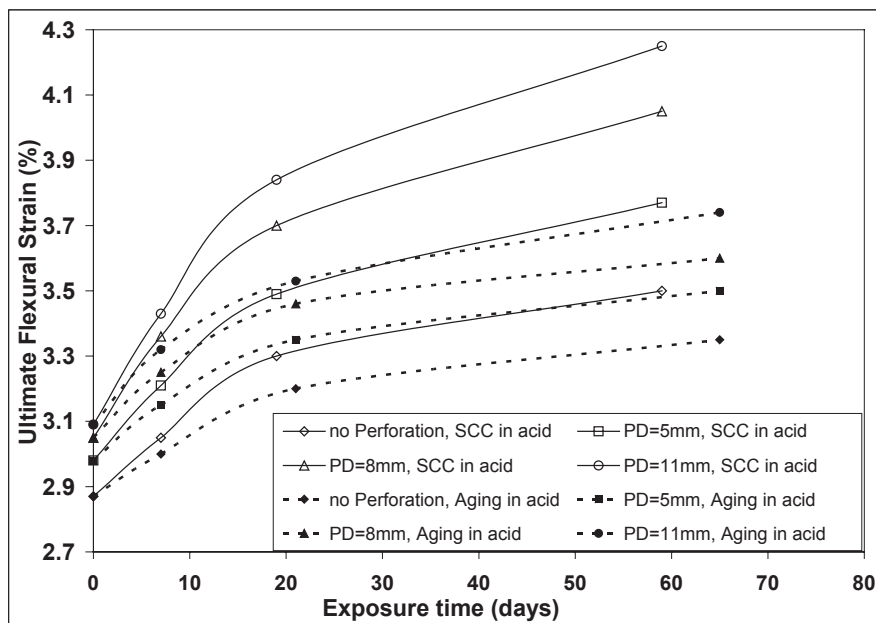


Figure 5.12 Variation in the ultimate flexural strain of perforated specimens aged in acidic solution as a function of conditioning time and perforation diameter

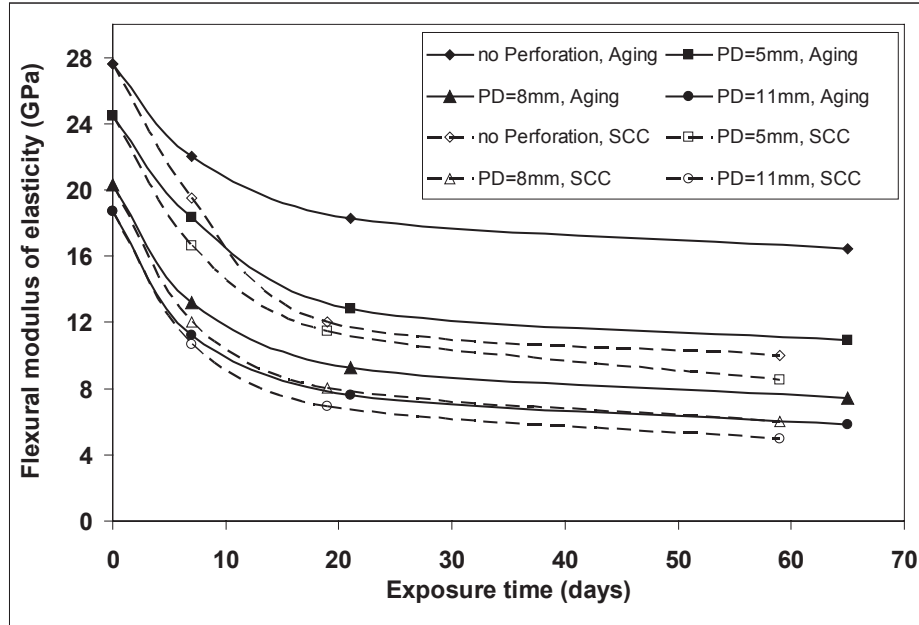


Figure 5.13 Degradation in the flexural modulus of elasticity of the perforated specimens as a function of time and perforation diameter (aged in water & acid)

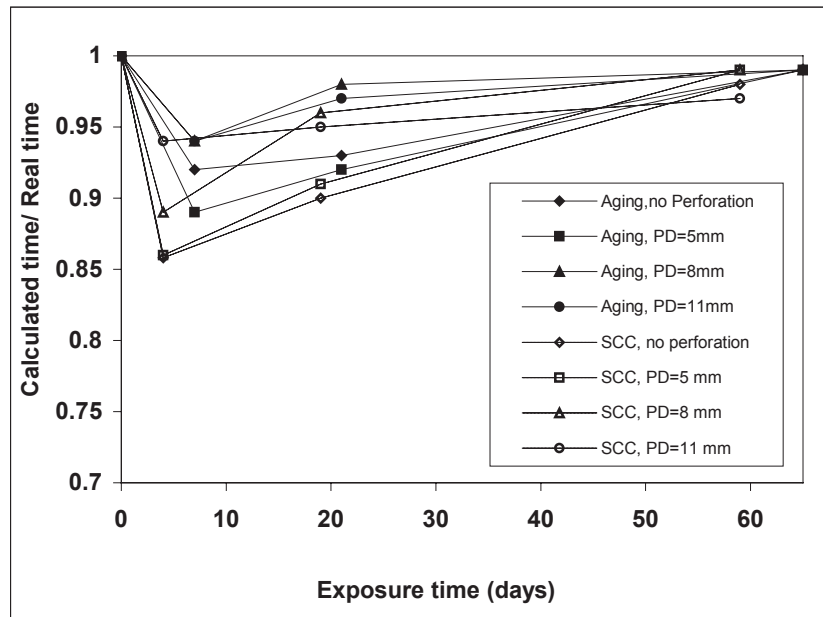


Figure 5.14 The accuracy of the proposed model for estimating the saturation time of the perforated specimens as a function of perforation diameter (aged in 15% sulphuric acid subject to external load)



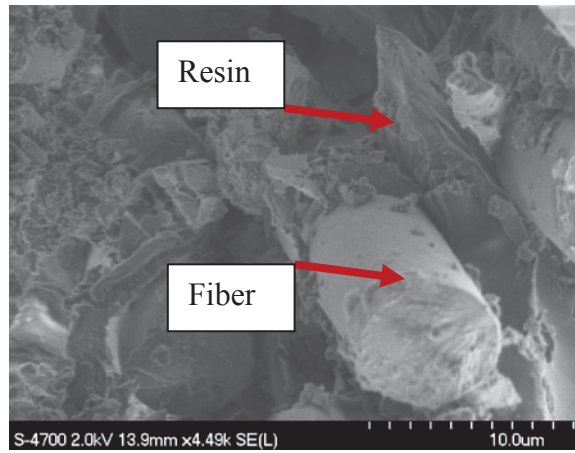
Figure 5.15 Typical delamination seen in the specimens due to the chemical degradation of the resin and fibers

5.5.3 MICROSCOPIC OBSERVATION

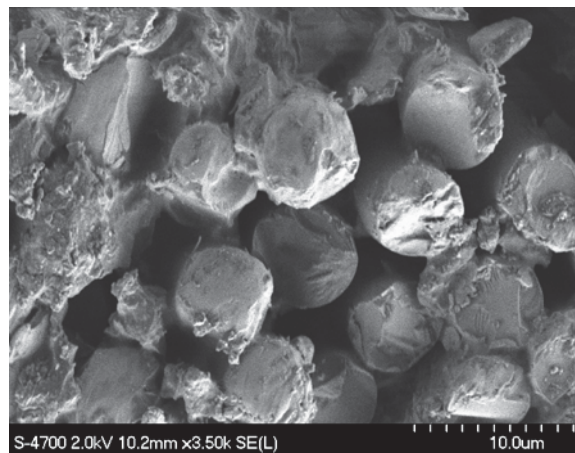
Scanning electron microscope (SEM) images were captured in order to study the influence of the acid diffusion on the microstructures of the perforated composite specimens.

Figure 5.16 shows SEM images of the glass/epoxy specimens before immersion in the acid and after aging and SCC tests in the acid. It can be seen that in the virgin specimen, the fibers had maintained good adhesion bond to the resin and the fiber/resin contact areas are all intact. However, after subjecting the specimens to the acidic medium under the elevated temperature, their interface bond became degraded and the resin regions thinned out (see Figures 5.16(b) and 5.16(c)).

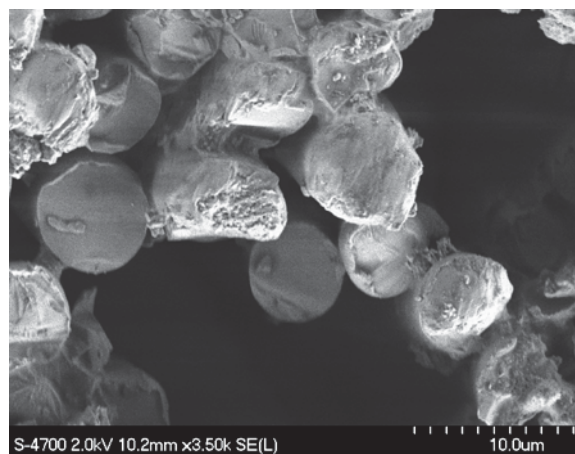
Figure 5.17 shows the effect of the acid attack on the fiber surfaces and the evidence for the presence of helical cracks on the surface. It is believed that the surface ions of the glass fibers that were exposed to acid were leached into the acid; as a result, a combined state of radial and tangential stresses was generated on the fiber's surface, and micro-cracks were initiated. Similar observation made by several researchers corroborates the previously mentioned phenomenon [9, 24].



(a) At virgin state

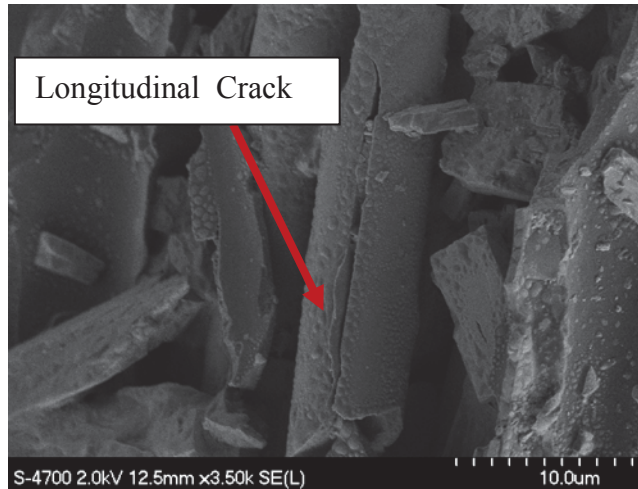


(b) After aging in 15% sulfuric acid medium

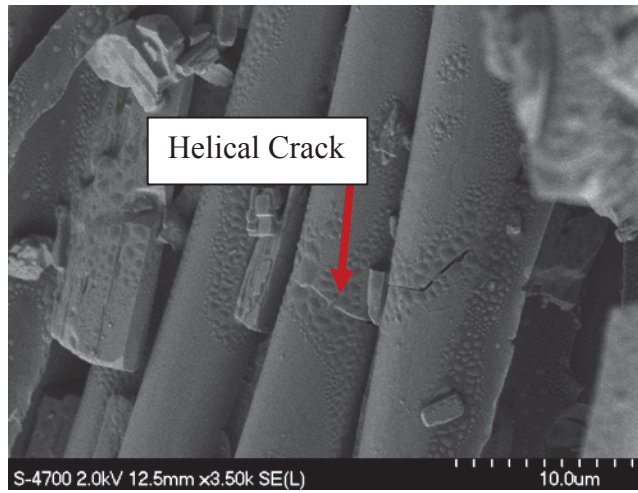


(c) After aging in 15% sulfuric acid subject to external load

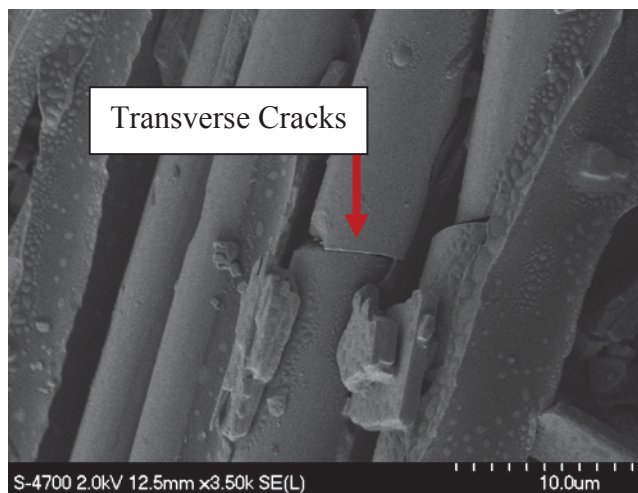
Figure 5.16 Typical failure surfaces of the GFRP specimens before and after immersion in acid



(a) Longitudinal crack on the corroded fibers surface



(b) Helical cracks on the corroded fibers surface



(c) Transverse cracks through the fiber

Figure 5.17 Effect of the acid on fibers surface

5.6 SUMMARY AND CONCLUSIONS

Aging and stress corrosion experiments were conducted on perforated glass/epoxy standard coupons, and the influence of the perforation size on the mass absorption behavior and level of degradation in the flexural properties of the composite specimens was examined. The mechanical tests results revealed that the increase in the perforation size led to an increase in the diffusion area, and in turn, the in mass absorption rate. The mass absorption also directly influences matrix integrity, thus degrading the flexural properties (i.e., strength and stiffness) of the composite. This was also accompanied by increasing the ultimate strain of the composite, which is believed to be the result of matrix plasticization phenomenon. It was also observed that mass absorption rate varied exponentially as a function of diffusion coefficient.

A semi-empirical model was developed for estimating the saturation time of the composite, which accounts for the increase in the edge surface area due to the presence of perforations. The model is also capable of accounting for the effects of stress corrosion. The proposed model can be used to estimate the time period after which the mechanical properties of GFRP composites, aged in harsh environments (e.g., acidic and hot environments), would be degraded.

Moreover, SEM examinations revealed that higher mass absorption accommodated by the larger edge surface area caused further de-bonding of the glass fibers from their surrounding matrix, causing further degradation in the flexural properties of the composite.

In conclusion, when considering the use of perforated GFRP in structural applications that will experience harsh environments (such as in oil wells), the influence of the environment on the composite should be carefully considered to ensure that the structure would perform satisfactorily during the anticipated service life.

5.7 ACKNOWLEDGEMENTS

The financial support of the Natural Sciences and Engineering Council of Canada (NSERC) in support of this work is gratefully acknowledged. The access to IRM (Institute of Research for Materials) SEM facilities is greatly appreciated.

5.8 REFERENCES

- [1] Shokrieh M M, Memar M. Stress corrosion cracking of Basalt/Epoxy composites under bending loading. *Appl. Compos. Mater.* 2010; 17: 121-35
- [2] Myres T J, Kytomaa H K, Smith T R. Environmental Stress corrosion cracking of fiber glass: Lessons learned from failures in the chemical industry. *J. Hazard. Mater.* 2007; 142: 695-704
- [3] Sapalidis S N, Hogg P J, Youd S J. High temperature acidic stress corrosion of glass fiber composites. *J. Mater. Sci.* 1997; 32: 309-16
- [4] Mula S, Bera T, Ray P K, Ray B C. Effects of Hydrothermal Aging on Mechanical Behavior of Sub-zero Weathered GFRP Composites. *J Reinf. Plas. & Compos.* 2006; 25: 673-80
- [5] Davies P, Mazeas F, Casari P. Sea Water Aging of Glass Reinforced Composites: Shear Behaviour and Damage Modelling. *J. Compos. Mater.* 2001; 35: 1343-72
- [6] Roy S. Prediction of Anomalous Hygrothermal Effects in Polymer Matrix Composites. *J. Reinf. Plast. Compos.* 1999; 19: 1197-207
- [7] Aditya P K, Sinha P K. Diffusion Coefficients of Polymeric Composites Subjected to Periodic Hygrothermal Exposures. *J. Reinf. Plast. Compos.* 1992; 11: 1035-47
- [8] Jones F R, Rock J W, Bailey J E. The environmental stress corrosion cracking of glass fiber- reinforced laminates and single E-glass filaments. *J. Mater. Sci.* 1983; 18: 1059-71
- [9] Maxwell A S, Broughton W R, Dean G, Sims G D. Review of accelerated aging methods and lifetime prediction techniques for polymeric materials. NLP report, DEPC MPR 016, National Physical Laboratory, Teddington, UK. 2005.
- [10] Caddock B D, Evans K E, Hull D. Stress corrosion failure envelopes for E-glass fiber bundles. *J. Mater. Sci.* 1990; 25: 1498-2502
- [11] Nakayama M, Hosokawa Y, Muraoka Y, Katayama T. Life prediction under sulfuric acid environment of FRP using X-ray analysis microscope. *J. Mater. Proc. Technol.* 2004; 155-156: 1558-63

- [12] Qiu Q, Kumosa M. Corrosion of E-glass fibers in acidic environments, *compos. Sci. & tech.* 1997; 57: 497-507
- [13] Kumar S, Sharma N, Ray B C. Acidic Degradation of FRP Composites. In: *Proc. the National Conference on Developments in Composites, India, 2007.*
- [14] Yilmaz T, Sinmazcelik T. Experimental investigation of acid environment influences on load-bearing performance of pin-connected continuous glass fiber reinforced polyphenylene sulfide composites. *Polym. Compos.* 2010; 31: 1-9
- [15] Jones RL, Stewart J. The kinetics of corrosion of E-glass fibers in sulphuric acid. *J Non-cryst Solids.* 2010; 356: 2433-6
- [16] Jones R L, Betz D. The kinetics of corrosion of E-glass fibers in hydrochloric acid. *J. Matls. Sci.* 2004; 39: 5633-7
- [17] Shen C H, Springer G S. Moisture Absorption and Desorption of Composite Materials. *J. Compos. Mater.* 1976; 10: 2-20
- [18] Eslami Sh, Taheri F. Degradation of perforated E-glass/epoxy plates submerged in water and acidic media under elevated temperature, In *Proc. the Second Joint US-Canada Conference on Composites, Montreal, Canada. 2011.*
- [19] Fahmy A A, Hurt J C. Stress dependence of water diffusion in epoxy resin. *Polym. Compos.* 1980; 1: 77-80
- [20] Whitaker G, Darby M I, Wostenholm G H, Yates B, Collins M H, Lyle A R, Brown B. Influence of temperature and hydrostatic pressure on moisture absorption in polymer resins. *J. Mater. Sci.* 1991; 26: 49-55
- [21] Carter H G, Kibler K. Langmuir-Type Model for Anomalous Moisture Diffusion in Composite Resins. *J. Compos. Mater.* 1978; 12: 118-31
- [22] ASTM D790-10, Standard test methods for flexural properties of unreinforced and reinforced plastics and electrical insulating materials, ASTM, West Coshohocken, PA, 2010

[23] ASTM D 5229, Standard Test Method for Moisture Absorption Properties and Equilibrium Conditioning of Polymer Matrix Composite Materials, ASTM, West Coshohocken, PA, 2004.

[24] Lewis G, Bedder S W. Stress corrosion of glass fibers in acidic environments. *J. Mater. Sci. Lett.* 1984; 3: 728-32.

CHAPTER 6 EXPERIMENTAL INVESTIGATION OF THE EFFECT OF AGING ON PERFORATED COMPOSITE TUBES UNDER AXIAL COMPRESSIVE LOADING*

Shiva Eslami, Ramadan A. Esmaeel* and Farid Taheri

Department of Civil and Resource Engineering, Dalhousie University

*Note: The structural testing and computational assessment presented in this chapter are conducted by Dr. R. Esmaeel

6.1 ABSTRACT

The use of fiber reinforced polymer composite materials (FRP) in various applications such as aerospace, automotive, sport equipment, and oil and gas industries has been growing at a steady rate in recent years. The potential use of perforated FRP tubes (pipes) in oil and gas industry related applications can become significantly greater, provided that the influence of the harsh environmental conditions specific to the industry could be tolerated by the materials used to form such tubes, with minimal degradation to the system's mechanical and physical properties. Unfortunately, there is no adequate database of information in the literature in regards to the long term response of perforated FRP tubes.

The purpose of this study is therefore to investigate whether FRP could be confidently used in structural applications that are primarily subjected to compressive loading and exposed to harsh environments, without significant deterioration of their physical and mechanical properties. For that, three sets of perforated glass fiber-reinforced plastic (GFRP) pipes were fabricated and subjected to accelerated aging conditions in an acid. Subsequently, the pipes were tested to failure under an axially applied compressive load. Results showed a considerable decrease in the load carrying capacity and axial stiffness of perforated pipes having certain D/t ratios, as a result of the aging.

Keywords: Axial loading; laminated cylindrical tubes; perforation; experimental investigation.

* Accepted for publication in the Advanced Composite Materials Journal

6.2 A BRIEF REVIEW OF THE RELEVANT RESEARCH

The use of FRP materials to fabricate waste water pipes has gained popularity in recent years as several wastewater treatment plants are currently replacing their traditional steel with pipes made of FRP. However, the presence of harsh environments can accentuate the corrosion process in FRP pipes. Due to the chemical nature of the polymeric matrix used in FRP, the loss in the mechanical properties can be attributed to the resin plasticization, and more importantly, to the degradation of the fiber/matrix interface bond [1]. The rate of degradation would be a strong function of the surrounding corrosive environment temperature. For instance, most epoxy matrices are recommended for use in environments with temperatures below 60 °C, as the thermally induced degradation is usually initiated at 70 °C [2]. Long-term exposure of FRP to corrosive environments at elevated temperatures has been shown to also strongly affect the fiber strength [3].

Startsev et al. [4] showed that the exposure of polymer composites to climatic aging would cause the through-the-thickness mechanical properties across the thickness to significantly degrade. Tsotsis et al. [5] observed that FRP specimens' aging process was significantly accelerated when the material was subjected to large pressure magnitudes (especially in those with $[\pm 45^\circ]_2s$ layup, which were subjected to a tensile load). Boukhoulda et al. [6] subjected artificially aged E-glass/polyester composite plates to impact forces by means of a drop-mass. They reported the non-Fickian and Langmuir-type characteristics of the moisture absorption kinetics of the plate specimens.

Using the fracture mirror measurements on the broken ends of the fibers, Liao et al. [7] provided clear evidence that the fiber strength of the pultruded glass fiber reinforced vinyl ester matrix composite coupons was decreased due to aging of the composite in water. Abdel-Magid et al. [8] studied aging of E-glass/epoxy composite specimens by conditioning their FRP specimens in a wet environment under an applied mechanical loading. Their results revealed that a noticeable loss in the mechanical properties (modulus and strength) took place as a result of the combined effects of loading, moisture and temperature. Bagherpour et al. [9] examined the effects of concentrated HCl acid on the mechanical response of a fiber-glass polyester composite. Their SEM micrographs

evidenced a considerable strength reduction due to the loss of the fiber/matrix interfacial bond.

The degradation of the mechanical properties of glass/epoxy tubular specimens as a result of environmental effects has also been studied experimentally by Ellyin and Maser [10]. They immersed their filament wound specimens in distilled hot water for four months and they noticed that the swelled matrix negatively impacted the functional failure of the specimens.

Moreover, the plasticization that occurred in the matrix reduced its stiffness considerably and also reduced the cohesion of the fiber/matrix interface, thus giving a greater chance for fiber pull out. Guedes et al. [11] studied the effect of moisture absorption on the creep response of glass-fiber/thermosetting-matrix composite pipes. As a conclusion, they stated that the use of the power law relationship could provide a good prediction of the long term response of such pipes. Yao and Ziegmann [12] performed an experimental investigation on the effects of moisture and temperature aging on the mechanical performance of glass/epoxy composite pipes under three point bending loading conditions. They suggested that moisture would exhibit a similar effect on aging as temperature. Almeida et al. [13] verified the Fick model's applicability for describing the water absorption response of glass/vinyl-ester composite pipes.

In this paper, the stability response of perforated E-glass/epoxy pipes, having been aged in an acidic environment, has been investigated experimentally. The response of the aged pipes was then compared to those of their healthy (un-aged) counterparts.

6.3 EXPERIMENTAL INVESTIGATION

In this study, full scale composite tube specimens were fabricated and tested in both healthy and aged states. Detailed description of specimen preparation, ageing conditions and experimental procedure is provided in the following sections.

6.3.1 FABRICATION AND CONDITIONING OF GFRP CYLINDRICAL SPECIMENS

All GFRP pipes considered in this study were fabricated by wrapping two or three layers of a stitched fabric having a typical ply sequence of $[45^{\circ}/-45^{\circ}/90^{\circ}]$ (angles are with

respect to the longitudinal axis of the pipes). To facilitate the release of the specimens from forming mandrel, a temperature resistant mold-release agent was applied to the outer surface of the mandrel. The alignment of the final pipe specimens was checked using a dial gauge having a resolution of 0.01 mm, while the thickness of the cured pipes was measured using a digital micrometer with 0.01mm accuracy. All specimens were then carefully cut to the specified length using a diamond coated saw, ensuring that their edges were parallel, and orthogonal to the pipe axial axis to facilitate a uniformly distributed load during testing. A total of 36 pipe specimens were fabricated, half of which were professionally perforated

The perforation pattern and the details of the geometrical features of the test specimens are clearly shown in Figure 6.1. The total length of each pipe specimen was $L= 300$ mm with a distance of $S = 50$ mm between the rows of perforations (see Figure 6.1). The 36 specimens were divided into two main categories; perforated and non-perforated. Each category was divided into three subcategories according to specimen's diameter to thickness ratio (i.e., $d/h=48.8$, 71.5 and 27.5 , respectively). More information on the specimen identification/classification codes and the dimensions are provided in Table 6.1. using a high speed milling machine.

Three out of six specimens per subcategory were submerged in a 15% diluted sulphuric acid solution and placed in a temperature controlled chamber at 60°C until saturation. The acid, its concentration and temperature were chosen to simulate the harsh chemical environment typically experienced by liners in directional oil wells. The purpose of the elevated temperature was to simulate the typical environment found in most directional oil wells, which expedites the aging process.

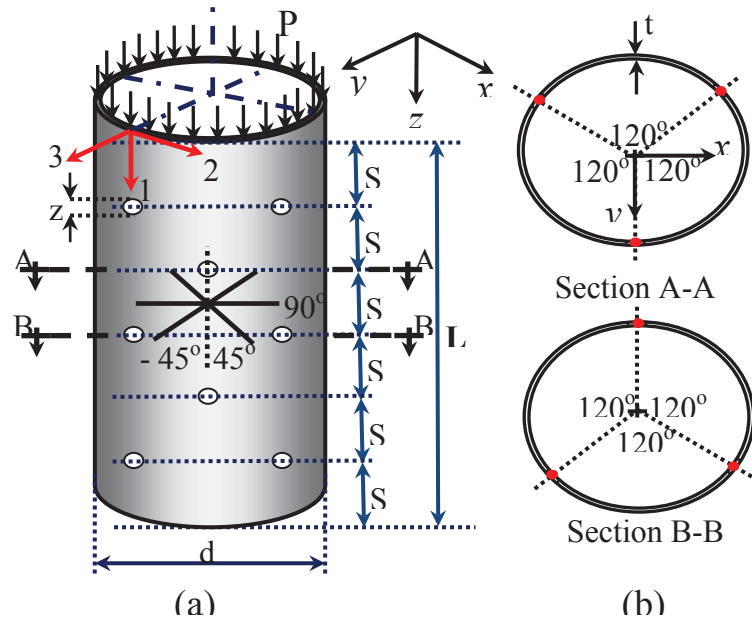


Figure 6.1 Perforated tube: (a) tube geometry, (b) cross sections showing perforation arrangements

Table 6.1 Test specimens' specification

Specimen ID	Inner Diameter, (mm)	Wall Thickness, (mm)	Lay up	Condition
AI	107.3	2.2	$[\pm 45^\circ/90^\circ]_3$	Intact
AP		2.2	$[\pm 45^\circ/90^\circ]_3$	perforated
BI	107.3	1.5	$[\pm 45^\circ/90^\circ]_2$	Intact
BP		1.5	$[\pm 45^\circ/90^\circ]_2$	perforated
CI	60.4	2.2	$[\pm 45^\circ/90^\circ]_3$	Intact
CP		2.2	$[\pm 45^\circ/90^\circ]_3$	perforated

6.3.2 TEST EQUIPMENT AND PROCEDURE

Specially designed grips were fabricated to hold the test specimen in the loading machine; this fixture is composed of two circular end plates having a 10 mm deep groove. The grooves were basically used to prevent the thin walled specimen from

slipping during the application of the compressive load. An INSTRON servo-hydraulic universal testing machine controlled with 8600+ electronics was used for testing the specimens. The grips and test set up are shown in Figure 6.2. To maintain a concentric axial load throughout the experiment, the upper circular plate was composed of two thick plates separated by a steel ball to prevent any misalignment due to the applied axial load. The specimens were loaded axially at a rate of 0.5 mm/min, and the applied load was measured using a 250 kN load cell, while the ends shortening was established through the actuator's crosshead movement, recorded by the electronics. For each specimen group, at least one specimen was instrumented with a set of strain gauges, mounted at the mid height of the specimen, on the two opposing faces. The main purpose of these gauges was to ensure that the axial load was applied in a concentric fashion and that the specimens were experiencing a uniformly distributed axial strain.

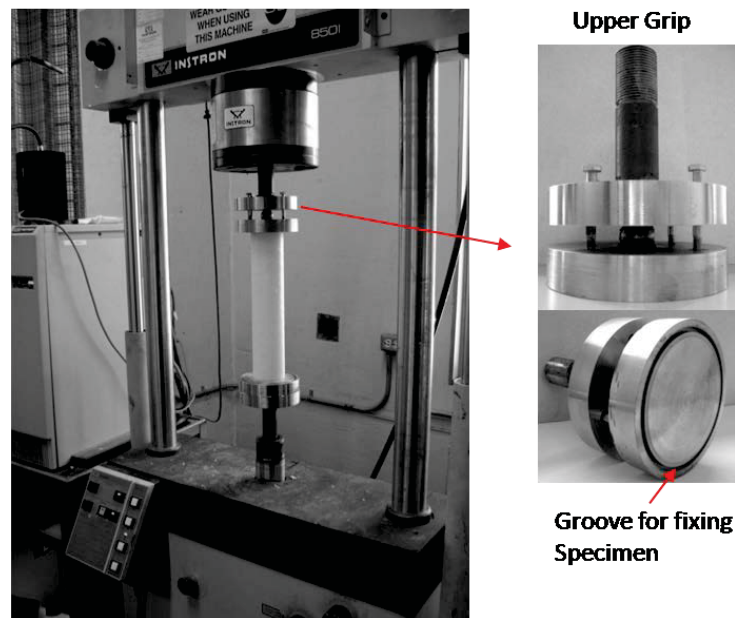


Figure 6.2 Buckling test facility

The aged specimens were tested immediately after having been taken out of the environmental chamber. Specimens were covered with plastic wrap to avoid the evaporation of the acid from the specimen during the transportation of the specimens from the chamber to the testing lab. For specimens receiving strain gauges, a small window was cut off of the plastic wrap to allow for the surface preparation and installation of the gauges. Since the aged specimens were submerged in the sulphuric acid

and were fully saturated by the acid, their surfaces needed to be neutralized using a sodium hydroxide solution before the strain gauges could be installed.

The strain gauge's data was captured through a data acquisition system with an analog input module (NI-9215, in cDAQ-9172 Compact Chassis, manufactured by the National Instruments Inc., Austin, Texas). The sampling frequency was kept at 20.0 kHz during all experiments.

6.4 RESULTS AND DISCUSSION

As stated, the foremost objective of this research work is to investigate the aging effects on the axial compressive load carrying capacity and stability response of the perforated GFRP pipes conditioned in an acidic environment. Typical failure patterns observed in the un-aged and aged specimens are illustrated in Figure 6.3. The visual inspection of the pipes, immediately after the specimens were taken out of the chamber, clearly evidenced a considerable loss of resin in the aged specimens. It was also evident that the material was fully saturated by the acid; as a result, the saturated specimens' wall-thickness was increased by approximately 10% compared to that of un-aged (virgin) counterparts.

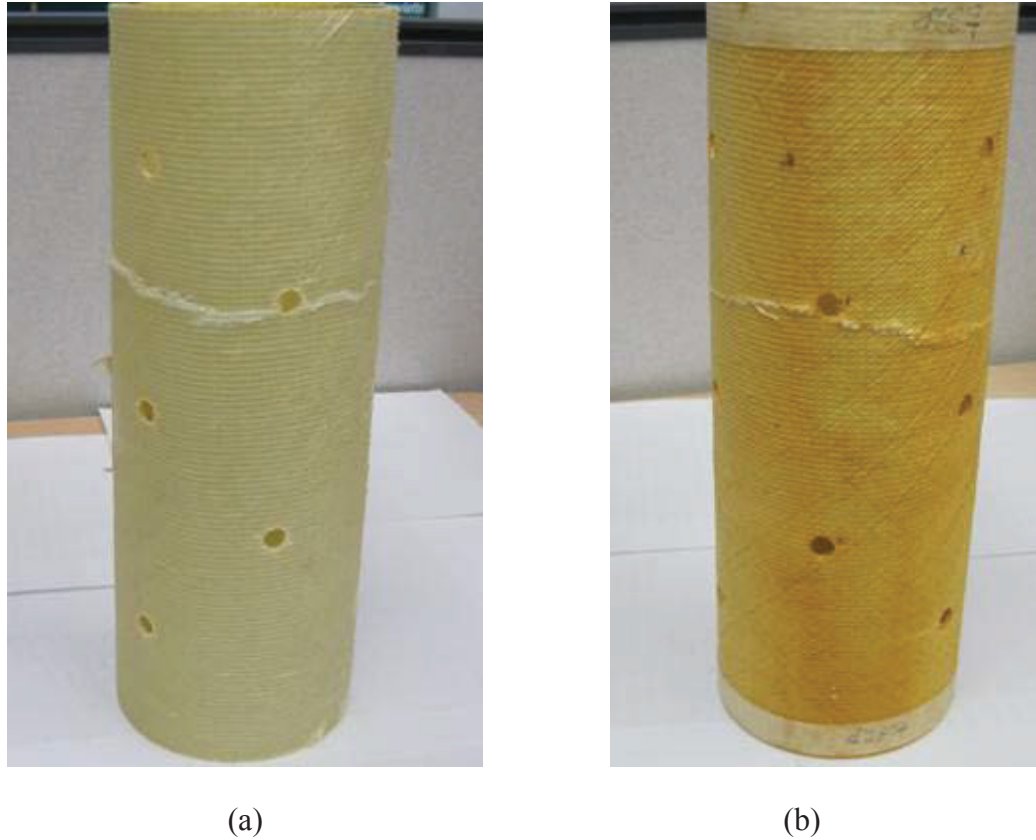


Figure 6.3 Typical failure patterns a) un-aged specimen b) aged specimen

6.4.1 INFLUENCE OF ACIDIC AND ELEVATED ENVIRONMENT ON THE MATERIAL

Prior to discussion of the test results, it would be prudent to briefly review the diffusion mechanism of liquids into composites. In polymer composites, the diffusion process could be modeled using Fick's solution, described by the following [13]:

$$\frac{M_{\%}}{M_m} = 1 - \frac{8}{\pi^2} \sum_{n=0}^{\infty} \frac{1}{(2n+1)^2} \exp \left[-D_c (2n+1)^2 \frac{\pi^2 t}{h^2} \right] \quad (6.1-a)$$

which can be simplified and represented by:

$$\frac{M_{\%}}{M_m} = \tanh \left[\frac{4}{h} \sqrt{\left(\frac{D_c t}{\pi} \right)} \right] \quad (6.1-b)$$

In the above equations, $M\%$ is the percent liquid (here, acid) absorbed at time t , and M_m is the maximum liquid contents, respectively, D_c is the diffusion coefficient and h is specimen's thickness.

The mass change rate in the specimens can be calculated by:

$$M_t = \frac{m - m_0}{m_0} 100\% \quad (6.2)$$

where m_0 , m and M_t are the initial mass, the mass content at time t and the absorbed mass percent at time t , respectively.

The weight change rate curves versus the square root of exposure time in aged specimens made from the materials used to fabricate the pipes are illustrated in Figures 6.4-6.6 for various composite thicknesses, diameters and perforation conditions. In these figures, the solid symbols illustrate the experimental test results and the solid line reflects the results obtained using the theoretical model (i.e., equation 6.1-b). Comparison of the absorption curves at different d/h ratio indicates that an increase in the ratio would increase the absorption rate; furthermore, it also implies that the perforations would facilitate further diffusion, hence accelerating the absorption rate.

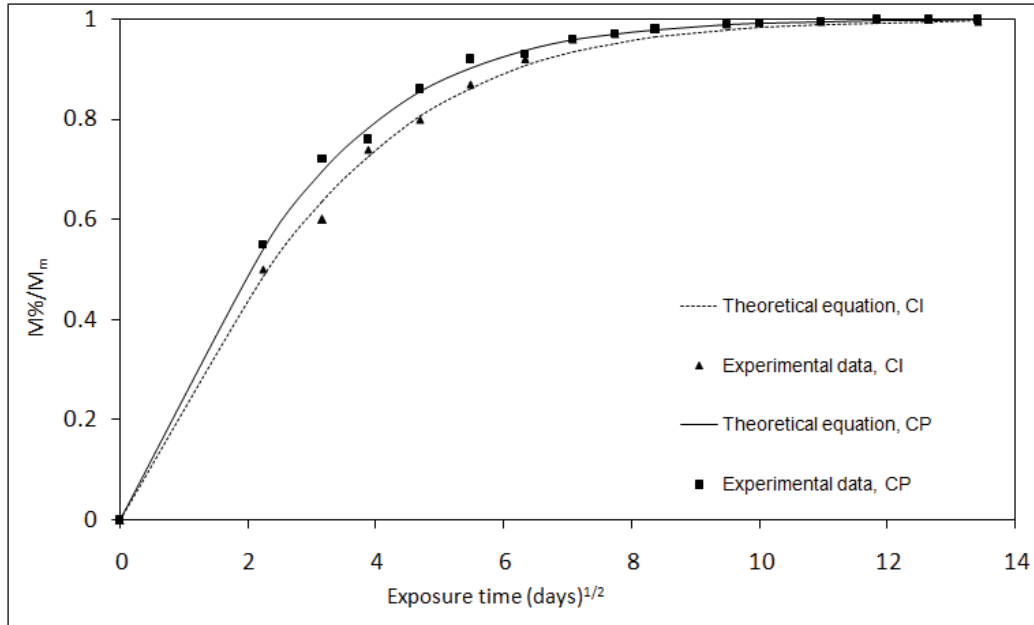


Figure 6.4 Variation of mass absorption as a function of time for pipe with $d/h=27.5$ aged in 15% sulfuric acid at $60\text{ }^{\circ}\text{C}$

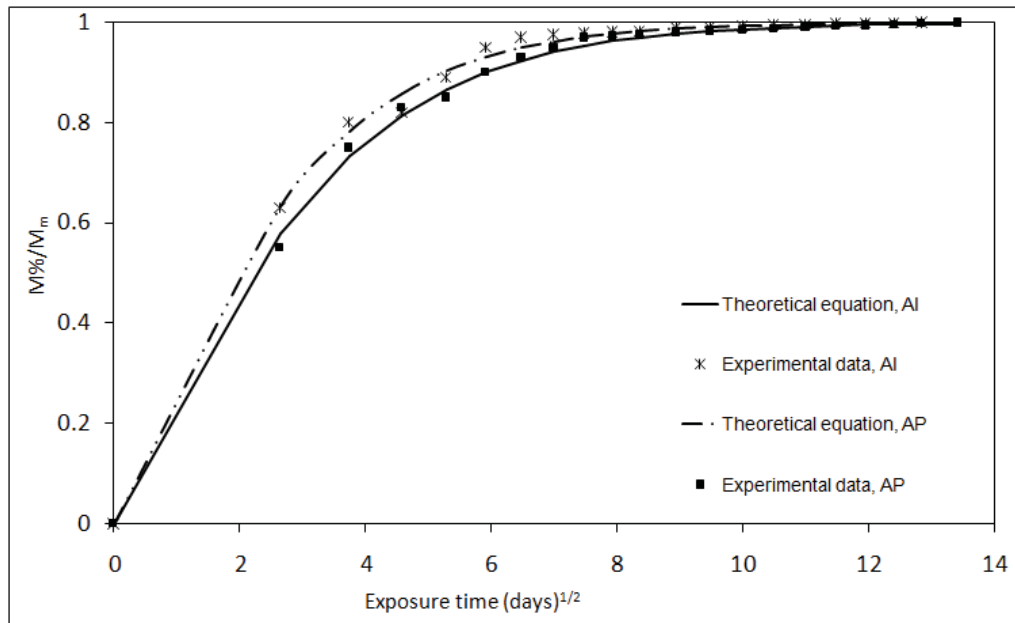


Figure 6.5 Variation of mass absorption as a function of time for pipe with $d/h=48.8$ aged in 15% sulphuric acid at $60\text{ }^{\circ}\text{C}$

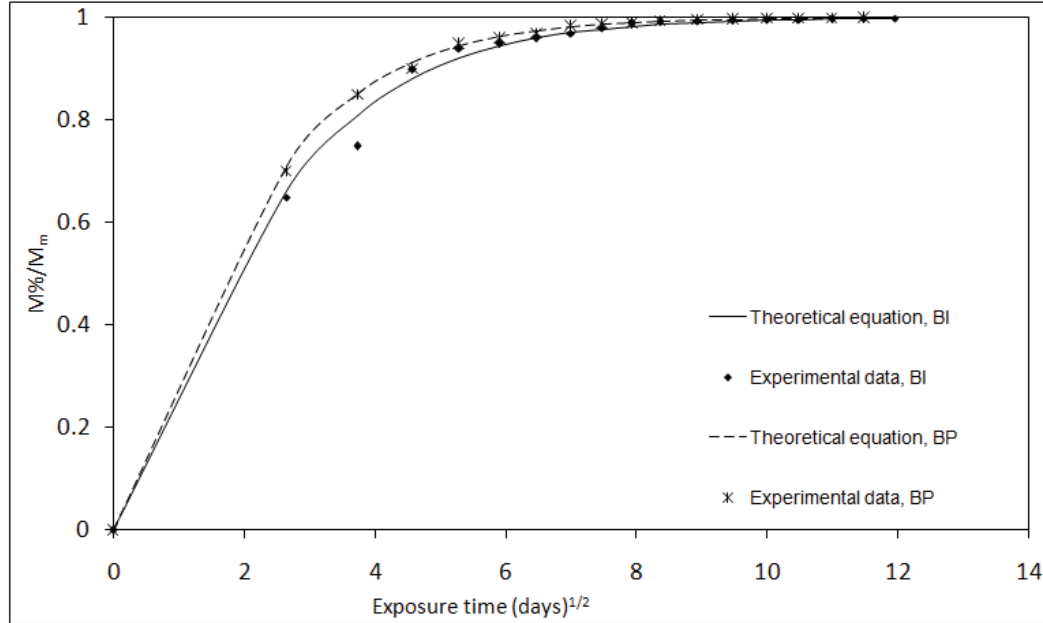


Figure 6.6 Variation of mass absorption as a function of time for pipe with $d/h=71.5$ aged in 15% sulphuric acid at 60 °C

6.5.2 INFLUENCE OF ACIDIC AND ELEVATED TEMPERATURE ON THE LOAD BEARING CAPACITY OF THE PIPES

Figure 6.7 shows the axial load versus end-shortening curves of typical virgin and aged non-perforated (intact) and perforated tubes with d/h ratio of 48.8. A considerable decrease in both the load carrying capacity and axial stiffness of the pipe is evident.

The load carrying capacity and axial stiffness of each group of specimens investigated in this study are reported in Table 6.2, based the specimen codes identified in Table 6.1. It can be seen from the results presented in this table that the axial stiffness of the aged pipes decreased by a maximum of 57%, leading to maximum end shortening of 46%, while the critical load was decreased by a maximum of 48%. Interestingly, the relative decrease in the ultimate strength of perforated pipes after aging was lower than that of the non-perforated aged pipes (by approximately 28%). Moreover, the aged non-perforated pipes exhibited greater end shortening than the perforated aged pipes; nevertheless, the overall axial stiffness of the aged perforated and non-perforated pipes were similar. As also seen, the responses of the aged specimens (for both virgin and perforated pipes) are somewhat nonlinear, evidencing the plasticization of the resin.

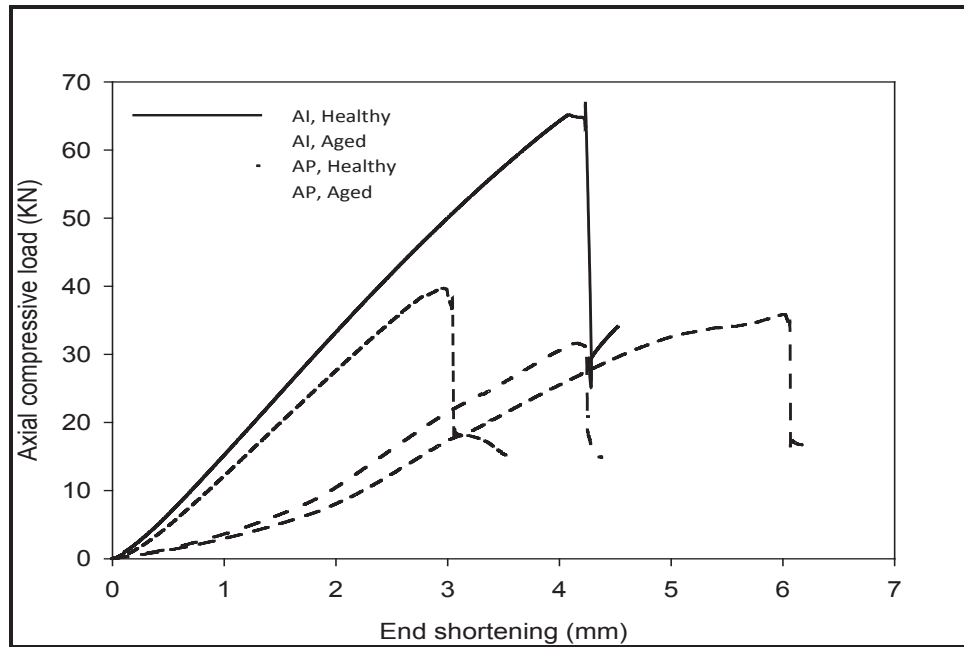


Figure 6.7 Experimental load versus end-shortening curves (AI and AP, D/t=48.8)

Table 6.2 Experimental results of buckling tests

		Axial stiffness (N/mm)	Critical load (N)	End-shortening (Mm)	Axial stiffness (N/mm)	Critical load (N)	End-shortening (mm)
		Healthy pipes			Aged pipes		
48.8	AI	18071	66295	4.15	7692	34128	6.07
	AP	15794	43122	3.08	9985	31050	4.24
71.5	BI	9622	28069	3.55	8750	26588	4.26
	BP	7849	18020	2.63	4800	15035	4.13
27.5	CI	10729	36276	4.01	10100	35384	4.39
	CP	9858	27563	3.31	9850	25213	3.57

The comparison of the axial and hoop strains of ($d/h=48.8$) group aged pipes is shown in Figure 6.8. As seen, the non-perforated pipes experience larger axial strain than the perforated pipes.

To further investigate the effect of aging of perforated pipes, the results of the second group of specimens ($d/h=71.5$) are shown in Figures 6.9 and 6.10. It should be noted that this set of pipes has the same inner diameter as the first group, but their wall-thickness is thinner ($2/3$ of the previous group). It can be inferred from Figure 6.9 that the steady axial stiffness (i.e., the slope of the major linear portion of the load-deformation curve) is only 14% lower than that of the healthy pipes, as a result of aging. However, for the perforated pipes this ratio jumped to almost 39%, as shown in Figure 6.9. This decrease in the axial stiffness can be attributed to the fact that the existence of perforations increased the acid absorption surface areas and hence decreases the overall stiffness of the aged pipes. In the case of the non-perforated pipes, there was virtually no change in the axial load carrying capacity of the virgin and aged pipes after aging. However, there was a noticeable decrease in the maximum sustained load by the perforated pipes of the same group. All the aged pipes in both categories exhibited a noticeably larger deformation before reaching the ultimate failure load. In fact, in some cases the aged pipes deformed more than one and half times of that of the virgin counterpart. The results obtained from the strain gauges placed at the mid-height of both healthy and aged pipes are shown in Figure 6.10. The nonlinear variation of the strain as a function of the applied load of the aged specimens, which is in concert to the response of aged specimens depicted in Figure 6.9, further confirms the resin plasticization phenomenon as a result of aging in the acidic solution.

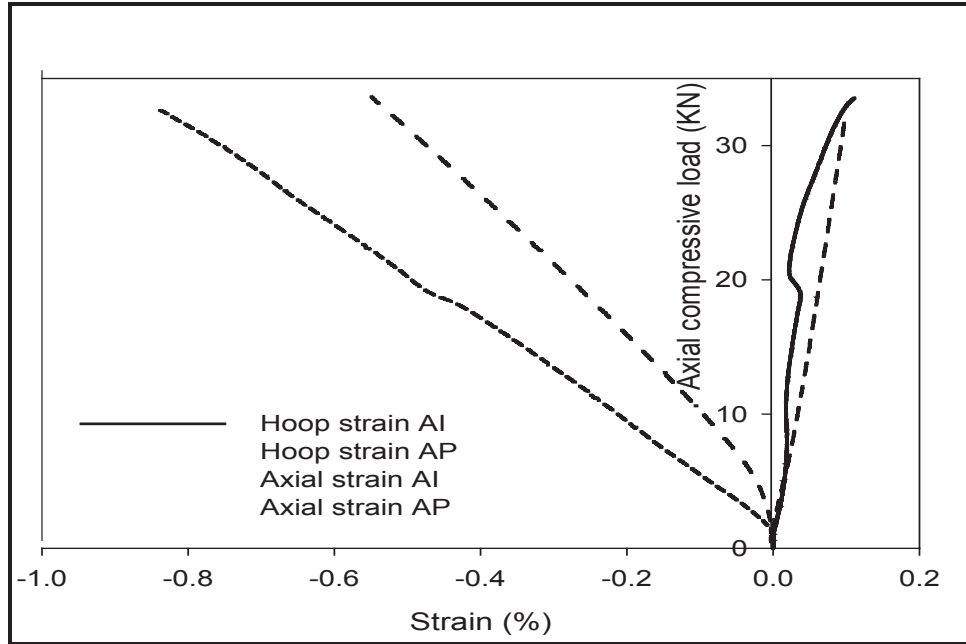


Figure 6.8 Hoop and axial strains for non-perforated and perforated pipes (AI and AP, $d/h=48.8$)

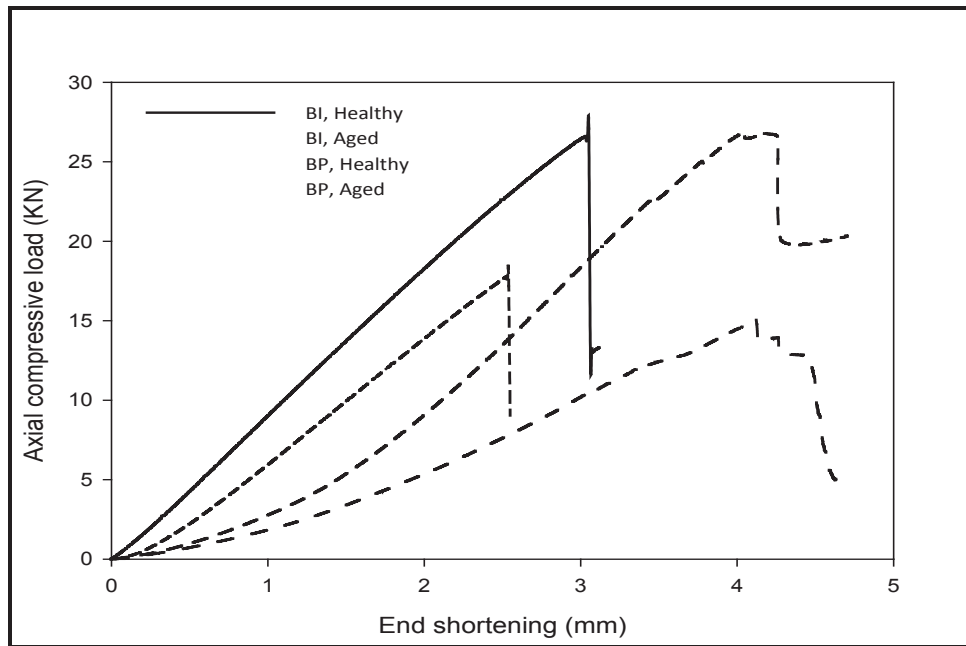


Figure 6.9 Experimental load versus end-shortening curves (BI and BP, $d/h=71.5$)

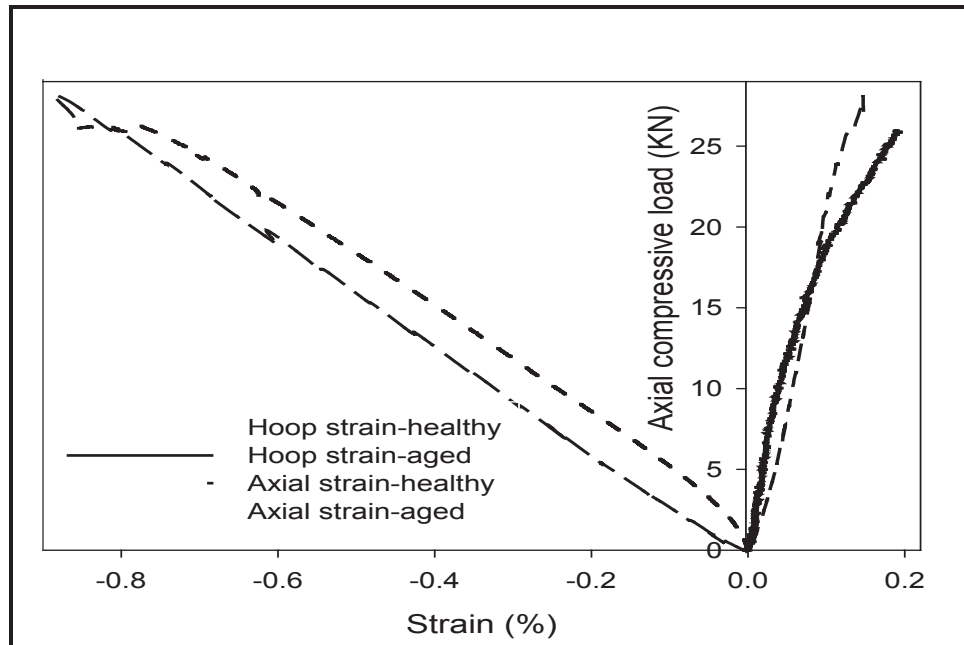


Figure 6.10 Hoop and axial strains for non-perforated pipes in both healthy and aged states (BI, $d/h=71.5$)

The third group of specimens, comprised of a set of a smaller diameter pipes (i.e., with $d/h=27.5$), when compared to the first two groups ($d/h= 48.8$ and 71.5), but had the same thickness as those in group 1. Figures 6.11 and 6.12 present third group's results. There was no significant change in either the axial stiffness or in the load carrying capacity as a result of the aging in comparison to the appreciable changes noted in the test results of the first two groups. The noted response is believed to be due to the comparatively limited surface areas for the acid to wick into the composite, since in comparison, both the surface area of the small diameter pipes and the total cross-section area of the perforations are lesser when compared to the first case. This hypothesis is further supported by noticing the slightly lower ultimate capacity exhibited by the perforated pipes of this group in comparison to the non-perforated pipes; there is indeed a marginally larger cross section area for the acid to wick into the composite in the case of the perforated pipes compared to the non-perforated pipes, though the area is not as appreciable as that in Group 1.

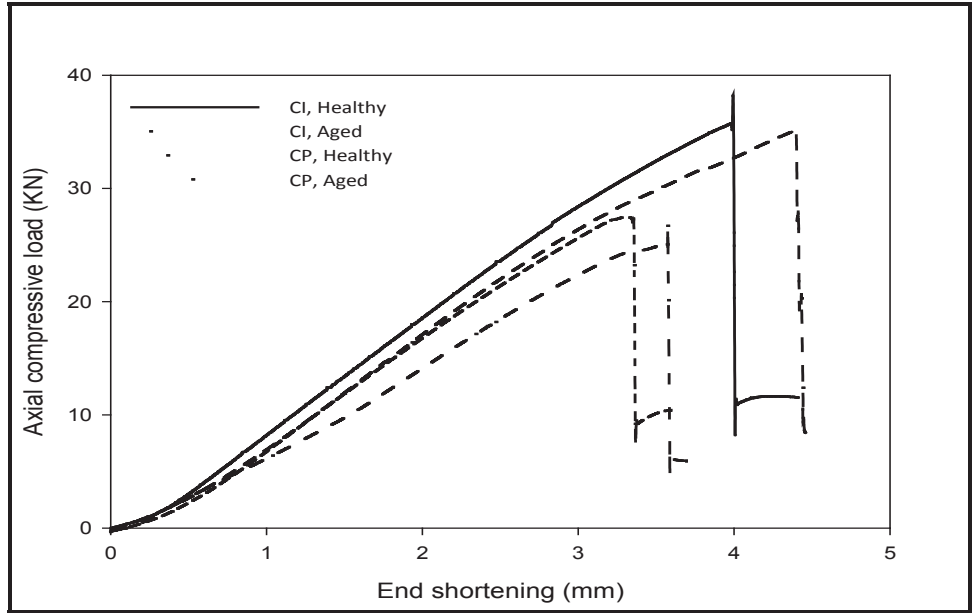


Figure 6.11 Experimental load versus end-shortening curves (CI and CP, $d/h=27.5$)

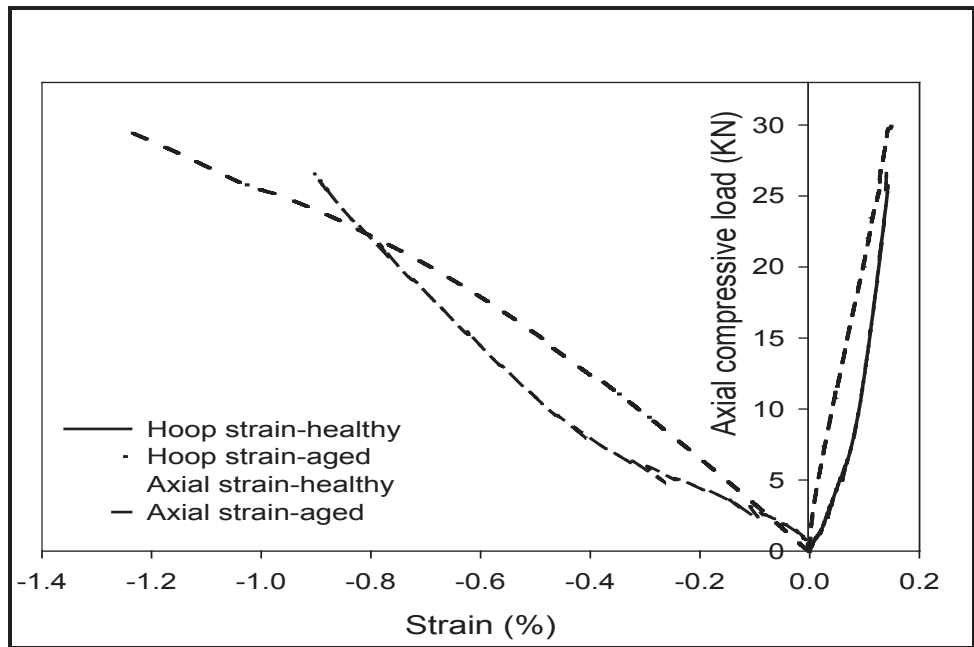


Figure 6.12 Hoop and axial strains for non-perforated pipes in both healthy and aged states (CI, $d/h=27.5$)

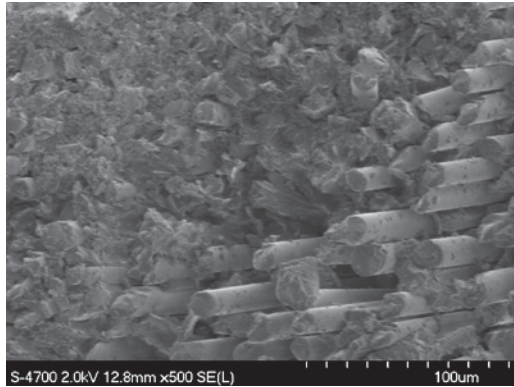
To complete the comparison, the strain gauges results of a representative pipes in this group are also presented in Figure 6.12.

6.5.3 INFLUENCE OF ACIDIC AND ELEVATED ENVIRONMENT ON THE MICROSTRUCTURE OF THE PIPES

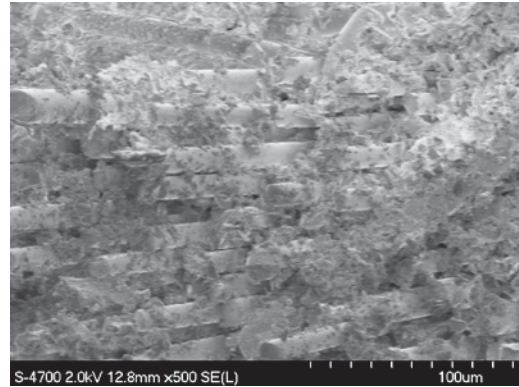
The influence of diffusion of the acidic solution on the perforated/non-perforated composite pipes, and its effect on their microstructures were also examined with the aid of scanning electron microscope (SEM) images.

Figure 6.13 shows the SEM pictures of the glass/epoxy pipes before, during and after acid immersion. Good adhesion between the fibers and matrix are observed in the images of the pipe material that was not exposed to acidic aging process. However, after having the material exposed to the corrosive medium at elevated temperature, their interfaces became weakened, leading to significantly reduced volume of resin surrounding the fibers.

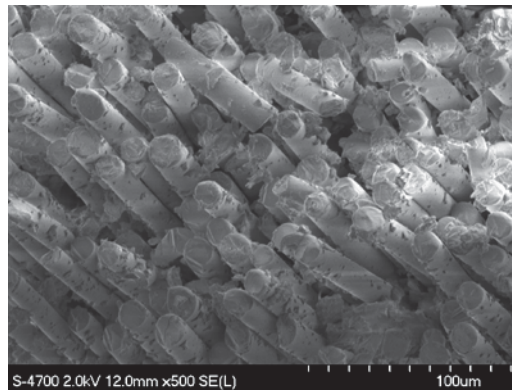
Further examination of the failed cross-section of the thicker-walled pipes clearly revealed that the corrosive outcome was more severe at specimen's surface, and gradually became milder when the specimen's interior core region is considered (see Figure 6.14). When the outer layer resin and fibers are degraded, due to exposure to acid, the stresses are shifted towards the fibers at the core region, thus leading to a decrease in the load bearing capacity of the fibers and the initiation of cracks. The combination of the tangential and radial stresses facilitates creation of the initial crack and the subsequent propagation in a helical pattern [14]. The evidence of such helical crack growth on the fibers can be seen in Figure 6.15.



(a) Virgin specimen

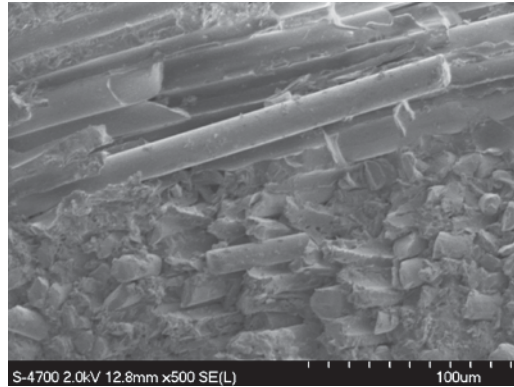


(b) During aging (prior to full saturation)

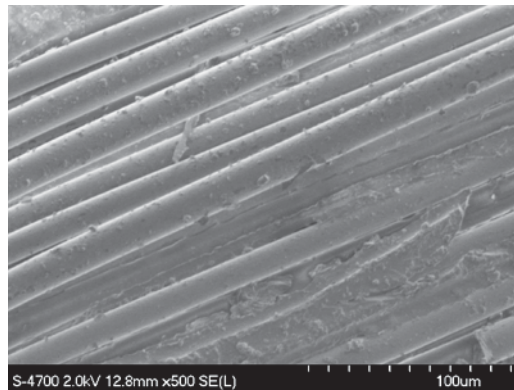


(c) Aged specimen (at fully saturated stage)

Figure 6.13 Comparison of the typical failure surfaces of the virgin and aged specimens

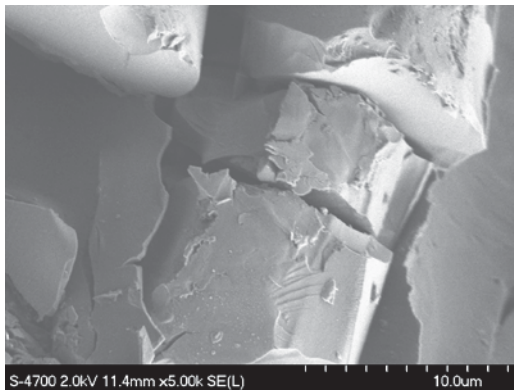


(a) Core region

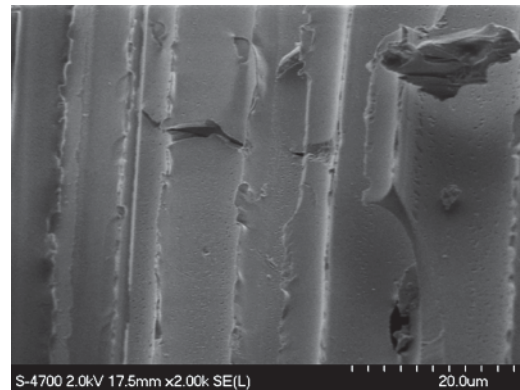


(b) Surface

Figure 6.14 SEM images (through-the- thickness) of the smallest D/t saturated pipe



(a) Transverse cracks through the fiber after aging in 15% sulphuric acid



(b) transverse cracks through fibers and the resin after aging 15% sulphuric acid

Figure 6.15 Transverse crack pattern through fibers

6.6 CONCLUSION

An experimental investigation was conducted in this study to assess the influence of aging on perforated glass/epoxy composite pipes within a combined harsh acidic and thermal environment, mimicking the ambient environment of most directional oil wells. As such, the specimens were soaked in a 15% diluted sulphuric acid solution at a constant temperature of 60°C within a digitally controlled thermal chamber for a period of 6 months. The specimens were then tested to failure under compressive axial load immediately after removing the specimens out of the chamber. The results obtained from the perforated and non-perforated aged specimens were then compared with their non-aged (virgin) counterparts. The concluding remarks of this study can be summarized as follows:

- The epoxy resin used to fabricate the FRP specimens was significantly affected and dissolved during the aging process.
- The remaining resin experienced a plasticization phenomenon, thereby rendering a nonlinear deformation. As a result, the aged pipes exhibited larger axial deformation prior to the final failure.
- Another major effect that can explain the loss in the load carrying capacity of the test specimens due to aging was the considerable loss of fiber/matrix interface adhesion.
- Pipes with larger d/h ratios showed more degradation in the mechanical properties and experienced more severe loss in their load carrying capacity as a result of aging in the combined acidic/thermal environment. This is believed to be due to the larger area available for the acid to wick into the composite.
- The degradation of the outer most layers due to acid exposure facilitated the transfer of the stress caused by the applied load toward the inner core region of the cross-section, thus creating helical cracks on the surface of glass fibers in that region.
- The existence of the perforation in the composite pipes proved to have more significant influence on the load carrying capacity and axial stiffness of the pipes in

comparison to the effect of aging. However, in order to reach to a more decisive conclusion on this observation, longer length perforated pipes should be fabricated, aged and tested, so to further establish the influence of the ratio of the exposed surface area to the perforation cross-section area on the overall degradation of perforated aged composites.

6.7 ACKNOWLEDGEMENT

The financial support of the Natural Sciences and Engineering Research Council of Canada is gratefully acknowledged. The assistance of Dr. Taheri-Behrooz in fabricating the pipes is gratefully acknowledged. The access to IRM (Institute of Research for Materials) SEM facilities is greatly appreciated.

6.8 REFERENCES

- [1] Perreux D, Suri C. A study of the coupling between the phenomena of water absorption and damage in glass epoxy composite pipes. *Compos. Sci. Technol.* 1997; 57: 1403-13
- [2] Bunsell A R. Hygrothermal ageing of composite materials. In *Proc. Compos. Mater. Petrol. Indust., Rueil-Malmaison.* 1994.
- [3] Aveston J, Kelly J, Sillwood J M. Long Term strength of glass reinforced plastics in wet environments. In *Proc. 3rd conf. compos. Mater., Oxford.* 1980; 556-68
- [4] Startsev O V, Krotov A S, Startseva L T. Interlayer shear strength of polymer composite materials during long term climatic ageing. *Polym. Degrad. Stabil.* 1999; 63: 183-6
- [5] Tsotsis T K, Keller S, Lee K, Bardis J, Bish J. Aging of polymeric composite specimens for 5000 hours at elevated pressure and temperature. *Compos. Sci. Technol.* 2001; 61: 75-86
- [6] Boukhoulda F B, Guillaumat L, Lataillade J L, Adda-Bedia E, Lousdad A. Aging-impact coupling based analysis upon glass/polyester composite material in hygrothermal environment. *Mater. Design.* 2011; 32: 4080-7

- [7] Liao K, Schultheisz C R, Hunston D L. Effects of environmental aging on the properties of pultruded GFRP. *Compos. Part B*. 1999; 30: 485-93
- [8] Abdel-Magid B, Ziaee S, Gass K, Schneider M. The Combined Effects of Load, Moisture and Temperature on the Properties of E-glass/epoxy Composites. *Compos. Struct.* 2005; 71: 320-6
- [9] Bagherpour S, Bagheri R, Saatchi A. Effects of concentrated HCl on the mechanical properties of storage aged fiber glass polyester composite. *Mater. Design*. 2009; 30: 271-4
- [10] Ellyin F, Maser R. Environmental effects on the mechanical properties of glass-fiber epoxy composite tubular specimens. *Compos. Sci. and Technol.* 2004; 64: 1863-74
- [11] Guedes R M, Sa A, Faria H. Influence of Moisture Absorption on Creep of GRP Composite Pipes. *Polym. Test*. 2007; 26: 595-605
- [12] Yao J, Ziegmann G. Equivalence of moisture and temperature in accelerated test method and its application in prediction of long-term properties of glass-fiber reinforced epoxy pipe specimen. *Polym. Test*. 2006; 25: 149-57
- [13] d'Almeida J R M, de Almeida R C, de Lima W R. Effect of water absorption of the mechanical behavior of fiberglass pipes used for offshore service waters. *Composite Structures*. 2008; 83: 221-5
- [14] Maxwell A S, Broughton W R, Dean G, Sims G D. Review of accelerated aging methods and lifetime prediction techniques for polymeric materials, NLP report, DEPC MPR 016, National Physical Laboratory, Teddington, UK. 2005.

CHAPTER 7 PERFORATED GFRP PIPES' RESPONSE TO HOSTILE MEDIA*

Shiva Eslami, and Farid Taheri

Department of Civil and Resource Engineering, Dalhousie University

7.1 ABSTRACT

The long term durability of GFRP pipes in hostile environments is a critical issue in industries involving corrosive media. In this study, a life assessment model has been developed for characterizing the response of perforated GFRP pipes, aged in both hot sulfuric acid and aqueous media, subjected to no external load as well as externally applied load. Experimental studies have been conducted to investigate the degradation in the flexural properties of the composites with different perforation sizes, subjected to various environmental conditions. The results indicate that perforation size and the presence of simultaneous external loading significantly influence the flexural properties of the composite.

Keywords: A. Glass; A. Polymer; B. SEM; C. Acid corrosion; C. Stress corrosion.

7.2 INTRODUCTION

Directional oil wells are the more preferred configuration for extracting oil due to their relatively higher productivity. In such wells, however, the installation and replacement of the so-called “liners” can be very costly. The liners, usually in the form of perforated steel pipes, stabilize oil wells; however, due to the corrosive environments in the wells, their service lives are usually short and they have to be replaced occasionally. The feasibility of the replacement of conventional steel liners with perforated glass fiber-reinforced plastic (GFRP) liners is currently being investigated as a new, viable alternative. However, the long term durability of such perforated GFRPs in hostile environmental conditions (e.g., elevated temperature, moisture and acidic media) has to be assessed in order to ascertain the applicability and viability of the concept.

* Submitted for publication in the journal of Corrosion Science

In general, the influence of corrosive media has been reported as one of the primary causes of failure in GFRP, mainly initiated by the chemical attack on the fiber's surface. However, most investigations have considered acidic solutions other than sulfuric acid. Moreover, investigations considering the response of GFRP in such hostile environment, especially at elevated temperatures have been scarce [1–6].

During corrosion process of glass fibers, the hydrogen ion concentration of the medium is considered as a governing parameter influencing the corrosion rate. Replacing the large metal ion on the surface of glass fibers by the smaller proton (H^+) supplied by the acid would generate stress concentration on the surfaces, thereby leading to crack generation [7].

The anions in the acidic media and the metal cations on the fibers can also combine and form an insoluble complex precipitant which, in turn, would increase the leaching process of the cations from fibers' surface [8, 9]. Jones and Stewart [10] showed that, in the case of E-glass fibers exposed to sulfuric acid medium, the formation of the precipitant was the key cause of the removal of calcium from the fibers, and not the acid ions' replacements. This was based on the observation that sulfuric acid concentration did not affect the rate of corrosion considerably.

According to the literature, liquid penetration into GFRP would be faster through edge surfaces. A perforated specimen would have a larger edge surface area due to the presence of the perforations, and hence, the rate of diffusion of liquid into such specimen would be higher. To the best of our knowledge, few studies have considered the influence of perforation on the resulting diffusion rate of sulfuric acid, especially when combined with stress corrosion cracking in GFRP.

This study is the continuation of a previous study which evaluated the influence of perforations in GFRP plates on acid and water absorption at an elevated temperature. In the current study, the resulting degradation in the flexural properties of perforated glass/epoxy composite pipes, and thereby indirectly evaluating the response of GFRP liners in a realistic environment, is explored. Both perforated and non-perforated specimens are considered; they are aged and also subjected to stress corrosion processes at elevated temperatures within a sulfuric acid solution and an aqueous medium.

Moreover, scanning electron microscopy (SEM) has been used to investigate the resulting microstructural changes in the GFRP pipes and the hydrolysis and corrosion caused by the exposed media.

7.3 LITERATURE REVIEW

In general, when composites are immersed in a hostile solution, the medium would be absorbed and mechanical properties of the materials would be degraded due to the hydrolysis and corrosion caused by the solution [11].

The liquid absorption process in a polymer composite immersed in a solution can be modeled by applying an equation developed based on Fick's law, illustrated by [12]:

$$\frac{M_{\%}}{M_m} = 1 - \frac{8}{\pi^2} \sum_{n=0}^{\infty} \frac{1}{(2n+1)^2} \exp\left[-D_c (2n+1)^2 \frac{\pi^2 t}{h^2}\right] \quad (7.1-a)$$

which can be simplified as [13]:

$$\frac{M_{\%}}{M_m} = \tanh\left[\frac{4}{h} \sqrt{\left(\frac{D_c t}{\pi}\right)}\right] \quad (7.1-b)$$

where $M_{\%}$ is the absorbed liquid at time t , M_{∞} is the maximum absorbed content at saturation point and h is the specimen thickness, respectively. In the above equation, D is the diffusion coefficient, which can be evaluated by [12]:

$$D = \pi \left(\frac{h}{4M_{\infty}}\right)^2 \left(\frac{M_2 - M_1}{\sqrt{t_2} - \sqrt{t_1}}\right)^2 \quad (7.2)$$

where $\frac{1}{M_{\infty}} \left(\frac{M_2 - M_1}{\sqrt{t_2} - \sqrt{t_1}}\right)$ is the slope of the initial linear portion of the curve of the

absorbed liquid versus time (i.e. $\frac{M_{\%}}{M_{\infty}}$ vs. \sqrt{t})

Moreover, the following coefficient can be used to evaluate the diffusion coefficient hosting equal diameter circular perforations [14]:

$$D_{MFS} = D \left(1 + \frac{h}{l} + \frac{h}{w} + \frac{n\pi dh}{2lw} \right)^{-2} \quad (7.3-a)$$

where d is the perforation diameter, l is the length and w is specimen's width and n is the number of the perforations.

The diffusion in a cylindrical pipe can be approximated by considering diffusion of a rectangular plate having an equivalent surface area, but with one less edge surface, using the following expression:

$$D_{MFS} = D \left(1 + \frac{h'}{l'} + \frac{n'\pi d'h'}{2l'w'} \right)^{-2} \quad (7.3-b)$$

where d' is the perforation diameter, h' is the pipe thickness, l' is the pipe length, w' is the lateral distance between perforations and n' is the number of the perforations.

Using eq. 7.3-b, the following equation can be used conducted for predicting the mass absorption of perforated GFRP pipes:

$$\frac{M_{\%}}{M_{\infty}} = \tanh \left(\frac{4}{h} \sqrt{\frac{D \left(1 + \frac{h'}{l'} + \frac{n'\pi d'h'}{2l'w'} \right)^{-2} \times t}{\pi}} \right) \quad (7.4)$$

The influence of external load on the diffusion process in epoxy has also been evaluated [15] and an equation for evaluating the diffusion coefficient, D_{σ} , in a stressed specimen has been proposed [15]:

$$D_{\sigma} = D_0 \left(1 + A \frac{\sigma}{G} \right) \quad (7.5)$$

where D_0 , σ , G and A are the diffusion coefficient in the unstressed state, the applied stress, the shear modulus and a constant (evaluated experimentally), respectively. It has been claimed that when the specimens are subjected to a tensile stress, then the magnitude of the diffusion coefficient would increase. In contrast, the application of a

compressive stress would reduce the diffusion coefficient and hence the resulting mass absorption. When the material is subjected to flexural stresses, however, the driving force due to the resulting tensile stress would be much higher than the resistance caused by the compressive stress; as a result, the diffusion would be enhanced [15, 16].

It has been shown that the degradation in the flexural strength of the GFP (immersed in one medium) as a function of perforation diameter, as well as the exposure time and applied stress causing stress-corrosion can be predicted as follows [14]:

$$\frac{\sigma_{residual}}{\sigma_0} = e^{-\left[\left\{\frac{D}{\phi^2}\right\}(A+B\sigma_{app})t\right]} \quad (7.6)$$

where $\sigma_{residual}$ is the flexural strength of the structure at time t , σ_0 is the flexural strength of the virgin (un-exposed) material, D is the diffusion coefficient calculated by equation 7.2 in the unstressed state, σ_{app} is the applied stress (which would be zero if the material is only subject to the aging processes), and A and B are empirical material constants. The constant A (i.e., the “aging constant”) is obtained from a basic aging test results; while factor B , or the “stress coefficient”, signifies the influence of the applied constant stress; its value is obtained from a basic SCC test. Finally, ϕ is a geometric factor, which- in this paper -should be calculated by the following equation:

$$\phi = \left(1 + \frac{h'}{l'} + \frac{n'\pi d'h'}{2l'w'}\right) \quad (7.7)$$

The primary aim of this study is to investigate the accuracy of the above models for assessing the mass absorption response of both perforated and non-perforated tubular GFRP in corrosive media.

7.4 EXPERIMENTAL INVESTIGATION

7.4.1 SPECIMEN PREPARATION

The tubular GFRP specimens used in our investigation were fabricated by applying epoxy to a stitched fabric of glass fibers having a layup sequence of [45°/-45°/90°] (with respect to the longitudinal axis of the pipes). The fabrication was done by wrapping three

layers of the fabric around a steel mandrel. A dial gauge with a resolution of 0.01 mm was used to check the alignment of the pipes and a digital micrometer with the accuracy of 0.01mm to measure the pipe thickness. Next, the pipes were trimmed by using a special diamond saw. Twelve specimens were left un-perforated, while the other 36 specimens were prepared with perforations of three different diameters (Figure 7.1). Perforations with 5, 8 and 11 mm diameters were then carefully machined into the specimens. The length of each pipe specimen was $L=200$ mm, diameter of $d=100$ mm, and spacing of $S = 50$ mm between the rows of perforations along the length of the tubes. The perforation pattern and specimens' geometries are shown in Figure 7.2.



Figure 7.1 Typical perforated and non-perforated pipe specimens

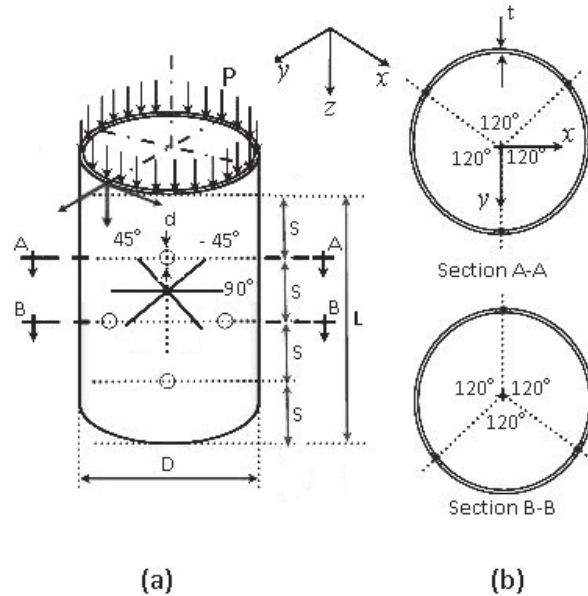


Figure 7.2 Typical perforation arrangement in specimens: (a) tube geometry and longitudinal arrangement of the perforations, (b) cross sections showing the circumferential arrangement of the perforations

7.4.2 EXPERIMENTAL METHODS

The tests were divided into two main categories; tests in water and tests in sulfuric acid. In each category, the specimens were immersed and kept in the hostile medium until they were saturated in two different testing conditions: (1) aging and (2) stress corrosion, and then were tested in a three-point bending configuration.

The experimental conditions of the specimens are summarized in Table 7.1. After recording the initial weight of each specimen, the first group of specimens, including perforated and non-perforated specimens with three perforation diameters, was put in a controlled environmental chamber and waterlogged at a temperature of 60°C to stimulate the aging process. The second group of specimens was subjected to a stress level equal to 25% of the ultimate strength of the specimens through a special frame designed for this purpose and immersed in the same medium at the temperature of 60°C to stimulate the stress corrosion phenomenon. The third group of specimens was aged in a 15% sulfuric acid solution at the same temperature of 60°C . Finally, the fourth group was subjected to

the same stress level as used for group 2 through a frame designed in-house, made of a corrosion resistant steel alloy, within 15% sulfuric acid solution at 60 °C. The weighing procedure was performed as per ASTM D5229 [17], and specimen's weights were measured periodically during the test, with least disturbance to the specimens, in a timely fashion, until saturation was completed.

Table 7.1 Details of the specimens and test condition

Specimen Type	Environment	Aging temperature (°C)	Test type	Perforation size (mm)	Number of specimens	
Pipes	Water	60	Aging	0	3	
				5	3	
				8	3	
				11	3	
		60	Stress corrosion	0	3	
				5	3	
				8	3	
				11	3	
	15% sulfuric acid solution	60	Aging	0	3	
				5	3	
				8	3	
				11	3	
		60	Stress corrosion	0	3	
				5	3	
				Corrosion	8	3
				11	3	

After saturation, the specimens were taken out of the chamber and then were tested in a bending test configuration, using a servo-hydraulic INSTRON universal testing machine controlled with 8500+ electronics, in order to evaluate the specimen's flexural response and degradation. As soon as the specimens were removed from the chamber, they were

wrapped with sawran wrap to prevent moisture loss, and were immediately tested. A set of totally virgin specimens (i.e. specimens not subjected to water/acid or heat) were also tested in flexure to provide the base-line data.

7.5 EXPERIMENTAL RESULTS AND DISCUSSION

7.5.1 ABSORPTION BEHAVIOR

The gained weight (mass absorption), M_t , in the specimens was calculated:

$$M_t = \frac{m - m_0}{m_0} 100\% \quad (7.8)$$

where m_0 and m are the specimen's mass at the initial stage and the mass at time t , respectively.

The mass absorption rates versus the square root of exposure time for all groups of specimens are illustrated in Figures 7.3 and 7.4. As shown, the specimens saturated as a function of the perforation diameter, since larger perforations would expose larger edge surface area, and thus saturate earlier. The absorption data (for different perforation sizes) also reveals an increasing trend in absorption in specimens subjected to SCC condition (i.e. aged while subjected to an applied load), in comparison to non-SCC aging groups. Moreover, the results indicate higher rates of diffusion for specimens aged in 15% sulfuric acid medium in comparison to the aqueous (water) medium. In these figures, the solid symbols illustrate the experimental test results and the solid lines are regarding the results obtained using the theoretical model (i.e., equation 7.1-b).

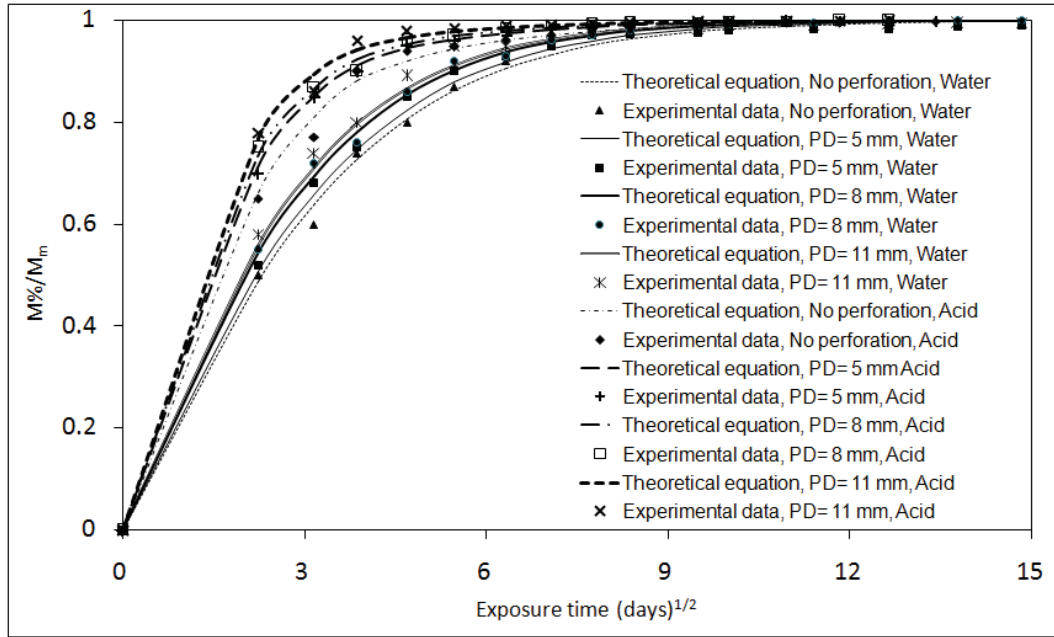


Figure 7.3 Variation of liquid absorption as a function of time for perforated pipes aged in water and 15% sulfuric acid at 60 °C; perforation size: 0, 5, 8 and 11 mm; testing condition: Aging

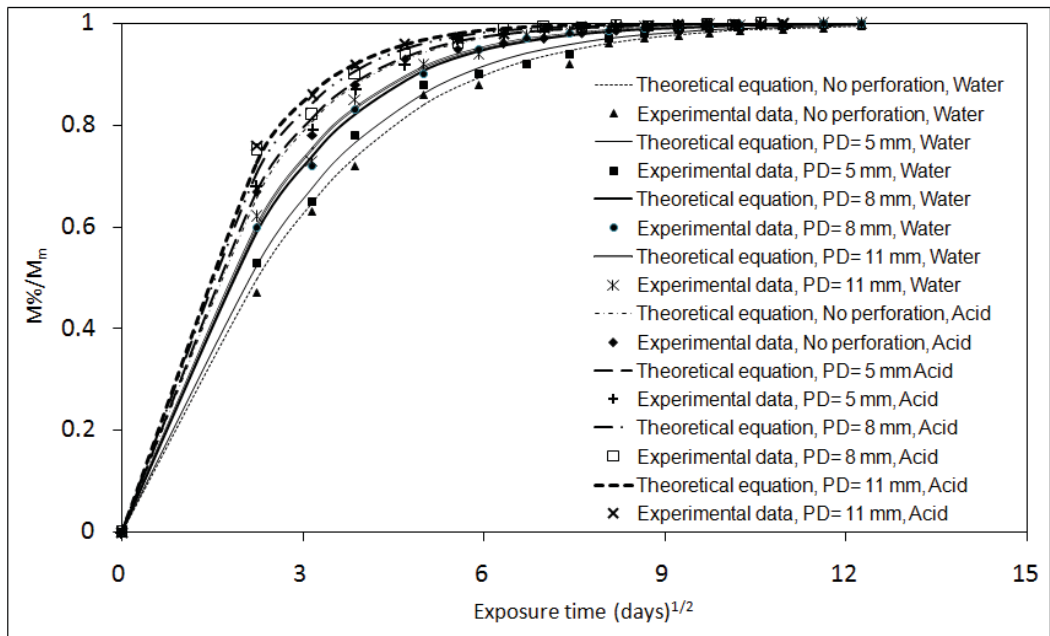


Figure 7.4 Variation of liquid absorption as a function of time for perforated pipes submerged in water and 15% sulfuric acid at 60 °C and subjected to external load (SCC); perforation size: 0, 5, 8 and 11 mm; testing condition: SCC

The results confirm that the absorption trend of aged and SCC pipes in various media could be predicted by the hyperbolic model, and they do not show very significant inconsistencies.

7.5.2 MECHANICAL CHARACTERIZATION

The three-point bending tests on pipes were conducted to evaluate the mechanical response of the specimens during and after the saturation process. The results are presented in Figures 7.5 and 7.6. The results indicate that the increase in the perforation diameter causes a decrease in the flexural stiffness and strength of the specimens. Moreover, the mechanical degradation is more significant in specimens that were subjected to SCC conditions. Moreover, the aged specimens and acidic solution caused more severe corrosion and degradation, as compared to aqueous media. Furthermore, the comparison between the ultimate strain of the specimens (See Figure 7.7), conditioned in the aqueous and acidic media (subjected or not subjected to the external loading), shows that the ultimate strain increases more in acidic medium as opposed to the aqueous medium, as a result of higher corrosion and thereby higher diffusion rate in the specimens; and also reveals that applying an external loading would enhance the ultimate strain in the specimens, causing an increase in the diffusion coefficient in the stressed specimens.

It should be mentioned that, in the three-point bending tests, plastic behavior was observed in the load-deflection diagrams for specimens exposed to the acidic media.

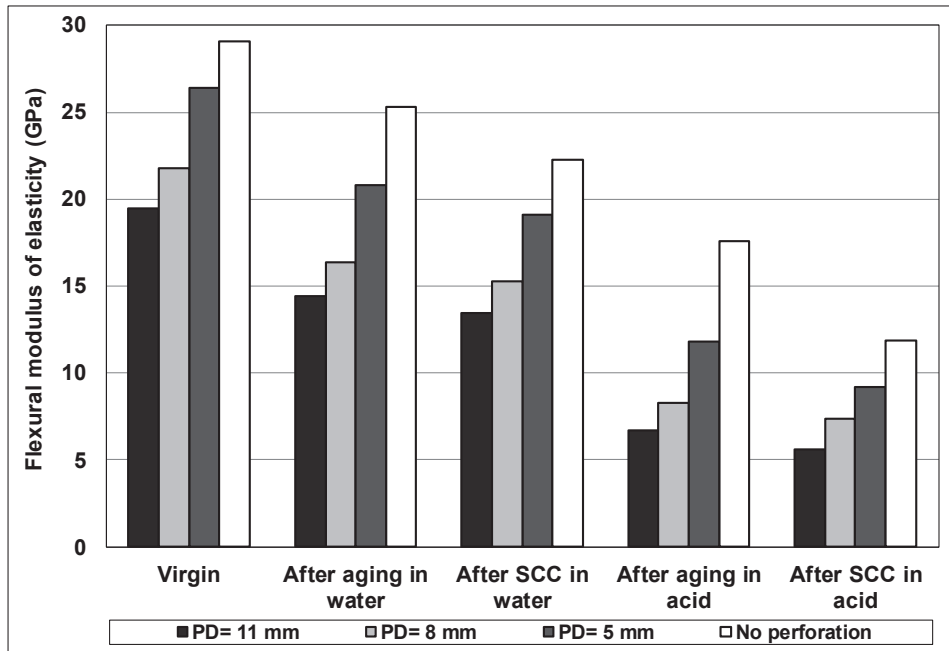


Figure 7.5 Degradation in the flexural modulus of elasticity of the perforated specimens as a function of perforation diameter and environmental conditions

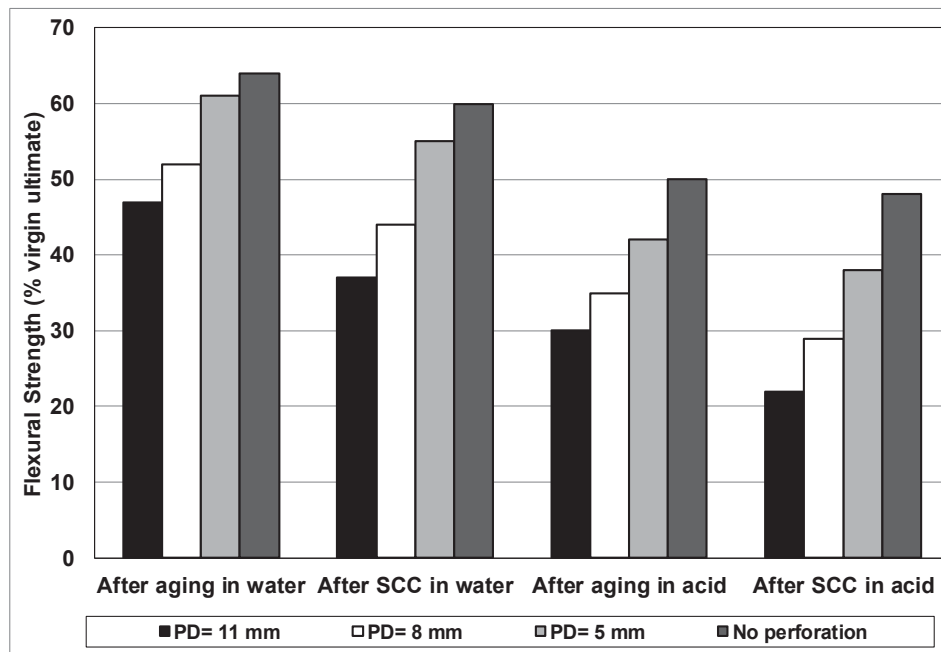


Figure 7.6 Degradation in the flexural strength of the perforated specimens as a function of perforation diameter and environmental conditions

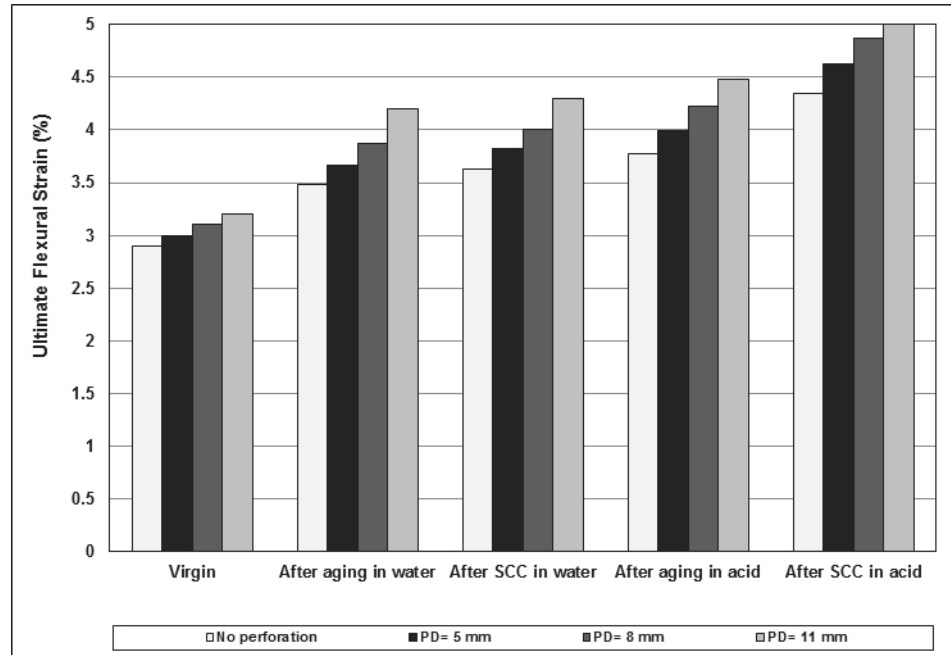


Figure 7.7 Variation in the ultimate flexural strain of perforated specimens as a function of perforation diameter and test conditions

Moreover, it was observed that the increase in perforation diameter created larger edge surface areas. The greater the surface areas, the higher diffusion rate thereby the more sever corrosion in the material and the more serious degradation in the flexural properties.

The saturation time, t , can be postulated using the general form of Eq.7.2 [14]:

$$t = \frac{\pi}{D} \left[\frac{h}{4} \tanh^{-1} \left(\frac{M_{\%}}{M_{\infty}} \right) \right]^2 \quad (7.9)$$

In this study, D will be considered as D_{MFS} . By applying Eq. 7.3-b, and following the approach used in deriving Eq. 7.5, and considering the influence of the external loading on the diffusion coefficient and perforation sizes, the integration of these equations results in a semi-empirical model that can be used to predict the saturation time for a perforated GFRP composite pipe exposed to aging or SCC in various solutions:

$$t = \frac{\pi}{D_0(A + B\sigma_{app}) \left(1 + \frac{h'}{l'} + \frac{n'\pi d'h'}{2l'w'}\right)^{-2}} \left[\frac{h}{4} \tanh^{-1} \left(\frac{M_{0\%}}{M_{\infty}} \right) \right]^2 \quad (7.10)$$

where t is the required time for specific saturated point, D_0 is the diffusion coefficient in the unstressed status, σ_{app} is the applied stress, which takes a value when a specimen is subjected to SCC or becomes zero for ordinarily aged specimens (i.e., not subject to an applied stress); A and B are empirical constant. The value of A is obtained from the conventional aging test results, while B is obtained from the SCC test results.

Using Eq. 7.6 for each medium, one can postulate a model to predict pipes' service life, with consideration of all affecting environments; The proposed model is expressed as:

$$\frac{\sigma_{residual}}{\sigma_0} = e^{-\left[\left\{ \frac{D_{Water}}{\phi^2} \right\} (A + B\sigma_{app})_{water} + \left\{ \frac{D_{Acid}}{\phi^2} \right\} (A + B\sigma_{app})_{Acid} \right] \times t} \quad (10.11)$$

The first part of the right hand of the above equation accounts for the strength degradation by water and the second part accounts for the role of the acidic solution in the strength degradation.

The above equation can be used to predict the useful life of a liner at a desired residual strength value. For that, we can set the residual strength as % of the ultimate strength of the material at its virgin state. Then the service-life, (time t), can be calculated from the above equation. Alternatively (and more practically), one can use Figure 8 for this purpose. As instance, Let's assume that we would like to estimate the service life for a perforated liner at the stage when the liner's strength reaches $x\%$ of its ultimate strength (in other words, the value of it is set to x). As an example, let's assume that the residual strength is set as 10% of liner's ultimate strength. The useful life can then be estimated by taking the x -axis value corresponding to the vertical axis value of -2.3, from the appropriate curve in Figure 7.8 (i.e., for the appropriate perforation diameter). It should be noted that the regression lines illustrated in the figure are in good agreement with the experimental data with $\pm 5\%$ standard deviation.

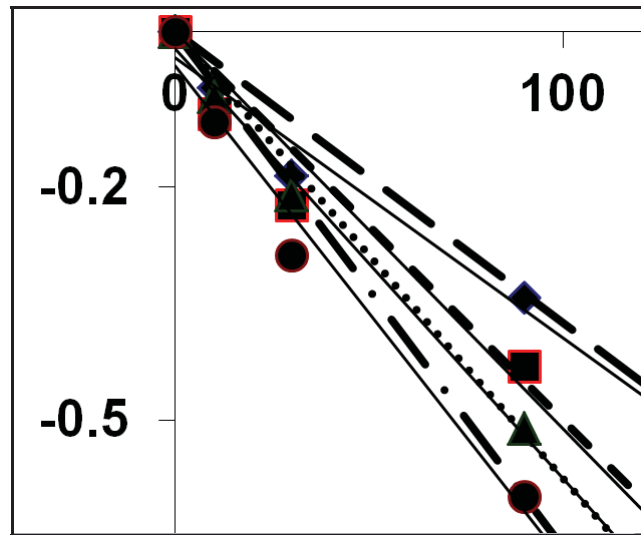
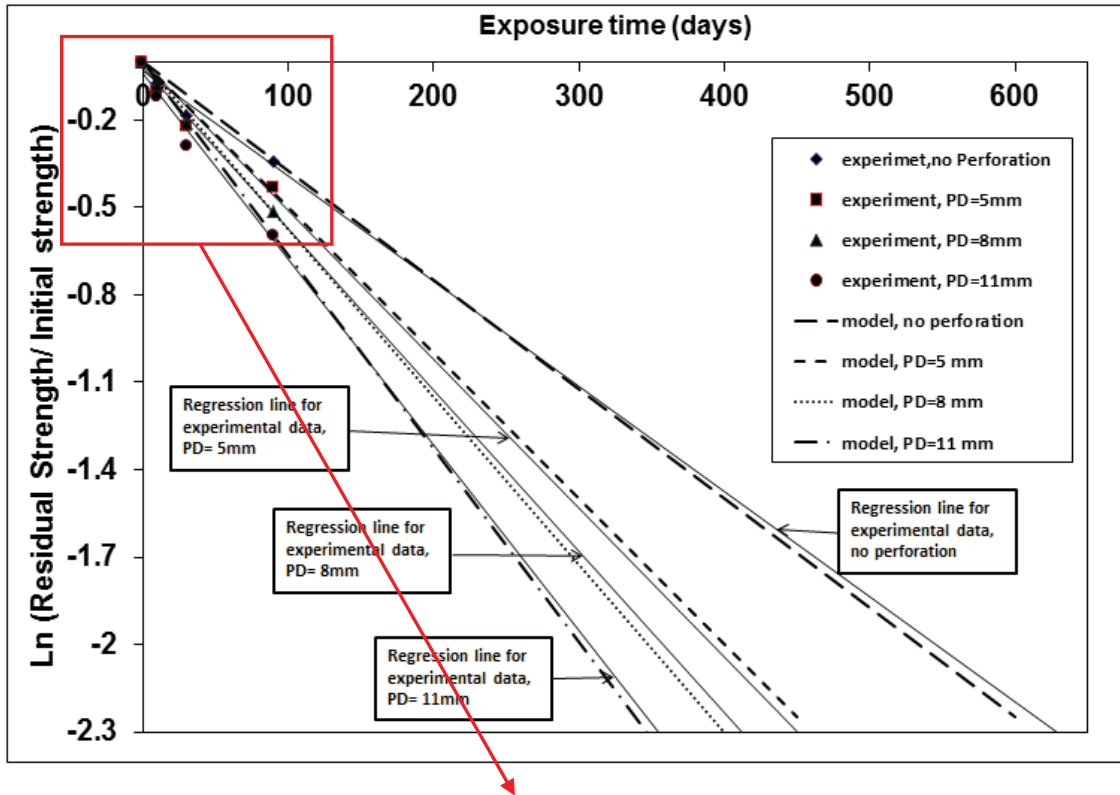


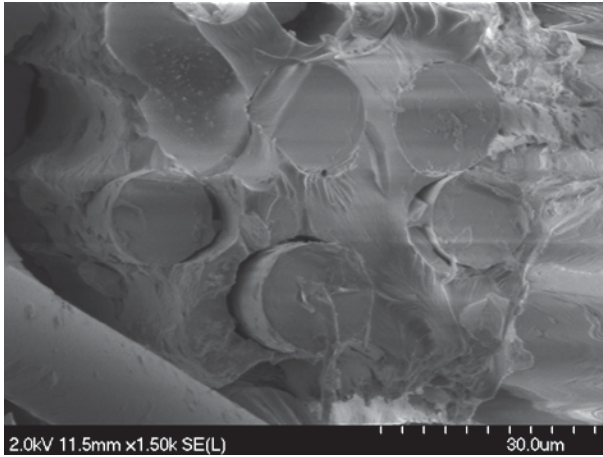
Figure 7.8 Comparison of the postulated model for service life and the regression line from experimental results for GFRP perforated specimens as a function of perforation diameter

7.5.3 MICROSCOPIC OBSERVATIONS

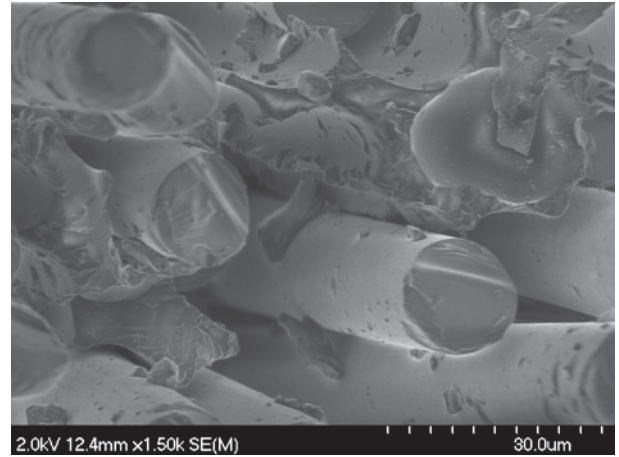
Scanning electron microscope (SEM) images of the specimens, before and after exposure to the solutions, were studied to ascertain the influence of solution diffusion on the microstructures of the perforated composite pipes.

Figure 7.9 shows SEM images of the GFRP specimens before immersion and after aging and SCC tests in the acid and water. It can be seen that in the virgin specimen, the fibers have good adhesion bond to the resin and the fiber/resin contact areas are all intact. However, after exposing the material to the aqueous and corrosive media under the elevated temperature, the interface bonds became degraded and the resin regions became thinned, particularly when the material is exposed to the acidic medium.

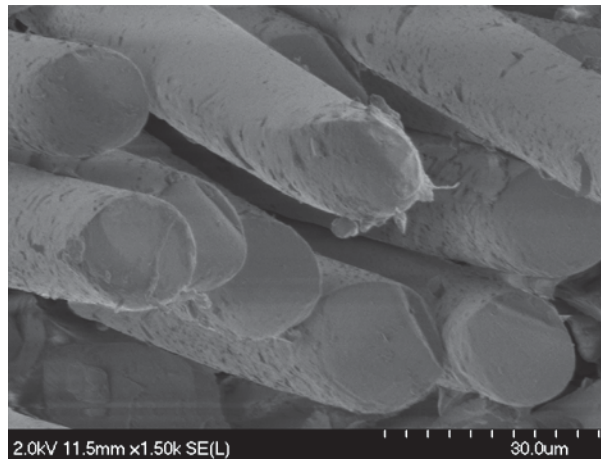
Figure 7.10 shows the effect of the acid attack on fibers' surface and the evidences for the presence of helical cracks on the surface as a result of a combined state of radial and tangential stresses on fibers' surface. This phenomenon could not be observed for fibers of GFRP specimens exposed to the aqueous environment.



a) Before exposing to media



B) After exposed to water



c) After exposed to 15% sulfuric acid medium

Figure 7.9 Typical fiber/resin interface of specimens subjected to various conditions

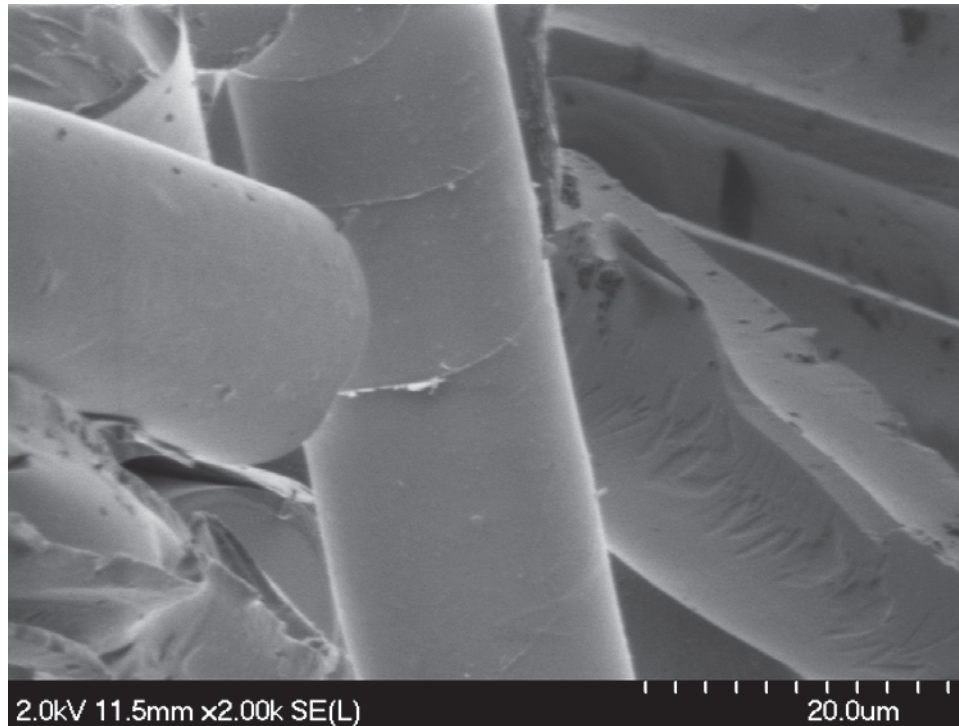


Figure 7.10 Helical cracks on the surface of a fiber (in specimens subjected to acidic environment) as a result of a combined state of radial and tangential stresses

7.6 SUMMARY AND CONCLUSION

Aging and stress corrosion experiments were conducted on perforated glass/epoxy pipes, and the influence of perforation diameter on the absorption behavior and the mechanical degradation of the material were examined. The mechanical tests' results showed that the increase in the perforation diameter led to an increase in the diffusion area, and in turn, the solution absorption rate. The solution absorption makes the matrix to be degraded and hence reduces the flexural strength, and modulus of elasticity of composite coupons.

It is also known that the absorbed content varies exponentially as a function of diffusion coefficient. A model was therefore developed by integrating the diffusion coefficient equations, both for non-stressed and stressed (SCC) specimens. A model was also developed by which degradation in the material's strength can be estimated as a function of time. In other words, the service life of the structure in sulfuric and aqueous medium and relatively high temperature (a similar environment in open-hole oil wells) can be predicted by the proposed model with a reasonable accuracy. Moreover, The SEM study

revealed that higher absorption due to higher diffusion area would cause more fiber/resin interface degradation and damage. Such interface damages are believed to be the cause of the observed decrease in the flexural properties of the GFRP.

In conclusion, when considering perforated GFRP for structural applications that are within harsh environments (e.g. in oil wells), the influence of the surrounding environment on the material performance should be considered to ensure the safety of such structural components in their intended service-life.

7.7 REFERENCES

- [1] Shokrieh M M, Memar M. Stress corrosion cracking of Basalt/Epoxy composites under bending loading. *Appl. Compos. Mater.* 2010; 17: 121-35
- [2] Myres T J, Kytomaa H K, Smith T R. Environmental Stress corrosion cracking of fiber glass: Lessons learned from failures in the chemical industry. *J. Hazard. Mater.* 2007; 142: 695-704
- [3] Sapalidis S N, Hogg P J, Youd S J. High temperature acidic stress corrosion of glass fiber composites. *J. Mater Sci.* 1997; 32: 309-16
- [4] Mula S, Bera T, Ray P K, Ray B C. Effect of hydrothermal aging on mechanical behavior of sub-zero weathered GFRP composites. *J. Reinf. Plast. Compos.* 2006; 25: 673-80
- [5] Davies P, Mazeas F, Casari P. Sea water aging of glass reinforced composites: shear behaviour and damage modelling. *J. Compos. Mater.* 2001; 35: 1343-72
- [6] Roy S. Prediction of anomalous hygrothermal effects in polymer matrix composites. *J. Reinf. Plast. Compos.* 1999; 19: 1197-207
- [7] Maxwell AS, Broughton WR, Dean G, Sims GD. Review of accelerated aging methods and lifetime prediction techniques for polymeric materials. NLP Report: DEPC MPR 016. 2005
- [8] Qiu Q, Kumosa M. Corrosion of E-glass fibers in acidic environments, *compos. Sci. & tech.* 1997; 57: 497-507

- [9] Kumar S, Sharma N, Ray B C. Acidic degradation of FRP composites. In: Proc. the National Conference on Developments in Composites, India, 2007.
- [10] Jones R L, Stewart J. The kinetics of corrosion of E-glass fibers in sulphuric acid. *J Non-cryst Solids*. 2010; 356: 243-6
- [11] Jones F R, Rock J W, Bailey J E. The environmental stress corrosion cracking of glass fiber- reinforced laminates and single E-glass filaments. *J. Mater Sci*. 1983; 18: 1059-71
- [12] Shen C H, Springer G S. Moisture absorption and desorption of composite materials. *J. Compos. Mater*. 1976; 10: 2-20
- [13] d'Almeida J R M, de Almeida R C, de Lima W R. Effect of water absorption of the mechanical behavior of fiberglass pipes used for offshore service waters. *Compos. Struct*. 2008; 83: 221-5
- [14] Eslami S, Taheri-Behrooz F, Taheri F. Long-term hygrothermal response of perforated GFRP plates with/without application of constant external loading. *Polym. Compos*. 2011; 33: 467-475
- [15] Fahmy A A, Hurt J C. Stress dependence of water diffusion in epoxy resin. *Polym. Compos*. 1980; 1: 77-80
- [16] Whitaker G, Darby M I, Wostenholm G H, Yates B, Collins M H, Lyle A R, Brown B. Influence of temperature and hydrostatic pressure on moisture absorption in polymer resins. *J. Mater. Sci*. 1991; 26: 49-55

7.8 ACKNOWLEDGEMENT

The financial support of the Natural Sciences and Engineering Council of Canada (NSERC) in support of this work is gratefully acknowledged. The access to IRM (Institute of Research for Materials) SEM facilities is greatly appreciated.

CHAPTER 8 SUMMARY AND CONCLUSIONS

8.1 SUMMARY

As stated earlier, due to the higher productivity of directional oil wells, they are considered as the preferred means for extracting oil. It was also highlighted that in such wells, however, the installation and replacement of the so-called “liners” can be costly. The liners (in the form of perforated steel pipes), stabilize the wells; however, due to corrosive environments in the wells, their service lives are usually short and they have to be replaced frequently.

As also stated, our literature search revealed that there has been no investigation into the effect of perforations on GFRP pipe’s response and durability. Moreover, no physical or mathematical model could be found by which one could predict the life cycle of perforated GFRP pipes. Therefore, this thesis presented a series of new data in regards to performance of non-perforated and perforated GFRP composites subject to various harsh environments. Another novel contribution in the thesis are the proposed models by which one can predict the effects of perforation size, stress level, and degradation due to water or acidic media aging on the aforementioned composites, and also for predicting their life-cycle.

As an alternative to the traditional steel liners, perforated glass fiber-reinforced plastic (GFRP) composite liners have been investigated. As part of the endeavor, it became necessary to conduct a systematic investigation to explore the long-term durability of such perforated GFRPs in hostile environmental conditions (e.g., at elevated temperature and in acidic media). For that, the degradation in the flexural properties of perforated GFRP plates and pipes hosting different perforation diameters in both warm aqueous and acidic media was systemically investigated. In addition, the resulting changes in their microstructural and absorption behaviors were carefully examined by SEM, and discussed. The aging experiments were conducted under no load, as well as under externally applied load (stress corrosion condition).

Subsequently, a semi-empirical model was proposed for evaluating the degradation of the mechanical properties of the composite over time, as a function of environmental and

loading conditions as well as geometric configurations. Finally a semi-empirical model was also developed for life cycle prediction of perforated GFRPs.

8.2 CONCLUSIONS

The observations and conclusion resulting from the experimental work followed by the analytical efforts are summarized as follows:

- It was observed that the mass absorption rate varied exponentially as a function of the diffusion coefficient.
- The modified Fick model could accurately describe the moisture absorption rate of the perforated GFRP specimens that were aged at room temperature, while the hyperbolic tangent model produced better predictions for the specimens conditioned at a higher temperature (i.e., 60°C).
- Moisture causes degradation in the matrix and in turn reduces the flexural stiffness and strength of the composite.
- The increase in temperature degraded the interface between the fibers and the matrix.
- The mechanical test results revealed that the increase in the perforation size led to an increase in the diffusion area, and as a result, the mass absorption rate increased. The mass absorption was also observed to directly influence matrix integrity, thus degrading the flexural properties (i.e., strength and stiffness) of the composite. This phenomenon was accompanied by an increase in the ultimate strain of the composite, which is believed to be a result of matrix plasticization phenomenon.
- The SEM study revealed that higher absorption occurring due to higher diffusion area caused more fiber/resin interface degradation and damage. Such interface damage is believed to be the cause of the observed decrease in the flexural properties of the GFRP.
- The degradation of the surface layers due to acid exposure facilitated the transfer of stress caused by the applied load toward the inner core region of the cross-section, thus creating helical cracks on the surface of glass fibers in that region.

- Under the axial compressive loading state, the aged pipes exhibited larger axial deformation prior to final failure. This can be related to the fact that after aging, the remaining resin underwent a plasticization phenomenon.
- Pipes with larger d/h ratios showed more degradation in their mechanical properties and experienced more severe loss in their load carrying capacity as a result of aging in the combined acidic/thermal environment. This is believed to be due to the larger surface area available to acid wicking into the composite.
- When considering perforated GFRPs for structural applications that are intended to serve in harsh environments (e.g. in oil wells), the influence of the surrounding environment on the material performance should be carefully considered. The result of such an investigation would ensure the safety of such structural components during their expected service-life.

8.3 RECOMMENDATIONS FOR FUTURE WORKS

Based on the work conducted in this thesis and the results, and the comprehensive review of the pertinent literature, the following future works are suggested:

- New research works have claimed that basalt fibers may have higher resistance to acids than glass fibers. Therefore, similar investigation could be carried out to assess the applicability and feasibility of basalt fiber-reinforced epoxy composite for the particular application considered in this thesis.
- As GFRP pipes have the potential to be used in other acidic and alkali media in addition to sulfuric acid, the integrity of the suggested GFRP pipes, however, would have to be assessed when subjected to other corrosive media (such as nitric acid and hydrochloric acid).
- As the liner can be exposed to other stresses and mechanical loading conditions in other applications (such as a comprehensive loading state resulting from thermal load and applied restraints), the integrity of the liner to such loading conditions (i.e. local buckling response) should be investigated.

- It would be desirable to conduct X-ray inspection of the specimens during their aging process to evaluate the diffusion rate of each element and the numbers of affected layers at specific intervals.

References

- Abdel-Magid B, Ziaee S, Gass K, Schneider M. The combined effects of load, moisture and temperature on the properties of E-glass/epoxy composites. *Compos. Struct.* 2005; 71: 320-6
- Adams R D, Singh M M. The dynamic properties of fibre-reinforced polymers exposed to hot, wet conditions. *Compos. Sci. Technol.* 1996; 56: 977-97
- Aditya P K, Sinha P K. Diffusion coefficients of polymeric composites subjected to periodic hygrothermal exposures. *J. Reinf. Plast. Compos.* 1992; 11: 1035-47
- Aditya P K, Sinha P K. Moisture diffusion in variously shaped fibre reinforced composites. *Comput. struct.* 1996; 59: 157-66
- Akay M, Kong Ah Mun S, Stanley A. Influence of moisture on the thermal and mechanical properties of autoclaved and oven-cured Kevlar-49/epoxy laminates. *Compos. Sci. and Technol.* 1997; 57: 565-71
- Alawsi Gh, Aldajah S, Rahmaan S A. Impact of humidity on the durability of E-glass/polymer composites. *Mater and Design.* 2009; 30: 2506-12
- Asaro R J, Lattimer B, Ramroth W. Structural response of FRP composites during fire. *Compos. Struct.* 2009; 87:382-93
- Assarar M, Scida D, El Mahi A, Poilane C, Ayad R. Influence of water aging on mechanical properties and damage events of two reinforced composite materials: flax_fibres and glass_fibres. *Mater and Design.* 2011; 32: 788-795
- ASTM D3171-09. Standard test methods for constituent content of composite materials.
- ASTM D5229. Standard test method for moisture absorption properties and equilibrium conditioning of polymer matrix composite materials.
- ASTM D790-10. Standard test methods for flexural properties of unreinforced and reinforced plastics and electrical insulating materials. West Conshohocken, USA. 2010.
- Aveston J, Kelly J, Sillwood J M. Long term strength of glass reinforced plastics in wet environments. In *Proc. 3rd conf. compos. Mater.*, Oxford. 1980; 556-68

- Azar J J. 'Oil and Natural Gas Drilling' in Encyclopedia of Energy. 2004; 4: 521-34
- Bagherpour S, Bagheri R, Saatchi A. Effects of concentrated HCl on the mechanical properties of storage aged fiber glass polyester composite. Mater. Design. 2009; 30: 271-4
- Bai Y, Keller Th, Vallée T. Modeling of stiffness of FRP composites under elevated and high temperatures. Composites. 2008; 68: 3099-106
- Bai Y, Post N L, Lesko J J, Keller Th. Experimental investigations on temperature-dependent thermo-physical and mechanical properties of pultruded GFRP composites. Thermochimica Acta. 2008; 469: 28-35
- Bai Y, Vallée T, Keller Th. Modeling of thermal responses for FRP composites under elevated and high temperatures. Compos. Sci. Technol. 2008; 68: 47-56
- Bao L R, Yee L f. Moisture diffusion and hygrothermal aging in bismaleimide matrix carbon fiber composites: part II—woven and hybrid composites. Compos. Sci. Technol. 2002; 62: 2111-19
- Bellarby J. 'Chapter 1: Introduction' in well completion design. Developments in Petroleum Science. 2009; 56: 1-14
- Berketis K, Tzetzis D, Hogg PJ. The influence of long term water immersion aging on impact damage behaviour and residual compression strength of glass fibre reinforced polymer (GFRP). Mater and Design. 2008; 29: 1300-10
- Bledzki A, Spaude R, Ehrenstein G W. Corrosion phenomenon in glass fibers and glass fiber reinforced thermosetting resins. Compos. Sci. Technol. 1985; 23: 263-85
- Boukhoulda B F, Adda-Bedia E, Madani K. The effect of fiber orientation angle in composite materials on moisture absorption and material degradation after hygrothermal ageing. Compos. Struct. 2006; 74:406-18
- Boukhoulda F B, Guillaumat L, Lataillade J L, Adda-Bedia E, Lousdad A. Aging-impact coupling based analysis upon glass/polyester composite material in hygrothermal environment. Mater. Design. 2011; 32: 4080-7

Bunsell A R. Hygrothermal ageing of composite materials. In Proc. Compos. Mater. Petrol. Indust., Rueil-Malmaison. 1994.

Caddock B D, Evans K E, Hull D. Stress corrosion failure envelopes for E-glass fiber bundles. J. Mater. Sci. 1990; 25: 1498-2502

Carter H G, Kibler K. Langmuir-type model for anomalous moisture diffusion in composite resins. J. Compos. Mater. 1978; 12: 118-31

Catania P, Wilson M. Horizontal drilling assessment in Western Canada. Appl. Energ. 1999; 64: 331-43

Catania P. Predicted and actual productions of horizontal wells in heavy-oil fields. Appl. Energ. 2000; 65: 29-43

Chou P J C, Ding D. Characterization of moisture absorption and its influence on composite structures. J. Thermoplast. Compos. Mater. 2000; 3: 207-25

d'Almeida J R M, de Almeida R C, de Lima W R. Effect of water absorption of the mechanical behavior of fiberglass pipes used for offshore service waters. Compos. Struct. 2008; 83: 221-5

Davies P, Mazeas F, Casari P. Sea water aging of glass reinforced composites: shear behaviour and damage modelling. J. Compos. Mater. 2001; 35: 1343-72

De La Osa O, Alvarezand V, Va' Zquez A. Effect of hygrothermal history on water and mechanical properties of glass/vinylester composites. J. Compos Mater. 2006; 40(22): 2009-23

Diffusion and Osmosis, Retrieved on 30/12/2010 from:

<<http://finleysciencep8.blogspot.com/2010/12/december-21-diffusion-and-osmosis.html>>

Drilling Sideways -- A review of horizontal well technology and its domestic application. A report from: Office of Oil and Gas, U.S. Department of Energy. DOE/EIA-TR-0565. 1993

Bindslev N. Drug-acceptor Interactions, Retrieved on 20/8/2009 from:

<http://journals.sfu.ca/coactionbks/index.php/Bindslev/article/view/3/16>

- Dutta P K, Hu, D. Low-temperature and freeze-thaw durability of thick composites. *Compos. Part B: Eng.* 1996; 27: 371-9
- Renaud C M, Greenwood M E. Effect of Glass fibres and environments on long-term durability of GFRP composites. Retrieved on 1/9/2011 from:
http://www.efuc.org/downloads/CLR_MEG_Paper_on_Advantex_E-CR_Glass.pdf
- Elbadry M, Elzaroug O. Control of cracking due to temperature in structural concrete reinforced with CFRP bars. *Compos. Struct.* 2004; 64:37-45
- Ellyin F, Maser R. Environmental effects on the mechanical properties of glass-fiber epoxy composite tubular specimens. *Compos. Sci. and Technol.* 2004; 64: 1863-74
- Ellyin F, Rohrbacher C. Effect of aqueous environment and temperature on Glass-fibre epoxy resin composites. *J. Reinf. Plast. Compos.* 2000; 19: 1405-27
- Eslami Sh, Taheri F. Degradation of perforated E-glass/epoxy plates submerged in water and acidic media under elevated temperature, In Proc. the Second Joint US-Canada Conference on Composites, Montreal, Canada. 2011.
- Eslami Sh, Taheri F. Effects of perforation size on the response of perforated GFRP composites aged in acidic media. *Corros. Sci.* 2013; 69: 262-269
- Eslami Sh, Taheri-Behrooz F, Taheri F. Long-term hygrothermal response of perforated GFRP plates with/without application of constant external loading. *Polym. Compos.* 2011; 33: 467-475
- Fahmy A A, Hurt J C. Stress dependence of water diffusion in epoxy resin. *Polym. Compos.*, 1980; 1: 77-80
- Gautier L, Mortaigne B, Bellenger V. Interface damage study of hydrothermally aged Glass-fiber reinforced polyester composites. *Compos. Sci. Technol.* 1999; 59: 2329-37
- Gentzis, Th. Stability analysis of a horizontal coalbed methane well in the Rocky Mountain Front Ranges of southeast British Columbia, Canada. *Int. J. Coal Geol.* 2009; 77: 328-37
- Giori C, Yamauchi T. Effects of ultraviolet and electron radiations on graphite-reinforced polysulfone and epoxy resins. *J. Appl. Polym. Sci.* 1984; 29: 237-49

- Gu P, Asaro R J. Designing sandwich polymer matrix composite panels for structural integrity in fire. *Compos. Struct.* 2008; 88:300-9
- Guedes R M, Sa A, Faria H. Influence of moisture absorption on creep of GRP composite pipes. *Polym. Test.* 2007; 26: 595-605
- Hadia N, Chaudhari L, Mitra S K, Vinjamur M, Singh R. Experimental investigation of use of horizontal wells in waterflooding. *J Petrol Sci Eng.* 2007; 56: 303-10
- High-performance concrete: A State-of-the-Art Report, Retrieved on 1/8/2009 from: <http://www.fhwa.dot.gov/publications/research/infrastructure/structures/hpc/97030/chap5.cfm>>
- High pressure and temperature wells, Retrieved on 4/6/2012, from: <https://www.rwe.com/web/cms/en/1475772/rwe-dea/know-how/drilling/high-pressure-and-temperature-wells/>
- Horizontal Environmental Well Handbook. Prepared by: Directed Technologies Drilling, Inc. 2004
- Huang G, Sun H. Effect of water absorption on the mechanical properties of glass/polyester composites. *Mater and Design.* 2007; 28 : 1647-50
- Hulatt J, Hollaway L, Thorne A. Preliminary investigations on the environmental effects on new heavyweight fabrics for use in civil engineering. *Compos. Part B: Eng.* 2002; 33: 407-14
- Imielinska K, Guillaumat L. The effect of water immersion ageing on low-velocity impact behaviour of woven aramid–glass fibre/epoxy composites. *Compos. Sci. Technol.* 2004; 64: 2271-8
- Jones F R, Rock J W, Bailey J E. The environmental stress corrosion cracking of glass fiber- reinforced laminates and single E-glass filaments. *J. Mater Sci.* 1983; 18: 1059-71
- Jones R L, Betz D. The kinetics of corrosion of E-glass fibers in hydrochloric acid. *J. Matls. Sci.* 2004; 39: 5633-7
- Jones R L, Stewart J. The kinetics of corrosion of E-glass fibers in sulphuric acid. *J Non-cryst Solids.* 2010; 356: 2433-6

- Karbhari V M (ed). Durability of composites for civil structural applications. woodhead publishings, Cambridge, UK. 2007.
- Karbhari V M, Zhao L. Use of composites for 21st century civil infrastructure. *Comput. Method. Appl. Mech . Eng.* 2000; 185: 433-54
- Kumar S, Sharma N, Ray B C. Acidic degradation of FRP composites. In: Proc. the National Conference on Developments in Composites, India, 2007.
- Leone M, Matthys S, Aiello M A. Effect of elevated service temperature on bond between FRP EBR systems and concrete. *Compos. Part B: Eng.* 2009; 40: 85-93
- Lewis G, Bedder S W. Stress corrosion of glass fibers in acidic environments. *J. Mater. Sci. Lett.* 1984; 3: 728-32
- Liao K, Schultheisz C R, Hunston D L. Effects of environmental aging on the properties of pultruded GFRP. *Compos. Part B.* 1999; 30: 485-93
- Lin M W, Berman J b, Khoshbakht M, Feickert C A, Abatan A O. Modeling of moisture migration in an FRP reinforced masonry structure. *Build. Environ.* 2006; 41: 646-56
- Majdi A, Mostafa-zadeh M, Sajjadian V A. Direction and prediction of well priority drilling for horizontal oil and gas wells (A case study). *J Petrol Sci Eng.* 2005; 49: 63-78
- Maxwell A S, Broughton W R, Dean G, Sims G D. Review of accelerated aging methods and lifetime prediction techniques for polymeric materials. NLP Report: DEPC MPR 016. 2005
- Mikhail A E, El Damatty A A. Non-linear analysis of FRP chimneys under thermal and wind loads. *Thin-Wall. Struct.* 1999; 35: 289-309
- Mula S, Bera T, Ray P K, Ray B C. Effect of hydrothermal aging on mechanical behavior of sub-zero weathered GFRP composites. *J. Reinf. Plast. Compos.* 2006; 25: 673-80
- Mula S, Bera T, Ray P K, Ray B C. Effects of hydrothermal aging on mechanical behavior of sub-zero weathered GFRP composites. *J Reinf. Plas. & Compos.* 2006; 25: 673-80

- Myres T J, Kytomaa H K, Smith T R. Environmental stress corrosion cracking of fiber glass: Lessons learned from failures in the chemical industry. *J. Hazard. Mater.* 2007; 142: 695-704
- Nakai A, Ikegaki S, Hamada H, Takeda N. Degradation of braided composites in hot water. *Compos. Sci. and Technol.* 2000; 60: 325-31
- Nakayama M, Hosokawa Y, Muraoka Y, Katayama T. Life prediction under sulfuric acid environment of FRP using X-ray analysis microscope. *J. Mater. Proc. Technol.* 2004; 155-156: 1558-63
- Neumann S, Marom G. Prediction of moisture diffusion parameters in composite materials under stress. *J. Compos. Mater.* 1987; 21: 68-80
- Neumann S, Marom G. Stress dependence of the coefficient of moisture diffusion in composite materials. *Polym. Compos.* 1985; 6: 9-12
- Neumann S.H, Marom G. Free-volume dependent moisture diffusion under stress in composite materials. *J. Mater. Sci.* 1986; 21: 26-30
- Pauchard V, Grosjean F, Campion-Boulharts H, Chateauminois A. Application of a stress-corrosion-cracking model to an analysis of the durability of glass/epoxy composites in wet environments. *Compos. Sci. Technol.* 2002; 62: 493-98
- Perreux D, Suri C. A study of the coupling between the phenomena of water absorption and damage in glass/epoxy composite pipes. *Compos. Sci. Technol.* 1997; 57:1403-13
- Pillay S, Vaidya U K, Janowski G M. Effects of moisture and UV exposure on liquid molded carbon fabric reinforced nylon 6 composite laminates. *Compos. Sci. Technol.* 2009; 69: 839-46
- Qiu Q, Kumosa M. Corrosion of E-glass fibers in acidic environments, *compos. Sci. & tech.* 1997; 57: 497-507
- Rao R, Chanda M, Balasubramanian M. Factors affecting moisture absorption in polymer composites, Part II: Influence of external factors. *J. Reinf. Plast. Compos.* 1984; 3: 246-53

- Ribeiro M C S, Novoa P R, Ferreira A J M, Marquez A T. Flexural performance of polyester and epoxy polymer mortars under severe thermal conditions. *Cement Concrete Comp.* 2004; 26: 803-9
- Roy S. Prediction of anomalous hygrothermal effects in polymer matrix composites. *J. Reinf. Plast. Compos.* 1999; 19: 1197-207
- Sala G. Composite degradation due to fluid absorption. *Compos. Part B.* 2000; 31(5): 357-73
- Sapalidis S N, Hogg P J, Youd S J. High temperature acidic stress corrosion of glass fiber composites. *J. Mater Sci.* 1997; 32: 309-16
- Schambron Th, Lowe A, McGregor H V. Effects of environmental ageing on the static and cyclic bending properties of braided carbon fiber/PEEK bone plates. *Compos. Part B: Eng.* 2008; 39: 1216-20
- Schutte C L. Environmental durability of glass-fiber composites. *Mater Sci Eng.* 1994; 13: 265-323
- Scida D, Abourab Z, Benzeggagh M L. The effect of ageing on the damage events in woven-fibre composite materials under different loading conditions. *Compos. Sci. and Technol.* 2002; 62: 551-7
- Sereir Z, Adda-Bedia E A, Tounsi A. Effect of temperature on the hygrothermal behaviour of unidirectional laminates plates with asymmetrical environmental conditions. *Compos. Struct.* 2006; 72: 383-92
- Shen C H, Springer G S. Moisture absorption and desorption of composite materials. *J. Compos. Mater.* 1976; 10: 2-20
- Shirrell C D, Leisler W H, Sandow F A. Moisture-induced surface damage in T300/5208 graphite/epoxy laminates, in nondestructive evaluation and flaw criticality for composite materials, ASTM STP 696, R. B. Pipes. ed. American Society for testing and materials, West Conshohocken, USA. 1979:209-23
- Shokrieh M M, Memar M. Stress corrosion cracking of Basalt/Epoxy composites under bending loading. *Appl. Compos. Mater.* 2010; 17: 121-35

Sim J, Park Ch, Young Moon D. Characteristics of basalt fiber as a strengthening material for concrete structures. *Compos. Part B: Eng.* 2006; 36: 504-12

Springer GS. Environmental effects on composite materials. vol. 3, Chapter 1 Lancaster, PA: Technomic Pub. Co. 1981

Startsev O V, Krotov A S, Startseva L T. Interlayer shear strength of polymer composite materials during long term climatic ageing. *Polym. Degrad. Stabil.* 1999; 63: 183-6

Strong M, Bozzini Ch, Hood D, Lowder B. Air and ozone sparging of TCE using a directionally drilled horizontal well. Retrieved on 20/8/2009 from: <http://www.horizontaldrill.com/resources/articles.htm>

Surathi P, Karbhari V M. Hygrothermal effects on durability and moisture kinetics of fiber-reinforced polymer composites, Technical Report No. SSRP06/15, University of California, Oakland. 2006

Suri C, Perreux D. The effects of mechanical damage in a glass fibre epoxy composite on the absorption rate. *Compos. Eng.* 1995; 5: 415-24

Tadeu A J B, Branco F J F G. Shear tests of steel plates epoxy-bonded to Concrete under temperature. *J. Mater. Civ. Eng.* 2000; 12: 74-80

The calculation of oil temperature in a well, SPE 17125, Society of Petroleum engineers, 1987

Tsotsis T K, Keller S, Lee K, Bardis J, Bish J. Aging of polymeric composite specimens for 5000 hours at elevated pressure and temperature. *Compos. Sci. Technol.* 2001; 61: 75-86

Verghese K N E, Hayes M D, Garcia K, Carrier C, Wood J, Riffle J R, Lesko J J. Influence of matrix chemistry on the short term hydrothermal aging of vinyl ester matrix and composites under both isothermal and thermal spiking conditions. *J of Compos. Mater.* 1999; 33: 1918-38

Wan Y Z, Wang Y L, Huang Y, He B M, Han K Y. Hygrothermal aging behaviour of VARTMed three-dimensional braided carbon-epoxy composites under external stresses. *Compos. A.* 2005; 36: 1102-09

Weitsman Y. Moisture in composites: sorption and damage, chap. 9, Fatigue of composite materials, Elsevier Science Publishers B.V. Amsterdam. 1991: 385-429

Whitaker G, Darby M I, Wostenholm G H, Yates B, Collins M H, Lyle A R, Brown B. Influence of temperature and hydrostatic pressure on moisture absorption in polymer resins. *J. Mater. Sci.* 1991; 26: 49-55

Woo R. S C, Zhu H, Leung Ch K y, Kim J K. Environmental degradation of epoxy-organoclay nanocomposites due to UV exposure: Part II residual mechanical properties. *Compos. Sci. Technol.* 2008; 68: 2149-55

Yao J, Ziegmann G. Equivalence of moisture and temperature in accelerated test method and its application in prediction of long-term properties of glass-fiber reinforced epoxy pipe specimen. *Polym. Test.* 2006; 25: 149-57

Yilmaz T, Sinmazcelik T. Experimental investigation of acid environment influences on load-bearing performance of pin-connected continuous glass fiber reinforced polyphenylene sulfide composites. *Polym. Compos.* 2010; 31: 1-9

APPENDIX A Copyright Permission Letter

**JOHN WILEY AND SONS LICENSE
TERMS AND CONDITIONS**

Jun 17, 2013

This is a License Agreement between shiva eslami ("You") and John Wiley and Sons ("John Wiley and Sons") provided by Copyright Clearance Center ("CCC"). The license consists of your order details, the terms and conditions provided by John Wiley and Sons, and the payment terms and conditions.

All payments must be made in full to CCC. For payment instructions, please see information listed at the bottom of this form.

License Number	3171431296127
License date	Jun 17, 2013
Licensed content publisher	John Wiley and Sons
Licensed content publication	Polymer Composites
Licensed content title	Long-term hygrothermal response of perforated GFRP plates with/without application of constant external loading
Licensed copyright line	Copyright © 2012 Society of Plastics Engineers
Licensed content author	Shiva Eslami,Fathollah Taheri-Behrooz,Farid Taheri
Licensed content date	Feb 26, 2012
Start page	467
End page	475
Type of use	Dissertation/Thesis
Requestor type	Author of this Wiley article
Format	Print and electronic
Portion	Full article
Will you be translating?	No
Total	0.00 USD
Terms and Conditions	

TERMS AND CONDITIONS

This copyrighted material is owned by or exclusively licensed to John Wiley & Sons, Inc. or one of its group companies (each a "Wiley Company") or a society for whom a Wiley Company has exclusive publishing rights in relation to a particular journal (collectively "WILEY"). By clicking "accept" in connection with completing this licensing transaction, you agree that the following terms and conditions apply to this transaction (along with the billing and payment terms and conditions established by the Copyright Clearance Center Inc., ("CCC's Billing and Payment terms and conditions"), at the time that you opened your RightsLink account (these are available at any time at <http://myaccount.copyright.com>).

Terms and Conditions

1. The materials you have requested permission to reproduce (the "Materials") are protected by copyright.
2. You are hereby granted a personal, non-exclusive, non-sublicensable, non-transferable, worldwide, limited license to reproduce the Materials for the purpose specified in the licensing process. This license is for a one-time use only with a maximum distribution equal to the number that you identified in the licensing process. Any form of republication granted by this license must be completed within two years of the date of the grant of this license (although copies prepared before may be distributed thereafter). The Materials shall not be used in any other manner or for any other purpose. Permission is granted subject to an appropriate acknowledgement given to the author, title of the material/book/journal and the publisher. You shall also duplicate the copyright notice that appears in the Wiley publication in your use of the Material. Permission is also granted on the understanding that nowhere in the text is a previously published source acknowledged for all or part of this Material. Any third party material is expressly excluded from this permission.
3. With respect to the Materials, all rights are reserved. Except as expressly granted by the terms of the license, no part of the Materials may be copied, modified, adapted (except for minor reformatting required by the new Publication), translated, reproduced, transferred or distributed, in any form or by any means, and no derivative works may be made based on the Materials without the prior permission of the respective copyright owner. You may not alter, remove or suppress in any manner any copyright, trademark or other notices displayed by the Materials. You may not license, rent, sell, loan, lease, pledge, offer as security, transfer or assign the Materials, or any of the rights granted to you hereunder to any other person.
4. The Materials and all of the intellectual property rights therein shall at all times remain the exclusive property of John Wiley & Sons Inc or one of its related companies (WILEY) or their respective licensors, and your interest therein is only that of having possession of and the right to reproduce the Materials pursuant to Section 2 herein during the continuance of this Agreement. You agree that you own no right, title or interest in or to the Materials or any of the intellectual property rights therein. You shall have no rights hereunder other than the license as provided for above in Section 2. No right, license or interest to any trademark, trade name, service mark or other branding ("Marks") of WILEY or its licensors is granted hereunder, and you agree that you shall not assert any such right, license or interest with respect thereto.
5. NEITHER WILEY NOR ITS LICENSORS MAKES ANY WARRANTY OR REPRESENTATION OF ANY KIND TO YOU OR ANY THIRD PARTY, EXPRESS, IMPLIED OR STATUTORY, WITH RESPECT TO THE MATERIALS OR THE ACCURACY OF ANY INFORMATION CONTAINED IN THE MATERIALS, INCLUDING, WITHOUT LIMITATION, ANY IMPLIED WARRANTY OF MERCHANTABILITY, ACCURACY, SATISFACTORY QUALITY, FITNESS FOR A PARTICULAR PURPOSE, USABILITY, INTEGRATION OR NON-INFRINGEMENT AND ALL SUCH WARRANTIES ARE HEREBY EXCLUDED BY WILEY AND ITS

LICENSORS AND WAIVED BY YOU.

6. WILEY shall have the right to terminate this Agreement immediately upon breach of this Agreement by you.

7. You shall indemnify, defend and hold harmless WILEY, its Licensors and their respective directors, officers, agents and employees, from and against any actual or threatened claims, demands, causes of action or proceedings arising from any breach of this Agreement by you.

8. IN NO EVENT SHALL WILEY OR ITS LICENSORS BE LIABLE TO YOU OR ANY OTHER PARTY OR ANY OTHER PERSON OR ENTITY FOR ANY SPECIAL, CONSEQUENTIAL, INCIDENTAL, INDIRECT, EXEMPLARY OR PUNITIVE DAMAGES, HOWEVER CAUSED, ARISING OUT OF OR IN CONNECTION WITH THE DOWNLOADING, PROVISIONING, VIEWING OR USE OF THE MATERIALS REGARDLESS OF THE FORM OF ACTION, WHETHER FOR BREACH OF CONTRACT, BREACH OF WARRANTY, TORT, NEGLIGENCE, INFRINGEMENT OR OTHERWISE (INCLUDING, WITHOUT LIMITATION, DAMAGES BASED ON LOSS OF PROFITS, DATA, FILES, USE, BUSINESS OPPORTUNITY OR CLAIMS OF THIRD PARTIES), AND WHETHER OR NOT THE PARTY HAS BEEN ADVISED OF THE POSSIBILITY OF SUCH DAMAGES. THIS LIMITATION SHALL APPLY NOTWITHSTANDING ANY FAILURE OF ESSENTIAL PURPOSE OF ANY LIMITED REMEDY PROVIDED HEREIN.

9. Should any provision of this Agreement be held by a court of competent jurisdiction to be illegal, invalid, or unenforceable, that provision shall be deemed amended to achieve as nearly as possible the same economic effect as the original provision, and the legality, validity and enforceability of the remaining provisions of this Agreement shall not be affected or impaired thereby.

10. The failure of either party to enforce any term or condition of this Agreement shall not constitute a waiver of either party's right to enforce each and every term and condition of this Agreement. No breach under this agreement shall be deemed waived or excused by either party unless such waiver or consent is in writing signed by the party granting such waiver or consent. The waiver by or consent of a party to a breach of any provision of this Agreement shall not operate or be construed as a waiver of or consent to any other or subsequent breach by such other party.

11. This Agreement may not be assigned (including by operation of law or otherwise) by you without WILEY's prior written consent.

12. Any fee required for this permission shall be non-refundable after thirty (30) days from receipt

13. These terms and conditions together with CCC's Billing and Payment terms and conditions (which are incorporated herein) form the entire agreement between you and WILEY concerning this licensing transaction and (in the absence of fraud) supersedes all prior agreements and representations of the parties, oral or written. This Agreement may not be amended except in writing signed by both parties. This Agreement shall be binding upon and inure to the benefit of the parties' successors, legal representatives, and authorized assigns.

14. In the event of any conflict between your obligations established by these terms and conditions

and those established by CCC's Billing and Payment terms and conditions, these terms and conditions shall prevail.

15. WILEY expressly reserves all rights not specifically granted in the combination of (i) the license details provided by you and accepted in the course of this licensing transaction, (ii) these terms and conditions and (iii) CCC's Billing and Payment terms and conditions.

16. This Agreement will be void if the Type of Use, Format, Circulation, or Requestor Type was misrepresented during the licensing process.

17. This Agreement shall be governed by and construed in accordance with the laws of the State of New York, USA, without regards to such state's conflict of law rules. Any legal action, suit or proceeding arising out of or relating to these Terms and Conditions or the breach thereof shall be instituted in a court of competent jurisdiction in New York County in the State of New York in the United States of America and each party hereby consents and submits to the personal jurisdiction of such court, waives any objection to venue in such court and consents to service of process by registered or certified mail, return receipt requested, at the last known address of such party.

Wiley Open Access Terms and Conditions

Wiley publishes Open Access articles in both its Wiley Open Access Journals program [<http://www.wileyopenaccess.com/view/index.html>] and as Online Open articles in its subscription journals. The majority of Wiley Open Access Journals have adopted the [Creative Commons Attribution License](#) (CC BY) which permits the unrestricted use, distribution, reproduction, adaptation and commercial exploitation of the article in any medium. No permission is required to use the article in this way provided that the article is properly cited and other license terms are observed. A small number of Wiley Open Access journals have retained the [Creative Commons Attribution Non Commercial License](#) (CC BY-NC), which permits use, distribution and reproduction in any medium, provided the original work is properly cited and is not used for commercial purposes.

Online Open articles - Authors selecting Online Open are, unless particular exceptions apply, offered a choice of Creative Commons licenses. They may therefore select from the CC BY, the CC BY-NC and the [Attribution-NoDerivatives](#) (CC BY-NC-ND). The CC BY-NC-ND is more restrictive than the CC BY-NC as it does not permit adaptations or modifications without rights holder consent.

Wiley Open Access articles are protected by copyright and are posted to repositories and websites in accordance with the terms of the applicable Creative Commons license referenced on the article. At the time of deposit, Wiley Open Access articles include all changes made during peer review, copyediting, and publishing. Repositories and websites that host the article are responsible for incorporating any publisher-supplied amendments or retractions issued subsequently. Wiley Open Access articles are also available without charge on Wiley's publishing platform, **Wiley Online Library** or any successor sites.

Conditions applicable to all Wiley Open Access articles:

- The authors' moral rights must not be compromised. These rights include the right of "paternity" (also known as "attribution" - the right for the author to be identified as such) and "integrity" (the right for the author not to have the work altered in such a way that the author's reputation or integrity may be damaged).
- Where content in the article is identified as belonging to a third party, it is the obligation of the user to ensure that any reuse complies with the copyright policies of the owner of that content.
- If article content is copied, downloaded or otherwise reused for research and other purposes as permitted, a link to the appropriate bibliographic citation (authors, journal, article title, volume, issue, page numbers, DOI and the link to the definitive published version on Wiley Online Library) should be maintained. Copyright notices and disclaimers must not be deleted.
 - Creative Commons licenses are copyright licenses and do not confer any other rights, including but not limited to trademark or patent rights.
- Any translations, for which a prior translation agreement with Wiley has not been agreed, must prominently display the statement: "This is an unofficial translation of an article that appeared in a Wiley publication. The publisher has not endorsed this translation."

Conditions applicable to non-commercial licenses (CC BY-NC and CC BY-NC-ND)

For non-commercial and non-promotional purposes individual non-commercial users may access, download, copy, display and redistribute to colleagues Wiley Open Access articles. In addition, articles adopting the CC BY-NC may be adapted, translated, and text- and data-mined subject to the conditions above.

Use by commercial "for-profit" organizations

Use of non-commercial Wiley Open Access articles for commercial, promotional, or marketing purposes requires further explicit permission from Wiley and will be subject to a fee. Commercial purposes include:

- Copying or downloading of articles, or linking to such articles for further redistribution, sale or licensing;
- Copying, downloading or posting by a site or service that incorporates advertising with such content;
- The inclusion or incorporation of article content in other works or services (other than normal quotations with an appropriate citation) that is then available for sale or licensing, for a fee (for example, a compilation produced for marketing purposes, inclusion in a sales pack)

- Use of article content (other than normal quotations with appropriate citation) by for-profit organizations for promotional purposes
- Linking to article content in e-mails redistributed for promotional, marketing or educational purposes;
- Use for the purposes of monetary reward by means of sale, resale, license, loan, transfer or other form of commercial exploitation such as marketing products
- Print reprints of Wiley Open Access articles can be purchased from:
corporatesales@wiley.com

The modification or adaptation for any purpose of an article referencing the CC BY-NC-ND License requires consent which can be requested from
RightsLink@wiley.com.

Other Terms and Conditions:

BY CLICKING ON THE "I AGREE..." BOX, YOU ACKNOWLEDGE THAT YOU HAVE READ AND FULLY UNDERSTAND EACH OF THE SECTIONS OF AND PROVISIONS SET FORTH IN THIS AGREEMENT AND THAT YOU ARE IN AGREEMENT WITH AND ARE WILLING TO ACCEPT ALL OF YOUR OBLIGATIONS AS SET FORTH IN THIS AGREEMENT.

v1.8

If you would like to pay for this license now, please remit this license along with your payment made payable to "COPYRIGHT CLEARANCE CENTER" otherwise you will be invoiced within 48 hours of the license date. Payment should be in the form of a check or money order referencing your account number and this invoice number RLNK501044825. Once you receive your invoice for this order, you may pay your invoice by credit card. Please follow instructions provided at that time.

**Make Payment To:
Copyright Clearance Center
Dept 001
P.O. Box 843006
Boston, MA 02284-3006**

For suggestions or comments regarding this order, contact RightsLink Customer Support: customer@copyright.com or +1-877-622-5543 (toll free in the US) or +1-978-646-2777.

Gratis licenses (referencing \$0 in the Total field) are free. Please retain this printable

6/17/13

Rightslink Printable License

license for your reference. No payment is required.

**ELSEVIER LICENSE
TERMS AND CONDITIONS**

Jun 17, 2013

This is a License Agreement between shiva eslami ("You") and Elsevier ("Elsevier") provided by Copyright Clearance Center ("CCC"). The license consists of your order details, the terms and conditions provided by Elsevier, and the payment terms and conditions.

All payments must be made in full to CCC. For payment instructions, please see information listed at the bottom of this form.

Supplier	Elsevier Limited The Boulevard, Langford Lane Kidlington, Oxford, OX5 1GB, UK
Registered Company Number	1982084
Customer name	shiva eslami
Customer address	1360 barrington st. , room D215 halifax, NS b3h4r2
License number	3171460067954
License date	Jun 17, 2013
Licensed content publisher	Elsevier
Licensed content publication	Corrosion Science
Licensed content title	Effects of perforation size on the response of perforated GFRP composites aged in acidic media
Licensed content author	Shiva Eslami, Farid Taheri
Licensed content date	April 2013
Licensed content volume number	69
Licensed content issue number	
Number of pages	8
Start Page	262
End Page	269
Type of Use	reuse in a thesis/dissertation
Portion	full article
Format	both print and electronic
Are you the author of this Elsevier article?	Yes
Will you be translating?	No
Order reference number	

Title of your thesis/dissertation	DURABILITY OF PERFORATED GFRP UNDER VARIOUS ENVIRONMENTAL CONDITIONS, WITH EMPHASIS ON ITS APPLICATION AS A LINER FOR DIRECTIONAL OIL WELLS
Expected completion date	Jun 2013
Estimated size (number of pages)	178
Elsevier VAT number	GB 494 6272 12
Permissions price	0.00 USD
VAT/Local Sales Tax	0.0 USD / 0.0 GBP
Total	0.00 USD
Terms and Conditions	

INTRODUCTION

1. The publisher for this copyrighted material is Elsevier. By clicking "accept" in connection with completing this licensing transaction, you agree that the following terms and conditions apply to this transaction (along with the Billing and Payment terms and conditions established by Copyright Clearance Center, Inc. ("CCC"), at the time that you opened your Rightslink account and that are available at any time at <http://myaccount.copyright.com>).

GENERAL TERMS

2. Elsevier hereby grants you permission to reproduce the aforementioned material subject to the terms and conditions indicated.

3. Acknowledgement: If any part of the material to be used (for example, figures) has appeared in our publication with credit or acknowledgement to another source, permission must also be sought from that source. If such permission is not obtained then that material may not be included in your publication/copies. Suitable acknowledgement to the source must be made, either as a footnote or in a reference list at the end of your publication, as follows:

“Reprinted from Publication title, Vol /edition number, Author(s), Title of article / title of chapter, Pages No., Copyright (Year), with permission from Elsevier [OR APPLICABLE SOCIETY COPYRIGHT OWNER].” Also Lancet special credit - “Reprinted from The Lancet, Vol. number, Author(s), Title of article, Pages No., Copyright (Year), with permission from Elsevier.”

4. Reproduction of this material is confined to the purpose and/or media for which permission is hereby given.

5. Altering/Modifying Material: Not Permitted. However figures and illustrations may be altered/adapted minimally to serve your work. Any other abbreviations, additions, deletions and/or any other alterations shall be made only with prior written authorization of Elsevier Ltd. (Please contact Elsevier at permissions@elsevier.com)

6. If the permission fee for the requested use of our material is waived in this instance, please be advised that your future requests for Elsevier materials may attract a fee.

7. **Reservation of Rights:** Publisher reserves all rights not specifically granted in the combination of (i) the license details provided by you and accepted in the course of this licensing transaction, (ii) these terms and conditions and (iii) CCC's Billing and Payment terms and conditions.

8. **License Contingent Upon Payment:** While you may exercise the rights licensed immediately upon issuance of the license at the end of the licensing process for the transaction, provided that you have disclosed complete and accurate details of your proposed use, no license is finally effective unless and until full payment is received from you (either by publisher or by CCC) as provided in CCC's Billing and Payment terms and conditions. If full payment is not received on a timely basis, then any license preliminarily granted shall be deemed automatically revoked and shall be void as if never granted. Further, in the event that you breach any of these terms and conditions or any of CCC's Billing and Payment terms and conditions, the license is automatically revoked and shall be void as if never granted. Use of materials as described in a revoked license, as well as any use of the materials beyond the scope of an unrevoked license, may constitute copyright infringement and publisher reserves the right to take any and all action to protect its copyright in the materials.

9. **Warranties:** Publisher makes no representations or warranties with respect to the licensed material.

10. **Indemnity:** You hereby indemnify and agree to hold harmless publisher and CCC, and their respective officers, directors, employees and agents, from and against any and all claims arising out of your use of the licensed material other than as specifically authorized pursuant to this license.

11. **No Transfer of License:** This license is personal to you and may not be sublicensed, assigned, or transferred by you to any other person without publisher's written permission.

12. **No Amendment Except in Writing:** This license may not be amended except in a writing signed by both parties (or, in the case of publisher, by CCC on publisher's behalf).

13. **Objection to Contrary Terms:** Publisher hereby objects to any terms contained in any purchase order, acknowledgment, check endorsement or other writing prepared by you, which terms are inconsistent with these terms and conditions or CCC's Billing and Payment terms and conditions. These terms and conditions, together with CCC's Billing and Payment terms and conditions (which are incorporated herein), comprise the entire agreement between you and publisher (and CCC) concerning this licensing transaction. In the event of any conflict between your obligations established by these terms and conditions and those established by CCC's Billing and Payment terms and conditions, these terms and conditions shall control.

14. **Revocation:** Elsevier or Copyright Clearance Center may deny the permissions described in this License at their sole discretion, for any reason or no reason, with a full refund payable to you. Notice of such denial will be made using the contact information provided by you. Failure to receive such notice will not alter or invalidate the denial. In no event will Elsevier or Copyright Clearance Center be responsible or liable for any costs, expenses or damage incurred by you as a result of a denial of your permission request, other than a refund of the amount(s) paid by you to Elsevier and/or Copyright Clearance Center for denied permissions.

LIMITED LICENSE

The following terms and conditions apply only to specific license types:

15. **Translation:** This permission is granted for non-exclusive world **English** rights only unless your license was granted for translation rights. If you licensed translation rights you may only translate this content into the languages you requested. A professional translator must perform all translations and reproduce the content word for word preserving the integrity of the article. If this license is to re-use 1 or 2 figures then permission is granted for non-exclusive world rights in all languages.

16. **Website:** The following terms and conditions apply to electronic reserve and author websites:
Electronic reserve: If licensed material is to be posted to website, the web site is to be password-protected and made available only to bona fide students registered on a relevant course if

This license was made in connection with a course,

This permission is granted for 1 year only. You may obtain a license for future website posting. All content posted to the web site must maintain the copyright information line on the bottom of each image,

A hyper-text must be included to the Homepage of the journal from which you are licensing at <http://www.sciencedirect.com/science/journal/xxxxx> or the Elsevier homepage for books at <http://www.elsevier.com> , and

Central Storage: This license does not include permission for a scanned version of the material to be stored in a central repository such as that provided by Heron/XanEdu.

17. **Author website** for journals with the following additional clauses:

All content posted to the web site must maintain the copyright information line on the bottom of each image, and the permission granted is limited to the personal version of your paper. You are not allowed to download and post the published electronic version of your article (whether PDF or HTML, proof or final version), nor may you scan the printed edition to create an electronic version. A hyper-text must be included to the Homepage of the journal from which you are licensing at <http://www.sciencedirect.com/science/journal/xxxxx> . As part of our normal production process, you will receive an e-mail notice when your article appears on Elsevier's online service ScienceDirect (www.sciencedirect.com). That e-mail will include the article's Digital Object Identifier (DOI). This number provides the electronic link to the published article and should be included in the posting of your personal version. We ask that you wait until you receive this e-mail and have the DOI to do any posting.

Central Storage: This license does not include permission for a scanned version of the material to be stored in a central repository such as that provided by Heron/XanEdu.

18. **Author website** for books with the following additional clauses:

Authors are permitted to place a brief summary of their work online only.

A hyper-text must be included to the Elsevier homepage at <http://www.elsevier.com> . All content posted to the web site must maintain the copyright information line on the bottom of each image.

You are not allowed to download and post the published electronic version of your chapter, nor may you scan the printed edition to create an electronic version.

Central Storage: This license does not include permission for a scanned version of the material to be stored in a central repository such as that provided by Heron/XanEdu.

19. **Website** (regular and for author): A hyper-text must be included to the Homepage of the journal from which you are licensing at <http://www.sciencedirect.com/science/journal/xxxxx> or for books to the Elsevier homepage at <http://www.elsevier.com>

20. **Thesis/Dissertation**: If your license is for use in a thesis/dissertation your thesis may be submitted to your institution in either print or electronic form. Should your thesis be published commercially, please reapply for permission. These requirements include permission for the Library and Archives of Canada to supply single copies, on demand, of the complete thesis and include permission for UMI to supply single copies, on demand, of the complete thesis. Should your thesis be published commercially, please reapply for permission.

21. **Other Conditions**:

v1.6

If you would like to pay for this license now, please remit this license along with your payment made payable to "COPYRIGHT CLEARANCE CENTER" otherwise you will be invoiced within 48 hours of the license date. Payment should be in the form of a check or money order referencing your account number and this invoice number RLNK501044872. Once you receive your invoice for this order, you may pay your invoice by credit card. Please follow instructions provided at that time.

**Make Payment To:
Copyright Clearance Center
Dept 001
P.O. Box 843006
Boston, MA 02284-3006**

For suggestions or comments regarding this order, contact RightsLink Customer Support: customercare@copyright.com or +1-877-622-5543 (toll free in the US) or +1-978-646-2777.

Gratis licenses (referencing \$0 in the Total field) are free. Please retain this printable license for your reference. No payment is required.
